



HAL
open science

Mechanical behavior of regularly spaced Cross Laminated Timber panels : Modeling and experimental validation in ambient and fire conditions

Lorenzo Franzoni

► **To cite this version:**

Lorenzo Franzoni. Mechanical behavior of regularly spaced Cross Laminated Timber panels : Modeling and experimental validation in ambient and fire conditions. Materials. Université Paris-Est, 2016. English. NNT : 2016PESC1113 . tel-01555571

HAL Id: tel-01555571

<https://pastel.hal.science/tel-01555571>

Submitted on 4 Jul 2017

HAL is a multi-disciplinary open access archive for the deposit and dissemination of scientific research documents, whether they are published or not. The documents may come from teaching and research institutions in France or abroad, or from public or private research centers.

L'archive ouverte pluridisciplinaire **HAL**, est destinée au dépôt et à la diffusion de documents scientifiques de niveau recherche, publiés ou non, émanant des établissements d'enseignement et de recherche français ou étrangers, des laboratoires publics ou privés.

UNIVERSITÉ — — PARIS-EST

Thèse présentée pour obtenir le grade de

Docteur de l'Université Paris-Est

Spécialité: Structures et Matériaux

par

Lorenzo Franzoni

École Doctorale : SCIENCES, INGÉNIERIE ET ENVIRONNEMENT

Mechanical behavior of regularly spaced Cross Laminated Timber panels

-

Modeling and experimental validation in ambient and fire conditions

Thèse soutenue le 24-11-2016 devant le jury composé de:

Prof. Hans Joachim Blass	KIT Karlsruhe	Rapporteur
Prof. Patrice Cartraud	EC Nantes	Rapporteur
Prof. Joseph Gril	LMGC Montpellier	Examineur
Dr. Reinhard Brandner	TU Graz	Examineur
Prof. Michael Flach	Innsbruck University	Examineur
Dr. Arthur Lebée	Laboratoire Navier	Co-encadrant
Dr. Florent Lyon	CSTB	Co-encadrant
Prof. Gilles Foret	Laboratoire Navier	Directeur de thèse

Abstract

Cross Laminated Timber (CLT) panels are engineered timber products composed of layers made of wooden lamellas placed side by side, glued on their upper and lower faces and stacked crosswise. In the present thesis, the influence of lateral spaces between lamellas of each layer on the panel's mechanical response is investigated with modeling and tests. Both configurations of standard panels having short spaces and innovative panels with large spaces are analyzed.

As a first approach, the bending behavior of standard CLT was modeled by means of an equivalent-layer model based on simplified hypotheses. The good agreement of the predicted behavior with an experiment of the literature allowed an investigation on several CLT properties by means of parameter studies.

Then, 4-points bending tests on standard and innovative CLT floors were performed in order to quantify the influence of periodic spaces on the panels' mechanical response. Moreover, available in-plane shear tests of the literature have been considered as reference in-plane behavior.

The spaced CLT have been subsequently modeled as periodic plates with a periodic homogenization scheme handled by a thick plate theory. Existing simplified methods were compared as well with refined modeling and test results. It appears that the bending behavior of spaced CLT can be predicted with a simplified method, while only the thick-plate homogenization can predict the in-plane and transverse shear behavior. Then, closed-form solutions for predicting spaced CLT elastic behavior were derived to encourage the application of these products in timber construction.

One further study within this thesis concerns the analysis of fire-exposed standard CLT floors. The comparison between test results and both advanced and simplified modeling led to a suggestion for a possible improvement the standard fire design model.

Résumé

Les panneaux en bois lamellé croisé (en anglais CLT - Cross Laminated Timber) sont des éléments de structure composés de couches en bois collées entre elles et empilées de façon croisée. Chaque couche est composée de planches en bois juxtaposées et généralement non collées sur leurs chants. Dans cette thèse, nous étudions l'influence des espacements entre planches sur le comportement mécanique des panneaux à l'aide d'une approche par modélisation et expérimentation. Les panneaux CLT standards sont considérés comme des panneaux avec des espacements de très faible dimension par opposition aux panneaux avec espacements importants que nous appelons panneaux innovants.

Nous modélisons dans un premier temps le comportement en flexion de panneaux standards à l'aide d'un modèle de couche homogène équivalente basée sur des hypothèses simplifiées de la mécanique d'une couche avec chants collés ou non collés. Nous observons un bon accord entre les résultats de notre modélisation et des résultats expérimentaux issus de la littérature. Des études paramétriques sont ensuite réalisées portant sur certaines propriétés des panneaux.

Nous avons ensuite réalisé des essais de flexion 4-points sur des panneaux CLT standard et innovants pour quantifier l'influence des espacements sur la réponse mécanique des panneaux. Nous observons alors que l'influence des effets de cisaillement transverse sur le comportement élastique et à la rupture augmente avec l'augmentation des vides dans le panneau.

Afin de prendre correctement en compte les effets du cisaillement, les CLT espacés sont ensuite modélisés comme des plaques épaisses périodiques à l'aide d'un modèle de plaque d'ordre supérieur. Ce modèle a été appliqué à la géométrie des panneaux CLT espacés avec un schéma d'homogénéisation périodique. Des méthodes simplifiées existantes ont également été comparées avec des résultats d'essais et le modèle de plaque. De plus, des résultats d'essais de cisaillement dans le plan des panneaux CLT standards issus de la littérature ont été comparés avec nos résultats. La raideur de flexion des CLT espacés peut être prédite avec des méthodes simples existantes alors que seule la modélisation que nous proposons permet de prédire le comportement en cisaillement transverse et dans le plan. Nous avons ensuite proposé des formules analytiques dans le but de prédire le comportement élastique des CLT espacés. Ces formules donnent une bonne approximation du comportement des CLT espacés et peuvent être utilisées dans le cadre d'une démarche pratique de dimensionnement.

Enfin, une étude concernant l'analyse du comportement au feu des panneaux CLT standard est présentée. La comparaison entre des résultats d'essais au feu et une modélisation avancée et simplifiée a permis de proposer une possible amélioration de la méthode standard de dimensionnement au feu.

Acknowledgments

I would like to acknowledge my supervisors Gilles, Arthur and Florent for giving me the opportunity to live the great working and human experience which has been my thesis. I want to thank my thesis director Gilles for his valuable advices during these three years and for the essential “background” work necessary to set up and fund my studies. Arthur has been a precious presence during my thesis, many thanks to you and to your patience during many computational issues. In my personal view, any modeling result obtained solving many computational issues loses a bit of value if not compared to experimental data. For this reason I’m really grateful to the CSTB institution and to my CSTB supervisor Florent for the organization of the experimental investigation and also for funding part of my thesis. Many thanks also to Dhionis, your advices have been a valuable help to carry on the study in fire conditions.

I want to acknowledge all the jury board for having accepted to examine my thesis. In particular, I would like to thank the representatives of the timber engineering research community, their presence in the jury board is important for me. Indeed, the exchanges during the timber engineering conferences I attended were simply enriching and inspiring, exactly as the people I met. I definitively hope that at least part of my future works will enrich the timber engineering research and consequently will contribute to the development of timber construction.

All my trips during my thesis would not be possible without the perfect and kind work of Marie-Francoise, many thanks also to you.

Finally, many thanks to all my Laboratory colleagues for the nice days together, to my friends, my family and my girlfriend for encouraging and supporting me since the beginning till today.

Lorenzo Franzoni
Paris, November 2016

Contents

1	Introduction	1
2	Bending behavior of standard CLT: modeling and parameter studies	13
2.1	Introduction	13
2.2	Reference experimental test	15
2.3	Modeling of CLT panels bending behavior	16
2.3.1	Mechanical behavior of solid wood	16
2.3.2	Van der Put's mixed failure criterion for wood	17
2.3.3	Equivalent CLT Layer model	19
2.3.3.1	Continuous Equivalent Layer	20
2.3.3.2	Discontinuous Equivalent Layer	20
2.3.4	Pagano's exact solution for laminates in bending	21
2.3.4.1	Uni-axial bending	22
2.3.4.2	Bi-axial bending	22
2.4	Comparison with the reference test	23
2.4.1	Global stiffness	23
2.4.2	Failure stages comparison	23
2.4.2.1	Continuous layer	24
2.4.2.2	Discontinuous layer	25
2.4.2.3	Discussion	26
2.5	Investigation on CLT panel properties	27
2.5.1	Influence of transverse shear effects	27
2.5.2	Varying the number of layers for a fixed total thickness	28
2.5.3	Varying cross layer orientation	29
2.6	Conclusion and perspectives	31
3	Experimental investigation	33
3.1	Introduction	33
3.2	4-points bending tests on full scale floors	34
3.2.1	Materials and methods	34
3.2.2	Results	36
3.2.3	Discussion	38
3.3	Small-scale tests on raw timber	38

CONTENTS

3.3.1	Materials and methods	38
3.3.2	Results	40
3.3.3	Discussion	42
3.4	CLT in-plane shear tests of literature	43
3.5	Conclusion	44
4	Homogenization of regularly spaced CLT panels	45
4.1	Introduction	45
4.2	Modeling of spaced CLT	47
4.2.1	Summary of the Bending-Gradient model	47
4.2.2	Homogenization scheme	48
4.2.2.1	Membrane and thin plate unit-cell problem	49
4.2.2.2	The generalized shear unit-cell problem	50
4.2.3	Application to a regularly spaced CLT panel	51
4.2.3.1	Boundary conditions and loads for the thin-plate and membrane unit-cell problem	53
4.2.3.2	Boundary conditions and loads for the thick-plate unit-cell problem	53
4.3	Results	56
4.3.1	Bending stiffness	56
4.3.2	In-plane shear and torsional stiffnesses	57
4.3.3	Thick-plate homogenization	61
4.3.4	Influence of predicted stresses on variation of failure modes	68
4.4	Conclusion	70
5	Closed-form solutions for spaced CLT	73
5.1	Introduction	73
5.2	Spaced CLT as beam space frame	74
5.3	Thin space frame	75
5.3.1	Energy of connected beams	76
5.3.2	Derivation of the spaced CLT stiffnesses	79
5.3.3	Membrane and bending stiffness of spaced CLT	80
5.3.4	In-plane shear and torsional stiffness of spaced CLT	81
5.4	Thick space frame	83
5.4.1	Transverse shear kinematics of blocks and related energy	85
5.4.2	Energy of connected beams	88
5.4.3	Derivation of the shear force compliance	89
5.5	Closed-form prediction of longitudinal and rolling shear stresses	92
5.5.1	Maximum longitudinal stress	93
5.5.2	Maximum rolling shear stress	93
5.6	Comparison	94
5.6.1	Bending stiffness	94

CONTENTS

5.6.2	In-plane shear and torsional stiffness	95
5.6.3	Shear force compliance	98
5.6.4	Maximum longitudinal and rolling shear stresses	100
5.7	Conclusion	103
6	Fire behavior of standard CLT floors: a stiffness-based approach	105
6.1	Introduction	105
6.2	Fire tests on CLT floors	107
6.2.1	Description of fire tests	107
6.2.2	Temperature profiles	107
6.2.3	Charring rates	110
6.2.4	Deflection of fire exposed CLT floors	110
6.3	Modeling	112
6.3.1	Advanced modeling of heat transfer	112
6.3.2	Thermo-mechanical modeling	113
6.3.3	Reduced Cross Section modeling	114
	6.3.3.1 Existing RCSM approaches	114
	6.3.3.2 Proposal for improving the RCSM	115
6.4	Comparison	116
6.5	Discussion	119
6.6	Conclusion	120
7	Conclusions and outlooks	121
7.1	Limitations	123
7.2	Outlooks	124
	Bibliography	127

CONTENTS

Chapter 1

Introduction

Timber is a bio-sourced construction material always present in human history. At the beginning of the 20th century, the classic log or lattice frame timber construction methods have been progressively replaced by the more economical human-made construction materials like masonry, steel and concrete, at least in Europe (Schickhofer et al 2009). Starting from about ten years ago, timber has sharply regained portions of the construction market, even within cities of European countries like Italy, Austria, Germany or France. This is mostly due to the introduction of a new massive timber construction method based on Cross Laminated Timber (CLT or crosslam) panels, two-dimensional engineered timber products composed of an uneven number of lumber layers stacked and glued crosswise (Figure 1.1). Each layer is made of lumber



Figure 1.1: Cross Laminated Timber panel (<http://hybrid-build.co/>)

boards placed side by side which can be glued or not on their lateral faces depending on the fabrication process. CLT panels have been introduced at the beginning of the 90's in central Europe, based on the well-known principle of orthogonal lamination of plywood applied to thick panels. The resulting thick and orthogonal element has more uniform hygroscopic behavior than glulam and can be used as a full size wall, floor or roof capable of bearing in-plane or out-of-plane loads. The main advantage of CLT building method with respect to traditional timber frame structures is the modular on-site assembly of full size prefabricated CLT that yields very short construction times. The CLT development in modern timber construction has so increased that tall 10-story buildings have been made for instance in London, Milan (Figure 1.2a) and Melbourne, and other having 20-story are in progress in Canada (Figure 1.2b) and

1. INTRODUCTION

France. Such heights are unprecedented in timber engineering, showing the potential of CLT construction system. Compared to linear beam elements made of Glued Lami-



Figure 1.2: Tall CLT buildings: (a) 9-story building in Milan (Bernasconi 2016) and (b) on-going project in Vancouver of a 18-story building with concrete cores (Fast et al 2014)

nated Timber (GLT), CLT panels have capacity of carrying in-plane and out-of-plane loads. Moreover, the crosswise lay-up yields a “system” effect which increases the raw material strength and stiffness, as highlighted by one of the first comprehensive experimental campaign on CLT in bending (Joebstl et al 2006). On this basis, recent state-of-art reports on CLT development suggested specific strength classes for CLT products (Brandner et al 2016; Schickhofer et al 2016). This effect increases when the two-dimensional load distribution capacity is exploited, as showed by Hochreiner et al (2013), Bogensperger and Jobstl (2015) and as will be pointed out in Chapter 2 of the present thesis.

Building with CLT means also connecting the panels between themselves or with other structural elements with connections capable of transferring the loads and ensuring the structural safety. Therefore, panels’ assembling plays a crucial role within CLT construction techniques and, indeed, connection systems are one of the main CLT research topics (Blass and Schadle 2011; Flatscher et al 2014; Polastri 2014). When dealing with dynamic loadings, the connections play a crucial role (Fragiacomo et al 2011; Gavric et al 2015; Scotta et al 2016), since the energy deriving from the wind or seismic acceleration has to be dissipated thanks to the ductility of connections systems. For instance, connections for anchoring CLT walls can consist in classical metallic fasteners (hold-down and angle brackets) or innovative connection systems (Figure 1.3a), while floor-to-floor connections are usually realized with screws (Figure 1.3b).

Increasing the height of timber buildings requires also an improved fire resistance, in

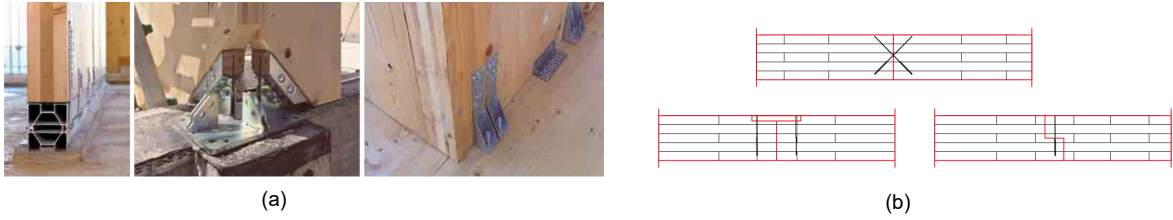


Figure 1.3: Connections in CLT construction: (a) metallic fasteners for anchoring CLT walls and (b) butt-joint between CLT panels (XlamDolomiti 2016)

order to guarantee the structural safety of the structure and also an adequate evacuation time. Since the massive CLT lay-up ensures slow charring rates (Frangi et al 2009b; Craft et al 2011), crosslam panels have also an improved fire resistance compared to linear beam elements. However, the current design model for timber members exposed to fire (EN1995-1-2 2004) has been recently identified to be sometimes non-conservative when dealing with timber floors exposed to fire (Schmid et al 2012). Chapter 6 of the present thesis suggests a possible approach for improving the current version of the structural fire design model of Eurocode 5 1-2 (EN1995-1-2 2004).

Finally, the prefabrication allows the possibility to use CLT panels as reinforcing elements for existing traditional buildings (Branco et al 2014; Soriano et al 2016) and also for the seismic retrofit and comfort rehabilitation (Viskovic et al 2016).

Figure 1.4 presents the CLT skeleton of the 9-storey building in London, showing CLT panels used as horizontal (floors) or vertical (walls) structural elements.



Figure 1.4: Structural skeleton of the 9-story Murray-Groove CLT building in London (<http://tesseract-design.com>)

CLT panels used as floors are submitted to out-of-plane bending. The mechanical

1. INTRODUCTION

response of standard and innovative CLT panels under out-of-plane bending is the main topic of the present thesis. When submitted to out-of-plane bending, the crosslam orthogonal structure leads to cross layers having negligible load-carrying capacity. This is due to the ratio in the range of 25-30 between wood's Young's modulus parallel and perpendicular to grains. Moreover, the cross layers are submitted to transverse shear in wood transverse RT -plane (also called *rolling* shear, Figure 1.5), which shows low values of stiffness and strength, making CLT shear compliant. For softwood, the ratios between RL and RT shear stiffness and strength are in the range of 5-10.

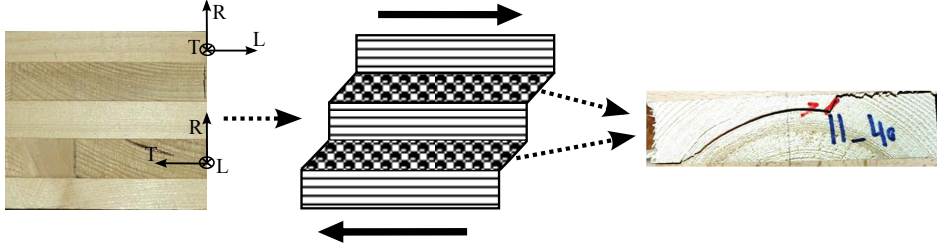


Figure 1.5: Rolling shear in CLT. From Mestek (2011) and Ehrhart et al (2015)

During last years many works have been done on rolling shear in CLT (Aicher and Dill-Langer 2000; Zhou et al 2014; Ehrhart et al 2015; Li et al 2014) in order to study the parameters that mostly influence rolling shear stiffness and strength. Many experimental bending tests on CLT panels proved that common failure modes are either rolling shear of transverse layers or tensile bending failure of bottom layers (Mestek 2011; Blass and Fellmoser 2004b; Hochreiner et al 2013; Czaderski et al 2007; Okabe et al 2014; Sikora et al 2016). The transition between bending and shear failure is influenced by the panel's slenderness but also by boards strength class (Hochreiner et al 2014). The strength classes (EN 2009) classify timber on the basis of the presence of natural heterogeneity (knots, fiber deviation) and the expected influence on the mechanical properties. The tensile strength is the most affected property by the heterogeneities, while timber shear stiffness and strength are generally considered to be independent from the strength class (Blass and Gorklacher 2000; Blass and Fellmoser 2004b; Grandvuiet and Muszynski 2016). Therefore, increasing the strength class of raw lamellas means favors rolling shear failure instead of tensile failure of CLT floors.

The shear compliance of CLT is due to the presence of cross layers at 90° , and hence varying the orientation of transverse layers may mitigate the shear effects and improve the bending performance. The recent studies of (Chen and Lam 2013) and Buck et al (2016) investigated experimentally on this topic (Figure 1.6), while in Chapter 2 of the present thesis a detailed numerical analysis on this subject is performed.

Dealing with calculation methods for out-of-plane loads, 3D Finite Elements (FE) or 3D analytical solutions can well reproduce the mechanical behavior of CLT panels (Sebera et al 2013; Sturzenbecher et al 2010) but they are computationally quite expensive. Crosslam panels can be also modeled as layered anisotropic plates, and their behavior can be well predicted by 2D plate theories, as showed by Sturzenbecher et al



Figure 1.6: Innovative orientation of transverse layers at 45° . From Buck et al (2016) (top) and Chen and Lam (2013) (bottom)

(2010). Due to the non-negligible shear compliance of crosslam, a thick plate theory to correctly predict transverse shear effects is needed. More than 3D or 2D approaches, several 1D simplified design methods exist, and some of them are implemented in European or national design codes (EN1995-1-1 2004; DIN 2004). Such methods are based on lamination theory for layered plates under uni-axial loads and are the k-method (Blass and Fellmoser 2004a) that neglects shear effects, the γ -method of the Eurocode 5 (EN1995-1-1 2004) which partially takes into account shear effects and the shear analogy method (Kreuzinger 1999) which is considered the most predictive method. The shear analogy method will be compared to refined modeling of spaced CLT in Chapter 4 and Chapter 5.

When the CLT floor supports directly the CLT wall, there is a local punching and compression perpendicular to grain, which is a significant research axis (Bogensperger et al 2011; Brandner and Schickhofer 2014; Serrano and Enquist 2010) that tries to show the enhanced compressive properties of CLT. Indeed, compared to glulam, CLT cross layers act as reinforcements with a “locking effect” that increase the CLT stiffness and strength perpendicular to grain (Schickhofer et al 2016). Again, within a CLT panel used as a wall under compressive loads, only the layers having the fibers aligned with the load direction have load-carrying capacity. Moreover, when the height-to-thickness ratio of the panel is sufficiently high, buckling of CLT wall can occur. Recent studies (Perret et al 2016; Thiel and Krenn 2016) pointed out that the rolling shear compliance of transverse layers has a significant influence on the buckling loads of CLT walls. The main focus of research studies concerning crosslam walls deals with the in-plane shear behavior (Figure 1.7a) and an adequate experimental set-up (Figure 1.7b) to determine in-plane shear stiffness and strength (Brandner et al 2013; Gagnon et al 2014; Araki et al 2014; Andreolli et al 2012; Brandner et al 2015). Indeed in-plane shear properties are important for CLT diaphragms and shear walls, especially when submitted to dynamic in-plane loads (Moroder et al 2016). The in-plane shear stiffness of spaced CLT panels is predicted in the present thesis with numerical (Chapter 4) and

1. INTRODUCTION

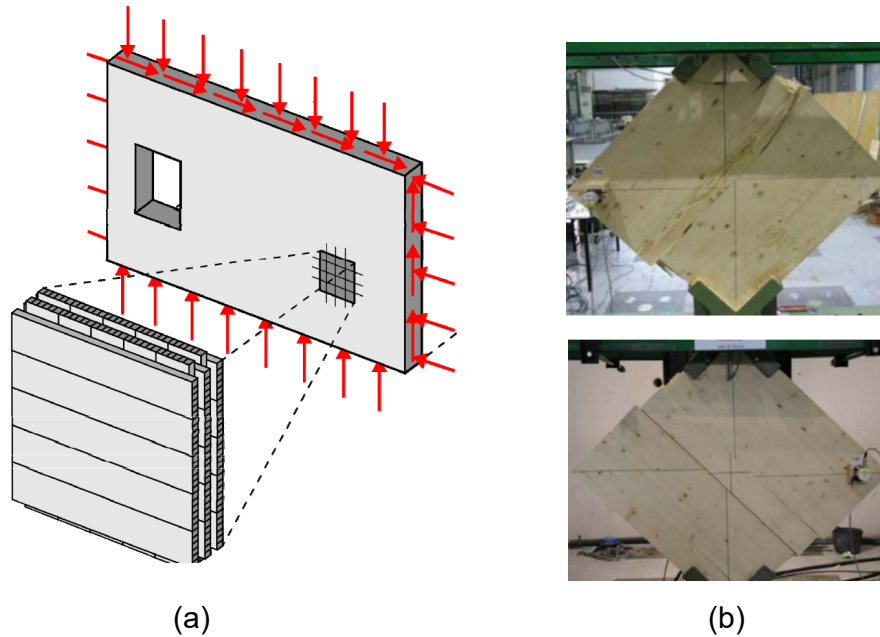


Figure 1.7: (a) CLT wall under loads in-plane (Bogensperger et al 2010) and (b) experimental set-up suggested by Andreolli et al (2012)

closed-form (Chapter 5) approaches, showing that the spaces between lamellas strongly influence the in-plane shear behavior, even for short spaces of standard panels.

The fast development of CLT application in modern construction led to many recent research studies on CLT challenging topics. As a consequence, an established knowledge on the main advantages and issues related to this product exists and brought to the publication of a north-American standard (ANSI/APA 2012) and manual (Gagnon and Pirvu 2013) and an European manual (Schickhofer et al 2009). The publication process of European standard requirements for CLT is on-going and the final draft is now available (EN-16351 2016), while the new version of the Eurocode 5 1-1 containing a section for CLT design is currently under revision (EN1995-1-1 2015).

The process of standardization tries to harmonize CLT production, fields of application and design methods, in order to make this product competitive against mineral-based construction materials. However, there still remain issues not covered or partially covered by the standards. For instance, the final version of EN-16351 (2016) allows the non-gluing of lateral boards of each layer and the presence of small gaps up to 6 mm (Figure 1.8) without specifying their influence on the mechanical behavior. Dealing with the out-of-plane behavior of crosslam the presence of such gaps has been found experimentally (Hochreiner et al 2013) and numerically (Flores et al 2016) to reduce the global-load carrying capacity, due to the presence of free edges between spaces that yields singularities of stress perpendicular to grain (Figure 1.9). This topic will be discussed in Chapter 4 of this thesis, where a comparison between modeling and test results quantifies the influence of small lateral gaps on the transverse shear behavior of standard CLT. Nevertheless, the most sensitive properties of crosslam having short

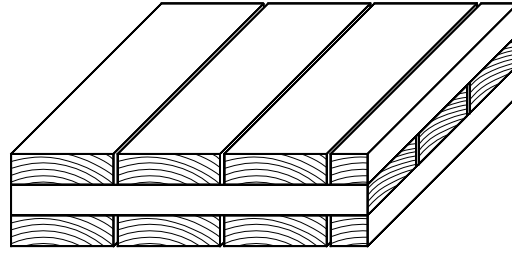


Figure 1.8: CLT panels with short spacing up to 6 mm as described in EN-16351 (2016)

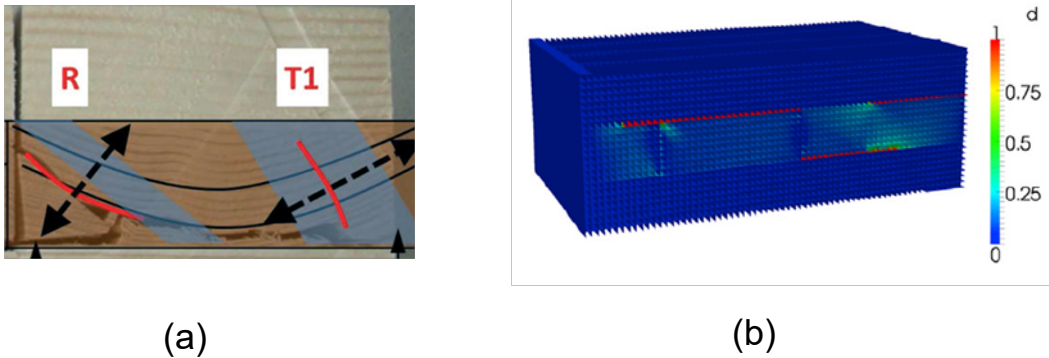


Figure 1.9: Stress concentration in laterally unglued transverse CLT boards due to free edges found (a) experimentally by Hochreiner et al (2013) and (b) numerically by Flores et al (2016) (b) for out-of-plane loads

spaces are related to in-plane behavior. Indeed, discontinuous CLT panels submitted to in-plane shear and in-plane bending (or torsion) shows an additional compliance mechanism related to torsion-like and in-plane rotation of lamellas. On the basis of this mechanism, Moosbrugger et al (2006) from Graz University suggested a simplified closed-form solution for predicting the in-plane shear stiffness and derived assuming an infinite number of layers. Then, the same research team of Graz University improved their approach fitting the closed-form solution on FE results (Bogensperger et al 2010; Silly 2010) for 3,5 or 7-ply configurations, leading to several fitting parameters. The current version of the reviewed Eurocode 5 1-1 for CLT design (EN1995-1-1 2015) includes such closed-form solution with the FE fitting parameters for taking into account the number of layers. In the present study, FE homogenization and closed-form solutions for predicting the in-plane shear and torsional stiffnesses of spaced CLT are compared to the existing closed-form approaches.

Increasing the spaces between narrow lamellas up to hundreds of millimeters yields innovative lighter CLT panels similar to space-frame structure (Figure 1.10). The regular voids can be used to receive equipment conduits or, when filled by insulating material, increase the acoustical and thermal efficiency as well as the fire resistance. Such innovative products match the increasing needs of lighter, more efficient and less expensive timber panels. Currently, there are no specific standards or design tools for the mechanical assessment of these innovative panels, which development is still

1. INTRODUCTION

limited for the resulting lack of knowledge. Similar engineered timber products have

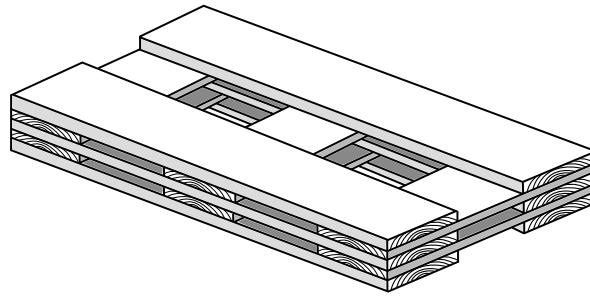


Figure 1.10: Innovative lightweight CLT panels having large spaces between lamellas

been tested by Blass and Gortlacher (2000) (Figure 1.11), who used the *gamma* design method for massive CLT (EN1995-1-1 2004) with wood mechanical properties reduced by the wood volume fraction in order to predict the bending behavior. It appeared that such approach can return a rather good prediction of the bending behavior of spaced timber floors. However, the simplified *gamma* method prevents an accurate description of the transverse shear behavior of the spaced panel. The simplified approach of combining wood volume fractions with a method for massive crosslam is common in engineering applications, and therefore a more refined method may be needed when dealing with spaced CLT floors. No experimental or numerical studies exist on in-

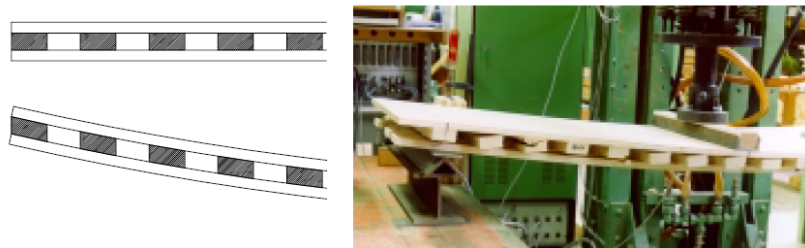


Figure 1.11: Bending tests by Blass and Gortlacher (2000) on spaced timber floors and rolling shear failure of transverse boards

plane behavior of largely spaced CLT. However, the closed-form solution derived by Moosbrugger et al (2006) contains terms related to bending and shear flexibility of cantilevered beams having the spaces as span, and therefore may be capable of reproducing the in-plane behavior of innovative CLT having large spaces. A comparison between such closed-form solution and more accurate modeling is showed in Chapter 4 and Chapter 5.

Contrary to common thoughts, massive timber members such as CLT exposed to fire ensure a safer fire behavior than other construction materials. Indeed, the low thermal conductivity of wood and the self-protection function of charred wood yield low charring rates. For this reason, the fire behavior of timber is more “predictable” than the fire behavior of other materials like steel or concrete that can show explosive

(concrete) or instability (steel) phenomena difficult to predict. Moreover, the low thermal conductivity of wood makes the region affected by high temperatures confined very close to the char front, while the rest of cross section remains at ambient temperature. For this reason, the current fire design approach of the Eurocode 5 1-2 (EN1995-1-2 2004) allows to consider mechanical properties at ambient temperature combined with a reduction of cross section (Reduced Cross Section Method - RCSM). The reduced cross section is predicted with two steps: (i) a first reduction due to charring and (ii) an additional removal of a layer having no mechanical properties (also called zero strength layer) in order to take into account the reduced properties of wood in the region close to the char front (Figure 1.12). In the current version of the Eurocode 5 1-2, such layer has

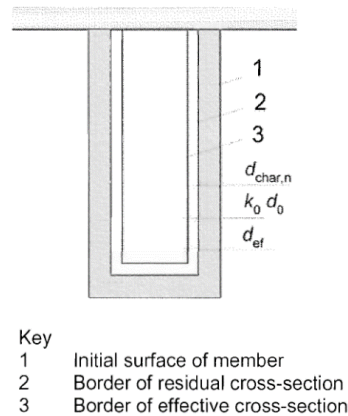


Figure 1.12: Principle of the Reduced Cross Section Method of the Eurocode 5 (EN1995-1-2 2004)

a constant value of 7mm. However, recent studies (Schmid et al 2012; 2014; Lineham et al 2016) showed that this value sometimes leads to non-conservative results, and the “exact” value of the additional layer to remove is difficult to predict since it depends on many parameters. For instance, in order to improve the current RCSM approach, Schmid et al (2012) suggested an additional depth to remove from the cross section as a function of the total thickness of the panel. In Chapter 6 of this thesis, an innovative approach for suggesting a possible improvement of the RCSM is presented. Basically, it is based on the exposure time-dependency of the additional layer to remove when applying the RCSM. Moreover, being laminated members, the glued interface between layers can lead to premature falling-off of layers due to the low mechanical properties of glue at high temperatures. Several experimental studies on fire-exposed crosslam (Frangi et al 2009b; Craft et al 2011; Osborne et al 2012; Klippel et al 2014; Lineham et al 2016) showed a discrepancy about the occurrence and the influence on the fire design of this phenomenon. In Chapter 6 of this thesis, the experimental deflection of fire-exposed crosslam floors that showed falling-off of layers is predicted with the approach of Frangi et al (2009b) for taking into account such delamination phenomenon and compared to other methods which neglect the falling-off.

Based on the current state of the art of CLT research, the main objective of

1. INTRODUCTION

the present thesis is to investigate on the influence of spaces between lateral boards on CLT mechanical behavior by means of modeling and tests. Both cases of small gaps of standard CLT and larger spaces of innovative panels are investigated. The comparison between refined modeling, test results and simplified methods aims to establish a reliable calculation tool for spaced CLT that could be used in practical applications. Additionally, a study on fire-exposed crosslam is presented in this thesis and aims to suggest a possible approach for improving the existing fire design model by means of a comparison between testing and advanced calculations.

In the following, the manuscript outline is summarized, while an overview of the thesis is presented in Figure 1.13.

First simplified approach: In this first approach presented in Chapter 2, laterally glued or unglued layers are modeled by means of an equivalent layer model based on simplified hypotheses on mechanical properties. The stress were predicted with a 3D solution and are the input for a wood failure criterion. The good match with a reference test of literature allows parameter studies on common and innovative crosslam properties in order to point out some interesting features about CLT applications.

Experimental investigation: Chapter 3 presents the conducted full-scale and small-scale experimental tests that aimed to point out the influence of spaces on elastic and failure behavior of spaced CLT floors. A reference in-plane shear test on CLT of the literature is presented as well.

Modeling-1: Homogenization: Spaced CLT panels are then modeled as thin and thick periodic plates by means of a numerical homogenization scheme. Chapter 4 presents the main features of such refined modeling and the implementation in the case of spaced crosslam, as well as the comparison with experimental results and existing simplified approaches.

Modeling-2: Closed-form solution: Chapter 5 presents the modeling procedure to derive a closed-form solution for spaced CLT based on beam theory. The obtained simplified formulations can then be used for practical spaced CLT applications.

Fire behavior: The analysis of standard CLT fire behavior is presented in Chapter 6. The available experimental data is firstly summarized, then both refined modeling based on reduced properties and simplified modeling based on reduced geometry are presented. The comparison between the two approaches led to a suggestion for a possible improvement of the current fire design model for timber structures of Eurocode 5 1-2 (EN1995-1-2 2004).

Conclusion and outlooks: The thesis concludes with Chapter 7, where the principal results, conclusion and outlooks of the presented study are presented.

Finally, in the present thesis, only the deterministic mechanical behavior of CLT panels is considered. No possible influence of obtained results on thermal, acoustical or hygroscopic behavior is taken into account. The predicted displacements and stresses are elastic fields, and failure is defined to be the reach of the material strength by the

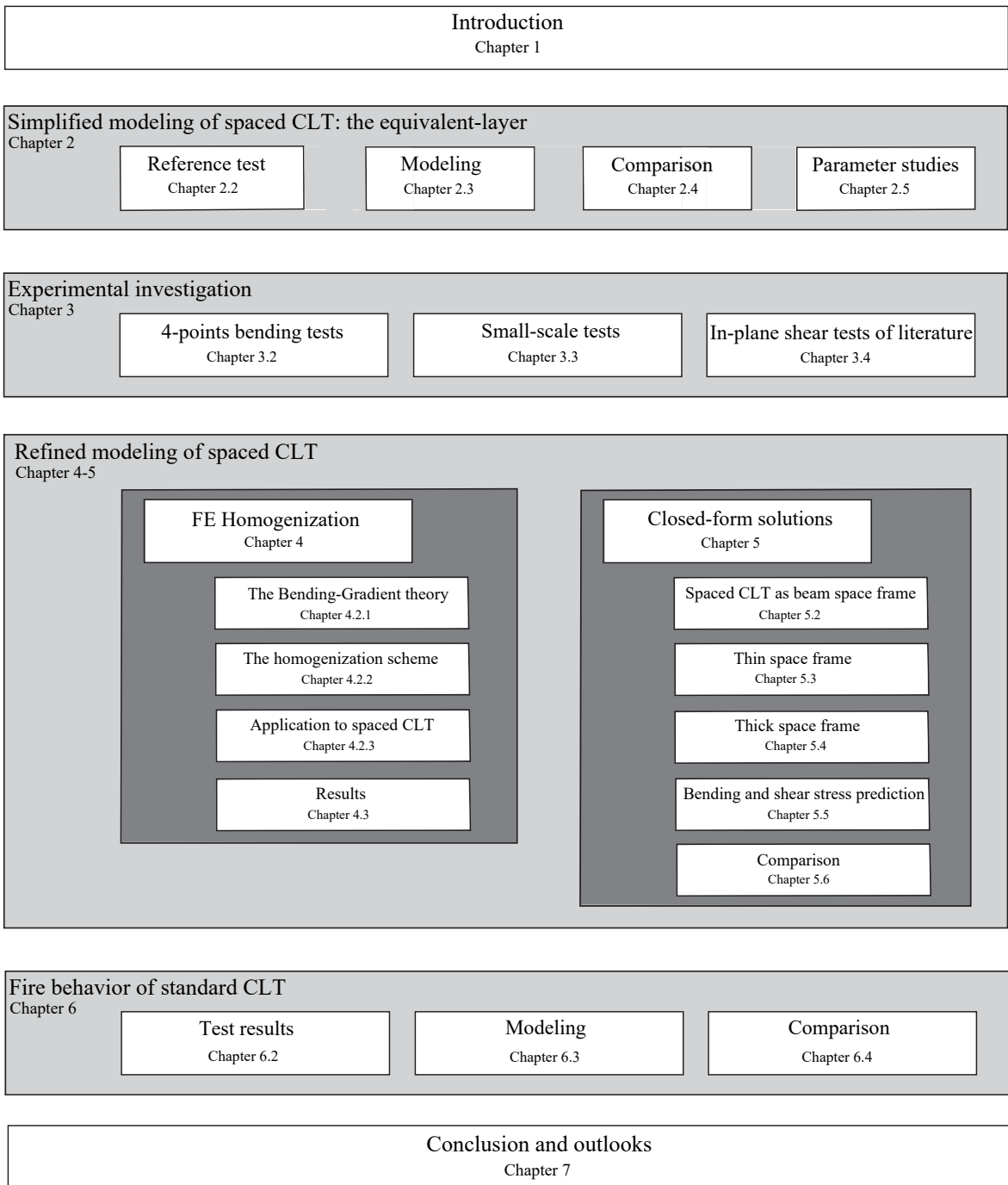


Figure 1.13: Schematic overview of the thesis

1. INTRODUCTION

elastic stresses. Moreover, the considered CLT are single panels without connections with other elements.

Chapter 2

Bending behavior of standard CLT: modeling and parameter studies

Note: This Chapter has been published in *European Journal of Wood and Wood Products* with the title *Influence of orientation and number of layers on the elastic response and failure modes of CLT floors: modeling and parameter studies* DOI: 10.1007/s00107-016-1038-x

Abstract. In this Chapter, the layers of CLT in bending are modeled as laterally glued or unglued layers by means of simplified hypotheses on mechanical properties. The simplified behavior is combined with the exact 3D elastic solution for layered plates in bending (Pagano 1969) and a failure criterion for wood. The predicted mechanical behavior is compared with an experiment of the literature in terms of global stiffness and variation of failure modes. Finally, parameter studies are performed on several panel's properties which can be interesting for practical application.

Résumé. Dans ce Chapitre, nous modélisons les couches de CLT en flexion comme des couches homogènes équivalentes dans lesquelles les planches sont collées ou non sur chants en prenant des hypothèses simplifiées sur les propriétés mécaniques. Ce comportement simplifié est couplé avec la solution exacte 3D pour multicouches en flexion (Pagano 1969) et un critère de rupture pour le bois. Le comportement prédit est comparé avec les résultats d'un essai issu de la littérature en termes de raideur globale et de variation des modes de ruine. Enfin, des études paramétriques sont conduites pour déterminer les propriétés des panneaux en fonction de leurs caractéristiques géométriques.

2.1 Introduction

The state-of-the-art presented in the previous Chapter revealed a comprehensive and well documented experimental study on CLT panels in bending (Hochreiner et al 2013). Therefore, the first purposes of this thesis have been reproducing the mechanical re-

2. BENDING BEHAVIOR OF STANDARD CLT: MODELING AND PARAMETER STUDIES

sponse observed during such experiments of the literature and performing parameter studies on CLT properties interesting for applications. This work allowed the identification of challenging topics from both scientific and practical point of view.

CLT plates in bending are affected by heterogeneities at different levels. First, at the material scale, timber features a pronounced variation in mechanical properties. Then, within each layer, two other kinds of heterogeneities can be differentiated. The local orientation of orthotropic coordinate system is *a priori* unknown due to the variation of annual ring pattern. Moreover, the discontinuities in the non-gluing of lateral lamellas have a non-negligible influence on the mechanical response, as the studies presented in Chapter 1 show. At the structural level, the multilayer and orthotropic lay-up makes crosslam panels layered shear-compliant plates with anisotropic behavior, and therefore an adequate model has to be implemented in order to predict the mechanical response. At the layer scale, an "equivalent-layer" mechanical model is suggested in this Chapter to take into account the CLT layer's heterogeneities, leading to simplified hypotheses on layer's behavior. Concerning the structural heterogeneity given by the multi-layer composition, the limits of the existing design methods presented in Chapter 1 lie in a simplified approach, which reduce the 2D problem into a 1D one and is suitable only for orthotropic (0° or 90°) lay-ups. In the present Chapter, the exact 3D theory for laminated plates in bending (Pagano 1969; 1970) is applied to CLT panels, in order to predict their mechanical response and to analyze plates with non-orthotropic lay-ups. Being a 3D solution, Pagano's theory can give a better estimation of stress distribution across the panel's thickness than simplified 1D or 2D approaches, especially when the panel is submitted to concentrated loads, as in the case of the reference test (Hochreiner et al 2013). The elastic bending solution is therefore combined with a failure criterion for wood, in order to extend the comparison with the reference test in terms of failure stages.

In the present Chapter, the main topic of interest is CLT mechanical behavior at the layer and structure scale, leading to a simplified modeling at the material scale. Whereas the wood variability has not been taken into account in this study, having a detailed description of 3D stress enables the estimation of interesting features of CLT mechanical behavior. Indeed, the influence on panel's bending behavior of having edge-glued or unglued layers is analyzed, as well as the effects of varying layers number and orientation. All the modeling tools are presented in Section 2.3 after the introduction, in Section 2.2, of the reference experimental behavior of CLT panels. In Section 2.4, the comparison between the predicted and actual behavior is made in terms of the plate's global stiffness and variations in failure stages. The good agreement with the reference results has led to an investigation on CLT properties by means of the parameter studies in Section 2.5. In this final Section, transverse shear effects occurring in CLT in bending are quantified, as well as further CLT advantages deriving from the variation of layer orientation and number.

2.2 Reference experimental test

Hochreiner et al (2013) tested square 3-ply and 5-ply CLT panels with slenderness ratios of 10 and 20 and made of Norway spruce lumber boards of strength class C24 (EN 2009). The plates had their four sides supported and were submitted to concentrated loads at their center. Thanks to a combined measuring system of acoustic emission, LVDTs and accurate cutting of specimens after the failure, progressive failure stages were determined as a function of load levels (Figure 2.1). At each failure stage, the corresponding crack type identified by the panel's cutting was assigned. The most complete documentation found in the reference paper is about the so-called specimen "EL4", a three-layer panel of slenderness ratio of 20. Figure 2.1 reproduces the reference test result for specimen "EL4" in terms of its load-displacement curve, failure stages and respective failure modes. The plate showed a global ductile behavior after the elastic limit, due to its bi-axial bending configuration, whose effect is to redistribute the stresses after the first cracks appear. This "system" effect is particularly evident in Stage 2, where the global linear behavior is not really affected by the appearance of rolling shear cracks.

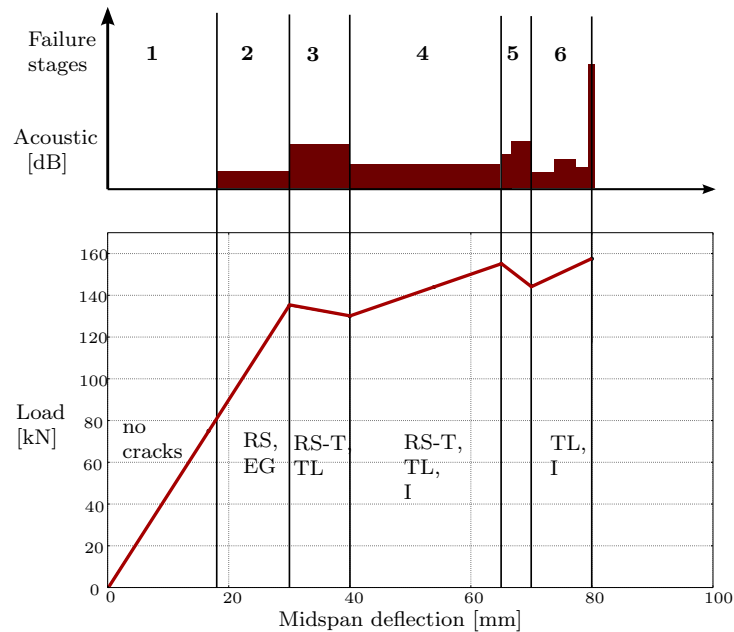


Figure 2.1: Schematic load - displacement curve with identified failure stages and associated crack modes found by Hochreiner et al (2013)

All the cracking modes found during the loading process are presented in Figure 2.2. The cracks appearing first called "RS" and "EG" stand respectively for rolling shear failure in cross-layers and edge-gluing failure between lateral boards of the same layer. The failure mode denoted "TL" is the tensile failure in direction parallel to grain, while "I" is the local indentation perpendicular to grain. The failure called "RS - T" is a complex cracking pattern occurring in cross layers at the end of the elastic limit and assumed to derive from interactions between rolling shear and tensile stresses.

2. BENDING BEHAVIOR OF STANDARD CLT: MODELING AND PARAMETER STUDIES

Moreover, the "RS - T" cracking pattern was also a consequence of the geometrical discontinuities appearing between boards of the same layer, after edge-gluing failure.

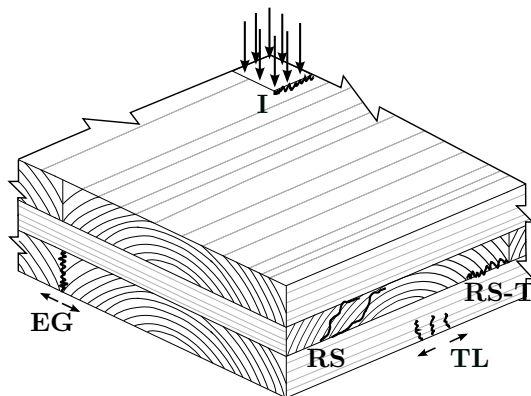


Figure 2.2: Failure modes of specimen EL4 (Hochreiner et al 2013)

The comparison between the predicted and experimental bending response is made in terms of the panel's global stiffness in the linear elastic load stage (stage 1 in Figure 2.1) and the variation of failure modes within the apparent elastic stage (until stage 3 in Figure 2.1).

2.3 Modeling of CLT panels bending behavior

At the material scale, wood is considered as an elastic, brittle and homogeneous material. The heterogeneities characterizing the CLT layers are taken into account by means of an equivalent and homogeneous layer, whose mechanical properties are defined both in terms of elasticity and failure. Once the simplified mechanical behavior is set, the exact 3D solution in elasticity for laminated plates in bending (Pagano 1969; 1970) is chosen in order to obtain precise estimation of the plate's mechanical response. Finally, a failure criterion suitable for wood (van der Put 1982) can point out the failure load and the corresponding dominant failure mode of CLT panels in bending.

2.3.1 Mechanical behavior of solid wood

Wood is an orthotropic material with three principal axes. The first one is aligned in the fiber or trunk direction (longitudinal direction, L). In the transverse plane, the remaining two axes are orthogonal to growth rings (radial direction, R) and tangential (tangential direction, T) to them. Figure 2.3 presents the axes of orthotropy of solid wood.

The chosen wood species is Norway spruce (*Picea abies*), since it is the most widely used wood species in Europe for CLT production and was also used in the reference experiment. The mechanical properties are chosen on the basis of tests in literature on specimens of *clear* spruce, without knots. Table 2.1 shows the elastic and strength properties of Norway spruce taken respectively from Keunecke et al (2008) and Dahl

2.3 Modeling of CLT panels bending behavior

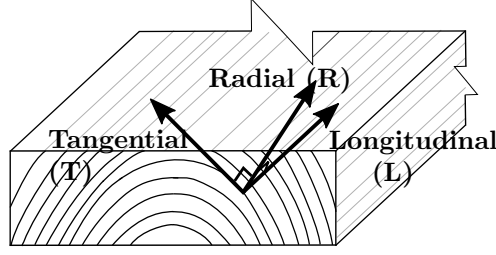


Figure 2.3: Material axes of orthotropy for solid wood

(2009). The first subscripts L , T and R represent the wood coordinate system, while the following t and c represent tensile or compressive strength. As it will be shown in the next paragraph, the failure analysis requires the complete set of nine spruce strength parameters, whose values are present only in Dahl (2009). Another experimental campaign on clear spruce strengths in the LT plane (Eberhardsteiner 2002) confirms the congruity of the chosen values, especially for the tensile strength. The failure behavior presented in Table 2.1 describes wood's strength with respect only to pure uni-axial stresses. Therefore, in order to perform an exhaustive failure analysis, a mixed failure criterion for wood is required.

Elasticity (Keunecke et al 2008)	E_L 12800	E_T 397	E_R 625	G_{RL} 617	G_{LT} 587	G_{TR} 53	ν_{LR} 0.36	ν_{LT} 0.45	ν_{RT} 0.48
Failure (Dahl 2009)	$f_{L,t}$ 63.4	$f_{L,c}$ 28.9	$f_{T,t}$ 2.8	$f_{T,c}$ 3.8	$f_{R,t}$ 4.9	$f_{R,c}$ 3.6	f_{RL} 7.1	f_{LT} 4.8	f_{TR} 2.0

Table 2.1: Elastic and strength properties of Norway spruce [MPa]

2.3.2 Van der Put's mixed failure criterion for wood

Failure criteria define the material failure by means of normalized expressions, which represent the material's strength surface. A stress state, that reaches or exceeds the failure surface, leads to inelastic phenomena such as damage or plastic strains. The most widely used isotropic failure criteria are based on von Mises maximum distortion energy. These criteria generally follow a quadratic expression which represents an elliptic surface. Dealing with anisotropic materials, the rotated and translated ellipsoid of Tsai-Wu (Tsai and Wu 1971) is the most common failure surface. The general quadratic expression for orthotropic materials can be written as:

$$\begin{aligned}
 f(\sigma) : & A\sigma_L^2 + B\sigma_T^2 + C\sigma_R^2 + D\sigma_L\sigma_T + E\sigma_L\sigma_R + \\
 & + F\sigma_T\sigma_R + G\sigma_L + H\sigma_T + I\sigma_R + \\
 & + L\tau_{LT}^2 + M\tau_{LR}^2 + N\tau_{RT}^2 = 1.0
 \end{aligned} \tag{2.1}$$

where σ and τ are respectively the longitudinal and shear stresses in orthotropic coordinates L , T , and R . The capital letters are function of the material strengths and

2. BENDING BEHAVIOR OF STANDARD CLT: MODELING AND PARAMETER STUDIES

they determine the geometry of the failure surface. While the coefficients of quadratic terms (A, B, C and L, M, N) represent the semi-axes of the elliptical surface, linear (G, H, I) and interaction (D, E, F) terms in (2.1) respectively translate and rotate the ellipsoid. The value of interaction terms in failure criteria for anisotropic materials is still nowadays under discussion. During his studies on failure criteria for wood, van der Put (1982) showed how the value of the interaction term has a negligible influence when the stress path is closed to the failure surface. Therefore, Van der Put's failure criterion is a function $f(\sigma)$ like (2.1) but without interaction terms. This failure criterion has been compared in Cabrero et al (1984) with other criteria applied to spruce failure, and it turned out to be one of the most predictive. Therefore, considering also its simple implementation due to the absence of interaction terms, Van der Put's failure function has been chosen for the failure analysis. The coefficients of Equation 2.1 derived in (van der Put 1982) are:

$$A = \frac{1}{f_{L,t}f_{L,c}}, \quad B = \frac{1}{f_{T,t}f_{T,c}}, \quad C = \frac{1}{f_{R,t}f_{R,c}}, \quad (2.2)$$

$$D = E = F = 0$$

$$G = \frac{1}{f_{L,t}} - \frac{1}{f_{L,c}}, \quad H = \frac{1}{f_{T,t}} - \frac{1}{f_{T,c}}, \quad I = \frac{1}{f_{R,t}} - \frac{1}{f_{R,c}} \quad (2.3)$$

$$L = \frac{1}{f_{LT}^2}, \quad M = \frac{1}{f_{RL}^2}, \quad N = \frac{1}{f_{TR}^2} \quad (2.4)$$

where wood's strength properties f_i have been discussed in Section 2.3.

If the failure criterion is proportional to the applied load, it is straightforward to find the failure load from a single linear solution. Whereas σ is already proportional to the applied load, the function $f(\sigma)$ derived by van der Put (1982) turns out not to be proportional. Hence, it is necessary to derive a new function $F(\sigma)$, which will describe the same failure surface, but also satisfy the condition

$$F(\lambda\sigma) = \lambda F(\sigma), \quad \lambda > 0 \quad (2.5)$$

Property (2.5) ensures the same variation λ of $F(\sigma)$, when varying the external load (and the related stress state σ) of a positive quantity λ . Rewriting the function $f(\sigma)$ of Equation 2.1 leads to:

$$f(\sigma) : {}^t(\sigma - \mathbf{k}_0)\mathbf{K}(\sigma - \mathbf{k}_0) - {}^t\mathbf{k}_0\mathbf{K}\mathbf{k}_0 = 1.0 \quad (2.6)$$

with

$$\boldsymbol{\sigma} = \begin{bmatrix} \sigma_L \\ \sigma_T \\ \sigma_R \\ \sigma_{TR} \\ \sigma_{RL} \\ \sigma_{LT} \end{bmatrix}, \quad \mathbf{k}_0 = \begin{bmatrix} g \\ h \\ i \\ 0 \\ 0 \\ 0 \end{bmatrix}, \quad \mathbf{K} = \begin{bmatrix} A & 0 & 0 & 0 & 0 & 0 \\ 0 & B & 0 & 0 & 0 & 0 \\ 0 & 0 & C & 0 & 0 & 0 \\ 0 & 0 & 0 & L & 0 & 0 \\ 0 & 0 & 0 & 0 & M & 0 \\ 0 & 0 & 0 & 0 & 0 & N \end{bmatrix} \quad (2.7)$$

2.3 Modeling of CLT panels bending behavior

$\boldsymbol{\sigma}$ stands for the stresses expressed in the wood's coordinate system, while \mathbf{k}_0 and \mathbf{K} include the wood's strength properties. Developing Equation 2.6 and comparing it term to term with Equation 2.1, we can find the following components of \mathbf{k}_0 :

$$g = \frac{f_{L,t} - f_{L,c}}{2}, \quad h = \frac{f_{T,t} - f_{T,c}}{2}, \quad i = \frac{f_{R,t} - f_{R,c}}{2} \quad (2.8)$$

As mentioned in Section 2.3.2, the function described by Equation 2.1 is not proportional to the external load. Then, we search a new function $F(\boldsymbol{\sigma})$, having the property of a homogeneous function of degree one:

$$F(\lambda\boldsymbol{\sigma}) = \lambda F(\boldsymbol{\sigma}), \quad \lambda > 0 \quad (2.9)$$

Substituting $\boldsymbol{\sigma} = \lambda\boldsymbol{\sigma}$ in (2.6) leads to

$$\lambda^2 {}^t\boldsymbol{\sigma}\mathbf{K}\boldsymbol{\sigma} - 2\lambda {}^t\boldsymbol{\sigma}\mathbf{K}\mathbf{k}_0 - 1 = 0 \quad (2.10)$$

The positive root of Equation 2.10 gives the multiplier coefficient λ with which the stresses $\lambda\boldsymbol{\sigma}$ produce a criterion's value of 1.0 and consequently, the material failure. Therefore, the function

$$\lambda(\boldsymbol{\sigma}) = \frac{{}^t\boldsymbol{\sigma}\mathbf{K}\mathbf{k}_0 + \sqrt{({}^t\boldsymbol{\sigma}\mathbf{K}\mathbf{k}_0)^2 + {}^t\boldsymbol{\sigma}\mathbf{K}\boldsymbol{\sigma}}}{{}^t\boldsymbol{\sigma}\mathbf{K}\boldsymbol{\sigma}} \quad (2.11)$$

returns the value with which the stresses should be multiplied in order to reach the rupture. The inverse of this function $F(\boldsymbol{\sigma}) = 1/\lambda(\boldsymbol{\sigma})$ is a homogeneous function of degree one whose values are

$$\begin{cases} F(\boldsymbol{\sigma}) \geq 1.0 & \text{if rupture occurs} \\ 0 < F(\boldsymbol{\sigma}) < 1 & \text{if rupture does not occur} \end{cases} \quad (2.12)$$

Finally, the function $F(\boldsymbol{\sigma}) = 1/\lambda(\boldsymbol{\sigma})$ can be derived from Equation 2.11. The value $\lambda(\boldsymbol{\sigma})$ represents the multiplier coefficient to reach the failure point. The spatial distribution within the CLT panel of $\lambda(\boldsymbol{\sigma})$ multiplied by the failure load F_c represents the load levels necessary to reach progressive failures under linear elastic hypotheses.

When the failure load is determined, it is of particular interest to establish the associated dominant failure mode. This can be achieved computing the ratios between each of the six stress components expressed in the wood's coordinates ($\sigma_L, \sigma_T, \sigma_R, \tau_{LT}, \tau_{RL}, \tau_{TR}$) and their respective strengths ($f_{L,c-t}, f_{T,c-t}, f_{R,c-t}, f_{LT}, f_{RL}, f_{TR}$). The maximum value of these ratios can point out the dominant failure mode. This ratio is computed at any point within the panel.

2.3.3 Equivalent CLT Layer model

Both complete (3D) and reduced (2D or 1D) solutions for layered plates in bending consider every layer as homogeneous. In practice, each CLT layer is made of boards

2. BENDING BEHAVIOR OF STANDARD CLT: MODELING AND PARAMETER STUDIES

placed side by side and it is affected by the heterogeneities presented before. Hence, it is necessary to set a homogeneous "Equivalent CLT Layer" model, which could take such heterogeneities into account. As presented before, the first complexity derives from the variation of growth rings' orientation inside each layer, which leads to an unknown orientation of the local orthotropic coordinate system. Moreover, in case of unglued lateral boards, the resulting discontinuities influence the equivalent layer. Note that, if the lateral edges of boards were initially glued, the experimental evidence showed that the edge gluing detachment is one of the first failure modes (see Section 2.2).

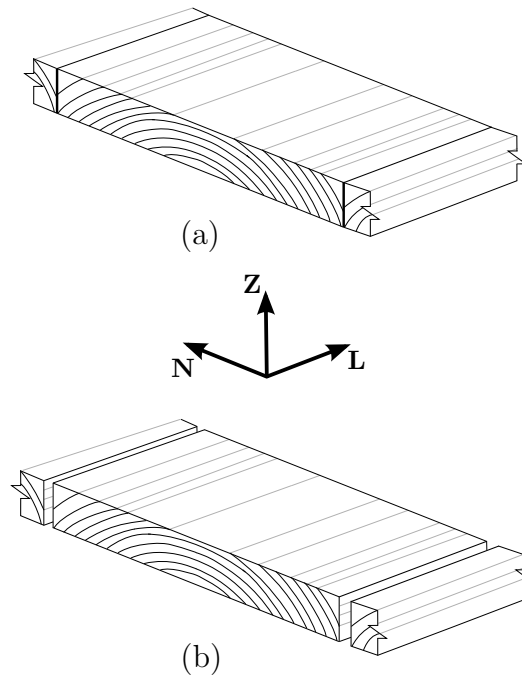


Figure 2.4: Schematic continuous (a) and discontinuous (b) Equivalent CLT Layers together with the layer's reference frame

2.3.3.1 Continuous Equivalent Layer

If the boards' lateral edges are glued, each wooden layer can be viewed as a continuous layer. The same material behavior in directions N and Z of the board's reference frame (Figure 2.4) is considered, in order to overcome the irregularity of growth rings. While the Z direction remains always the same, directions L and N change together with the orientation of the considered layer. Table 2.2 presents the elastic and strength properties of the continuous Equivalent Layer. The defined elastic moduli for the N or Z direction are the mean values between the corresponding T and R ones for solid wood (Table 2.1), while the strength parameters are the lower values.

2.3.3.2 Discontinuous Equivalent Layer

When CLT boards are not glued together on their lateral edges, or when in-plane stress caused the edge-gluing detachment, each layer becomes discontinuous (Figure 2.4b) and

2.3 Modeling of CLT panels bending behavior

Elasticity	E_L	E_N	E_Z	G_{ZL}	G_{LN}	G_{NZ}	ν_{LZ}	ν_{LN}	ν_{ZN}
	12800	511	511	602	602	53	0.41	0.41	0.48
Failure	$f_{L,t}$	$f_{L,c}$	$f_{N,t}$	$f_{N,c}$	$f_{Z,t}$	$f_{Z,c}$	f_{ZL}	f_{LN}	f_{NZ}
	63.4	28.9	2.8	3.6	2.8	3.6	4.8	4.8	2.0

Table 2.2: Elastic and strength properties of a continuous CLT layer [MPa]

such discontinuities preclude any transmission of stresses between separated boards. This also means that failure in N -direction cannot occur. Table 2.3 shows the considered mechanical behavior of an equivalent and discontinuous layer made of Norway spruce. Intuitively, due to the gaps between lateral boards, the equivalent layer's plane shear modulus G_{LN} may be set to zero (Mestek et al 2008). However, all layers are glued on their upper and lower faces and hence the discontinuous CLT panel has a (reduced) in-plane shear stiffness (Moosbrugger et al 2006). The same conclusion can be deduced for the plane shear strength of a discontinuous layer. A more accurate investigation on the actual plane shear behavior of a discontinuous layer will be the object of further studies. In this first simplified approach, it is assumed that the in-plane shear behavior of layers equals the wood's behavior. The Poisson's ratios ν_{LN} and ν_{ZN} represent the layer's strain in direction N , due to the imposed strain in directions L and Z , respectively. Considering layers with discontinuities along direction N as in Figure 2.4b, the values of these coefficients are assumed to be zero.

Elasticity	E_L	E_N	E_Z	G_{ZL}	G_{LN}	G_{NZ}	ν_{LZ}	ν_{LN}	ν_{ZN}
	12800	0.0	511	602	602	53	0.41	0.0	0.0
Failure	$f_{L,t}$	$f_{L,c}$	$f_{N,t}$	$f_{N,c}$	$f_{Z,t}$	$f_{Z,c}$	f_{ZL}	f_{LN}	f_{NZ}
	63.4	28.9	-	-	2.8	3.6	4.8	4.8	2.0

Table 2.3: Elastic and strength properties of a discontinuous CLT layer [MPa]

2.3.4 Pagano's exact solution for laminates in bending

Once the model for an equivalent and homogeneous CLT layer is set, the analytical bending solution can be chosen between complete or reduced approaches. 1D theories (Blass and Fellmoser 2004a; EN1995-1-1 2004; Kreuzinger 1999) have very low computational costs but give approximate results. 2D plate theories for laminates in bending (Lebée and Sab 2011a; Thai et al 2013) are still reduced approaches, but return more precise results than beam theories. Nevertheless, the specimens of the reference test were submitted to concentrated loads, which produce complex stress states close to loading area, difficult to predict with reduced approaches. Therefore, the complete 3D solution from Pagano (1970; 1969) was chosen in order to obtain a precise estimation of CLT bending behavior. Pagano derived such solution for plates having homogeneous layers and perfect connections between them under uni-axial (Pagano 1970) or bi-axial (Pagano 1969) bending configurations. The bi-axial bending solution is used

2. BENDING BEHAVIOR OF STANDARD CLT: MODELING AND PARAMETER STUDIES

for the comparison with the reference test, while the uni-axial solution is applied to the parameter studies on CLT properties.

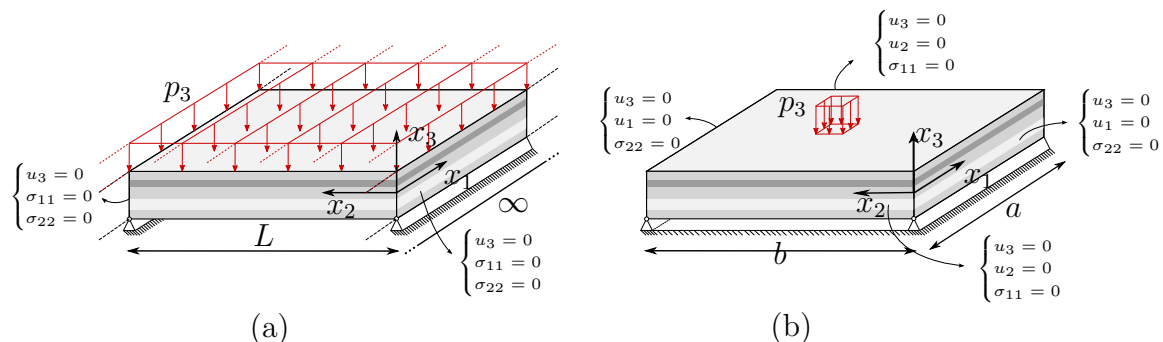


Figure 2.5: Pagano's uni-axial (a) and bi-axial (b) bending configurations with corresponding applied loads and boundary conditions. u_1 , u_2 and u_3 stand for the displacements in directions x_1 , x_2 and x_3 respectively

2.3.4.1 Uni-axial bending

The most common bending configuration for structural panels is represented by a plate simply supported on two sides. Pagano's 3D solution for layered plates in uni-axial bending represents such a bending configuration. A plate under uni-axial, or *cylindrical*, bending has only two sides supported along the same direction, while the other direction is assumed as infinite and there are no boundaries (Figure 2.5a). The displacement field is assumed to be a single Fourier-like series, like the out-of-plane load p_3 , acting on the plate's upper or lower surface. In Pagano's uni-axial bending, the only imposed condition on the bounded edges is zero vertical displacement u_3 , leaving free the in-plane displacements.

2.3.4.2 Bi-axial bending

CLT panels tested in the framework of the reference experiment were supported on their four sides, which corresponds to the bi-axial bending solution from Pagano. This solution is valid for rectangular orthotropic plates, whose axes are aligned with the axes of the supports. In this case, all the plate's sides are simply supported (Figure 2.5b) and the displacements as well as the surface load p_3 are expressed as double Fourier-like series. The boundary conditions, which make possible Pagano's solution in bi-axial bending, consist in restraining vertical and *tangential* displacements at the plate's bounded sides. As Figure 2.5b shows, the tangential displacements for edges along direction 2 and 1 are respectively u_2 and u_1 . However, since the tangential displacements of the reference panel's edges were not restrained, the experiment configuration has more degrees of freedom than the bending solution. Further analyses not reported here showed that the reference slenderness ratio of 20 gives a difference of about 10% between the estimated deflection preventing or not edges' tangential

2.4 Comparison with the reference test

displacements. Hence, when choosing Pagano’s bi-axial solution to reproduce the reference test, it is expected to find a global stiffness about 10% higher than the reference one.

2.4 Comparison with the reference test

In this Section, the predicted bending behavior is compared with the reference behavior in terms of the panel’s global stiffness and failure stages.

2.4.1 Global stiffness

Table 2.4 shows the plate’s global stiffness comparison between the reference test and each model for an equivalent CLT layer.

Continuous panel (0 - 50 kN)	Global Stiffness [$\frac{kN}{mm}$]	measuring error
Experimental reference	4.60	$\pm 5.0\%$
Predicted	5.03 (+9.3%)	-
Discontinuous panel (80 - 120 kN)	Global Stiffness [$\frac{kN}{mm}$]	measuring error
Experimental reference	4.14	$\pm 5.0\%$
Predicted	4.60 (+11.1%)	-

Table 2.4: Plate’s global stiffness comparison

When the lateral boards are glued to each other, the panel is continuous and its global stiffness is the slope of the load-displacement curve in the proportional limit (from 0 to 50 kN). Then, when the edge-gluing detachment occurs (≈ 80 kN), the panel presents gaps between boards and its stiffness slightly decreases. For each case, the corresponding equivalent-layer model is used to predict the CLT plate’s global stiffness. Because of the experimental uncertainty, a 5.0% margin of error in measuring the reference value of the plate’s stiffness is assumed. Taking into account the discrepancy between modeled and actual boundary conditions described in 2.3.4.2, a predicted plate’s stiffness about 10% greater than the reference stiffness is expected. Indeed, as Table 2.4 shows, for both the continuous and discontinuous case, the predicted global stiffnesses are about 10% higher than the reference stiffness. A CLT plate made of continuous layers shows higher stiffness compared to the one predicted using a discontinuous model, due to the absence in the latter of any contribution of fibers along direction N (see Table 2.3). However, the hypotheses made on elastic properties of continuous and discontinuous CLT layers lead to a relatively small difference between their elastic response in terms of vertical displacements.

2.4.2 Failure stages comparison

In addition to the elastic panel’s deflection, Pagano’s solution can precisely estimate the stress distributions within the panel. In Section 2.3.2, the identification of failure load

2. BENDING BEHAVIOR OF STANDARD CLT: MODELING AND PARAMETER STUDIES

and the corresponding dominant failure mode are described. A progressive increase in the load after the first failure, leads to a proportional variation of the function $F(\sigma)$ within the panel. Therefore, considering simultaneously the spatial distributions of the failure criterion $F(\sigma)$ and the related failure mode, leads to the derivation of failure stages under linear elastic hypothesis. A preliminary analysis revealed that, when considering the plate's cross-section, the first failures take place under the concentrated load at the plate's center. Hence, an investigation on the variation of failure modes along the plate's axes of symmetry is sufficient. The reference specimen is a CLT 3-ply and its failure stages were introduced in Section 2.2. For both continuous and discontinuous cases, the distributions of failure load are plotted for the plate's cross-sections at $x_1 = a/2$ and $x_2 = b/2$ (see Figure 2.5b). This distribution highlights the load level necessary to reach the failure along the plate cross-sections. Over such a distribution, the superimposition of the dominant failure modes points out the progressive failure stages. Table 2.5 presents the chosen abbreviations for the failure modes within a layer of a CLT panel.

Failure mode	Abbreviation
Tensile Longitudinal	L-t
Compressive Longitudinal	L-c
Tensile Direction-N	N-t
Compressive Direction-N	N-c
Tensile Direction-Z	Z-t
Compressive Direction-Z	Z-c
Transverse (rolling) shear ZN	RS
Transverse shear ZL	ZL
Plane shear LN	LN

Table 2.5: Abbreviations of failure modes

2.4.2.1 Continuous layer

Figure 2.6a shows the distribution of failure load and failure modes within the panel's cross section predicted with a continuous equivalent layer. For a better presentation, the ratio between the panel's thickness and span is scaled at about 10:1. The first failure mode occurs at about 50 kN of load level. Such a failure mode is a perpendicular compressive failure close to the punching area (N-c), which is actually difficult to observe experimentally. Detailed analyses of stresses revealed how this area is affected by a tri-axial stress state. Therefore, the contribution to material failure derives from all the compression components in direction L , N and Z , with the latter as the dominant one. This is a very local phenomenon not affecting the linear response of the panel at a very short distance from the punch. Moreover, the punch, being modeled as a uniformly distributed load, cannot take into account the actual contact phenomena occurring in the experiment. The subsequent failure stage is tensile failure of the bottom layer in

2.4 Comparison with the reference test

direction N ($N-t \approx 70$ kN). Such a predicted failure could explain the corresponding edge-gluing (EG) separation found in the experimental test at similar load levels (see Section 2.2) along direction N of boards. Rolling shear failure of cross layers (RS ≈ 90 kN) and longitudinal tensile failure of bottom layer (L-t ≈ 100 kN) are the next failure modes. Both of them are estimated at load levels, which slightly deviate from the experimental evidence, especially the tensile failure.

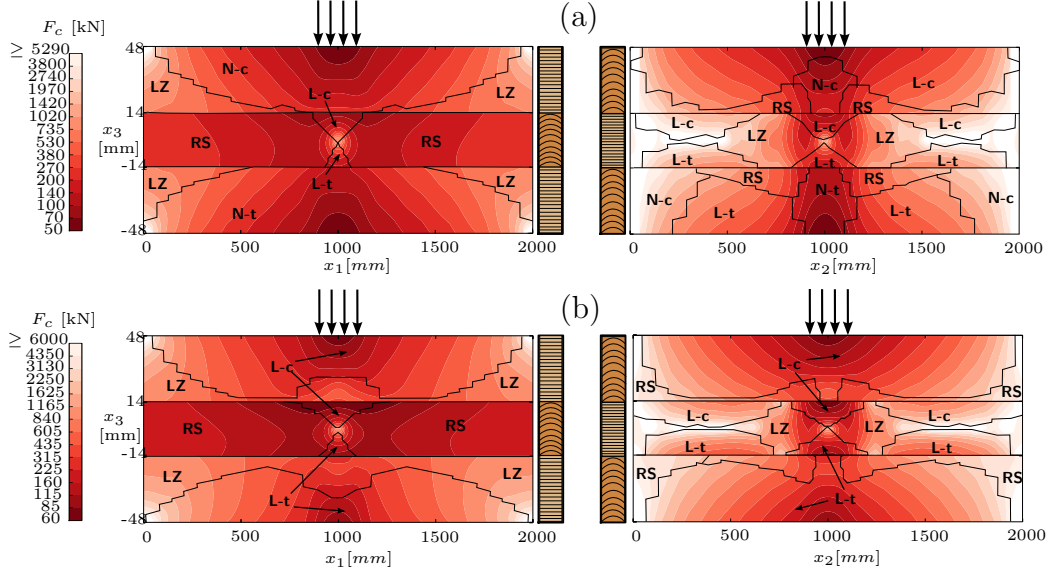


Figure 2.6: Variation of failure load and failure modes at $x_1 = a/2$ and $x_2 = b/2$ inside the panel predicted with the continuous (a) and discontinuous (b) models

2.4.2.2 Discontinuous layer

Since the first significant observed damage is the edge-gluing detachment, it is worth investigating a discontinuous equivalent layer. Figure 2.6b presents the predicted failure stages for a discontinuous equivalent layer. As introduced before, the modeling of discontinuous layers prevents wood's failure in N -direction (Figure 2.4b). Therefore, the first compressive failure close to the punching area is a contribution of only compression in direction L and Z , where the former is the dominant one ($L-c \approx 60$ kN). Again, the modeling of wood's mechanical behavior led to a compressive failure close to the punching area, which does not affect the plate's global behavior. Rolling shear failure in the cross layer is the following predicted failure, with a corresponding load level (RS ≈ 80 kN) in accordance with the reference test. Moreover, the propagation of such a failure from the plate's center to its' edges is in agreement with the experimental evidence, as Figure 2.7 shows. Finally, the predicted failure stage at 120 kN is longitudinal tensile failure in the L -direction (L-t) of the bottom layer, which is in a good agreement with the reference behavior (see Figure 2.1).

2. BENDING BEHAVIOR OF STANDARD CLT: MODELING AND PARAMETER STUDIES

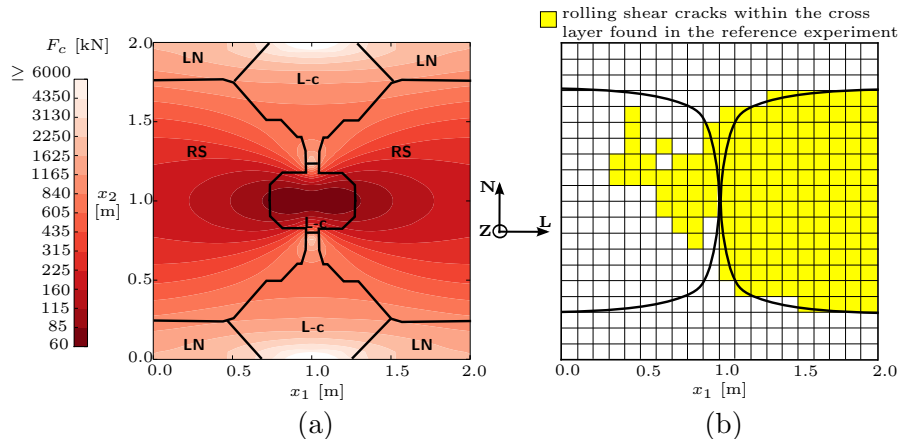


Figure 2.7: Horizontal section of the plate at $x_3 = +13mm$. Failure stages predicted with the discontinuous model (a) and the corresponding cracking pattern found in the reference experiment (b)

2.4.2.3 Discussion

Table 2.6 summarizes the predicted failure stages with continuous or discontinuous CLT layer and compares them to the experimental evidence.

Load level [kN]	Failure modes		
	Reference test	Continuous	Discontinuous
50	-	N-c	-
60	-	N-c	L-c
70	-	N-t	L-c
80	RS/EG	N-t	RS
90	RS/EG	RS	RS
100	RS/EG	L-t	RS
120	L-t	L-t	L-t

Table 2.6: Summary of predicted failure stages in comparison with the experimental evidence

As for the elastic stiffness comparison, each equivalent-layer model is in accordance within ranges of load levels, which correspond to glued or unglued lateral boards. Indeed, the continuous CLT layer gives good prediction on failure modes at low load levels, when the narrow boards are still glued. Notwithstanding the compressive indentation under the punch, the first predicted failure in this stage is tensile failure in the tangential direction within the bottom layer, which could cause the actual edge-gluing failure of neighboring layers found in the experiment. The discontinuous model fits well the experimental evidence at higher load levels, where the actual rise of rolling shear and tensile failures are predicted with a more accurate precision than in a continuous geometry. Finally, it appears that the edge-gluing of narrow boards makes the panel a little stiffer but, being the first failure mode, the already “damaged” discontinuous model gives better prediction of global load-carrying capacity of the panel. Therefore

2.5 Investigation on CLT panel properties

the discontinuous equivalent-layer model will be used for the parameter studies on CLT properties presented in the next section.

Like every modeling procedure, the predicted bending behavior with the present model depends on the chosen mechanical properties of raw materials. Surprisingly, elastic and strength parameters of clear spruce lead to an accurate prediction of the experimental bending behavior, even if the reference CLT panel was made of boards of strength class C24 having knots. When dealing with CLT in bending, elastic and strength responses mainly derive from either tensile or (rolling) shear effects (Mestek 2011; Hochreiner et al 2014; Czaderski et al 2007), as the previous Section 2.4.2 also shows. While rolling shear stiffness and strength are commonly assumed to be independent from the presence of defects (ETA 2013; Blass and Fellmoser 2004b;a; Blass and Gorlacher 2000; Grandvuinet and Muszynski 2016), tensile properties strongly depend on lumber strength class. Generally, dealing with C24 strength class, a mean elastic modulus value of 11.0 GPa (EN 2009) and a mean tensile strength of about 30 MPa (Stapel and van de Kuilen 2014) are assumed. Further simulations showed that when using such mean values of wood having knots, the predicted stiffness and failure stages deviate significantly from the experimental reference. In Section 2.4, a good agreement between the predicted and actual bending behavior is found using an elastic modulus of 12.8 GPa and a tensile strength of 63 MPa. This could be explained by a “system effect” when assembling lumber boards in a CLT configuration, which increases the panel stiffness and tensile strength, as also suggested by Joebstl et al (2006).

2.5 Investigation on CLT panel properties

Since the discontinuous equivalent-layer gives a good prediction of crosslam bending behavior, parametric studies with this model are carried out in order to better understand CLT properties and quantify their advantages and limits. The considered bending configuration is a uni-axial bending and the out-of-plane load is an evenly distributed load. In this Section only the mechanical and deterministic behavior is considered.

2.5.1 Influence of transverse shear effects

The transverse shear weakness of CLT panels is due to the presence of cross layers and their low shear strength and stiffness. Shear effects in bending elements become more significant, while the slenderness ratio decreases. Figure 2.8 shows the failure load and mid-span deflection for a 3-ply and 5-ply CLT as a function of the plate’s slenderness ratio L/h . The total plate’s thickness h is assumed to be constant at 20cm for both 3-ply and 5-ply panels, while only the plate’s span L changes.

The slope variation of the failure load trend in Figure 2.8a points out the change of failure mode as a function of the slenderness ratio. This derives from the linear and quadratic dependency of, respectively, shear and bending failure load from the

2. BENDING BEHAVIOR OF STANDARD CLT: MODELING AND PARAMETER STUDIES

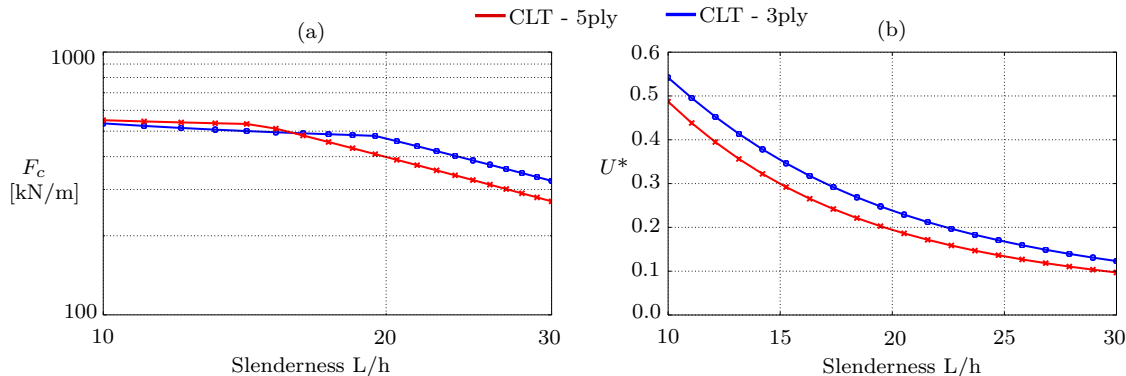


Figure 2.8: Failure load (a) and deflection (b) trends for 3-ply and 5-ply CLT in uni-axial bending when varying slenderness. $U^* = \frac{U_{3, Pag} - U_{3, Kir}}{U_{3, Pag}}$

slenderness ratio. Moreover, for a plate under a uniform uni-axial load, there is no interaction between bending and shear forces. While for low slenderness ratios the dominant failure mode is rolling shear (RS) in cross layers, when the plate is slender, the bending failure (namely L-c of upper layer) becomes the dominant failure mode. The transition slenderness from bending to shear failure turns out to be 15 for a 5-ply and 19 for a 3-ply. The 5-ply panel, having lower transition slenderness and higher shear failure load, shows less weakness to rolling shear stresses than the 3-ply CLT.

The difference between the deflection predicted using Pagano’s solution ($U_{3, Pag}$) and the deflection predicted using the Kirchhoff-Love plate theory for laminates (March 1936) ($U_{3, Kir}$) which neglects the shear deformation, can quantify the shear contribution to the total deflection. Figure 2.8b presents the variation of this difference as a function of the CLT panel’s slenderness ratio. When the plate’s span increases, the increasing slenderness yields a negligible shear deflection and an increasing bending one. However, even when the panel is slender and the failure mode is bending, the shear contribution to deflection is still about 10 %.

2.5.2 Varying the number of layers for a fixed total thickness

Of particular interest in CLT applications is the optimal number of layers in the cross section to obtain the best mechanical behavior. Therefore, this study aims to show how the CLT mechanical response changes when the number of layers increases from 3 to 23 for a fixed total thickness, which involves a progressive thinning of layers. The results are as follows expressed in terms of the panel’s maximum vertical displacement U_3 and failure load F_c . The two cases when the plate is thick or slender are presented. For a better visualization, mid-span deflection values are normalized to the Kirchhoff-Love deflection (Kirchhoff 1850) of a corresponding “solid wood” panel ($U_{3, sw, Kir}$) having only one longitudinal layer. Figure 2.9 presents the variation of failure load F_c and mid-span deflection U_3 as a function of the number of layers for slender and thick CLT plates. The panel’s dimensions are $L = 5m$, $h = 20cm$ for the panel having a slenderness ratio of 25 and $L = 2m$, $h = 20cm$ for the thicker plate.

2.5 Investigation on CLT panel properties

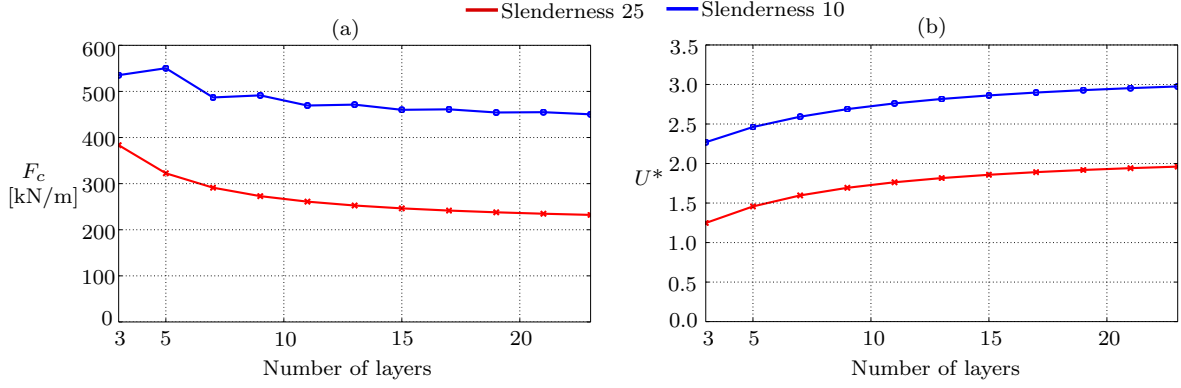


Figure 2.9: Variation of CLT failure load F_c (a) and normalized mid-span deflection U_3 (b) as a function of the increasing number of layers for thick and slender panels. $U^* = \frac{U_{3,Paq}}{U_{3,sw,Kir}}$

For a plate in uni-axial bending only the layers parallel to the main direction bear the bending stresses, while the transverse layers do not contribute to global stiffness and strength. Hence, the progressive decreasing of the total thickness of longitudinal layers leads to higher deflections and lower failure loads. Unlike the slender case, the variation of failure load when the dominant effect is shear, decreases with oscillations (see Figure 2.9a). This is because CLT panels with a central longitudinal layer (5ply, 9ply etc.) have the cross layers placed at a distance from the cross-section's center (where the shear stresses are maximum), while for the other lay-ups (3ply, 7ply etc.), the central layer is cross and shear-compliant. Therefore, the trend of shear failure load is dependent on the kind of lay-up, in addition to the number of layers within the cross section.

From a deterministic point of view, homogenizing the panel in uni-axial bending by means of progressive thinner layers has a negative impact on the mechanical response. However, taking into account wood's defects such as knots (reliability approach), thinner layers could lead to more uniform CLT mechanical properties.

2.5.3 Varying cross layer orientation

A solution to mitigate CLT shear weakness could be varying the in-plane orientation of transverse layers, in order to change their actual shear stiffness and strength from TR to RL . Hence, in this section the effect of a progressive rotation of transverse layers on CLT bending behavior is analyzed. Four different configurations with varying layer lamination have been studied. Configurations called 1a and 1b (Figure 2.10 - top) are five-layer panels and the difference between them is the opposite orientation of transverse layers. Configuration 1b is the same tested at $\theta = 45^\circ$ by Buck et al (2016) who found experimentally increased stiffness and strength of panels having such new lay-up compared to classical CLT. Configuration 2 comes from another study present in literature (Chen and Lam 2013) (with again $\theta = 45^\circ$) which, however, did not clearly highlight the effects of the new lamination. Finally, configuration 3 is a 3-ply plate

2. BENDING BEHAVIOR OF STANDARD CLT: MODELING AND PARAMETER STUDIES

whose central layer has variable orientation. At $\theta = 90^\circ$, all the configurations have the crosswise CLT lamination, while at $\theta = 0^\circ$ they behave like a Glued Laminated Timber. Figure 2.10 illustrates the variation of elastic mid-span deflection U_3 as a function of the layers' orientation θ for the four configurations having the same total thickness $h = 200\text{mm}$. Both cases of a thick and slender panel are analyzed using respectively a span of 2m and 5m.

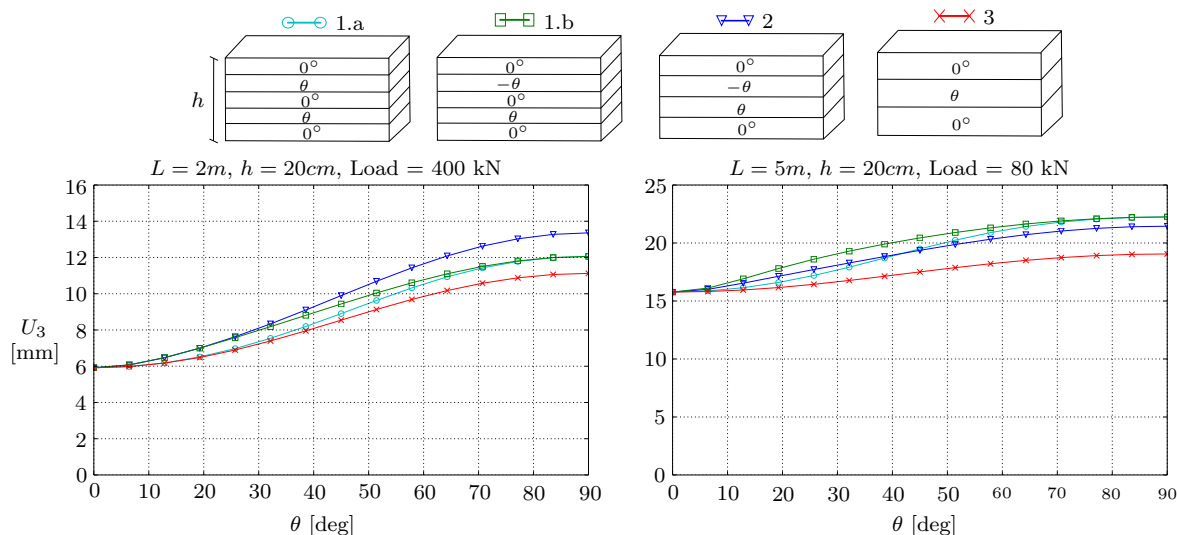


Figure 2.10: Variation of deflection U_3 as a function of layer orientation for slenderness ratios of 10 (left) and 25 (right)

While changing the panel's lamination from GLT to CLT, the deflection increases. This effect is particularly evident at a low slenderness ratio, showing that a variation of the actual shear modulus from G_{TR} to G_{RL} mitigates the shear deflection. The influence of the cross layers' direction on the panel's deflection is lower when increasing the slenderness ratio. For a thick panel, CLT 1a generally shows lower values of deflection than 1b which has opposite lamination of transverse layers. Configuration 2 leads to the highest values of deflection at low slenderness ratio, due to the considerable thickness of its central shear-compliant layers. When the bending effects become dominant, the configuration 2 shows lower values of deflection than the panels with five layers. This derives from the greater thickness of its upper and lower longitudinal layers (the middle one does not really contribute) than in CLT 5-ply. For the same reason the plate 3 with three layers presents generally the lowest values of deflection at every slenderness ratio when varying its transverse layer's orientation.

Figure 2.11 presents the variation of failure load F_c and failure mode as a function of the orientation of transverse layers.

While for a dominant shear regime, varying transverse layer orientation leads to an increasing failure load (Figure 2.11-left), when dealing with a slender CLT, the effect of rotating cross layers becomes less significant (Figure 2.11-right). Interestingly, and contrary to the deflection case, the difference between failure load trends for solutions 1a and 1b is significant, especially at a low slenderness ratio. This means that imposing an

2.6 Conclusion and perspectives

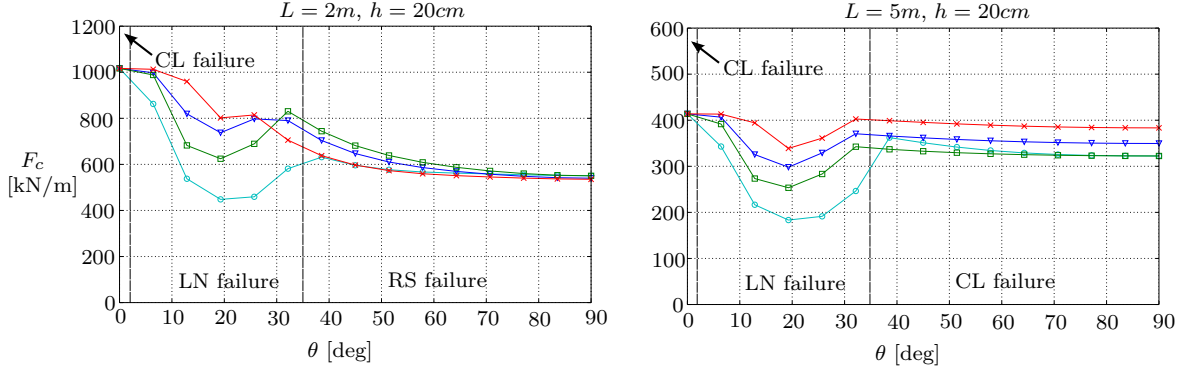


Figure 2.11: Variation of failure load F_c as a function of layer orientation for slenderness ratios of 10 (left) and 25 (right)

opposite lamination of transverse layers leads to higher shear strengths while changing their orientation. At values of θ between about 10° and 40° , all the CLT configurations of both slenderness present sharp drops in the failure load. Further analysis proved that in this range of θ , the transverse layers are submitted to torsional effects which produce high in-plane shear stresses, leading to an unexpected plane shear failure (LN) of layers. When testing crosslam panels in bending having slenderness 18 with configuration 1b, Buck et al (2016) found a variation of failure modes from bending or rolling shear at $\theta = 0^\circ$ to bending or longitudinal shear $\theta = 45^\circ$, that is very close to the failure mode transition angle showed in Figure 2.11. The associated failure load was found to be about 30% higher than the failure mode of CLT with classical orthogonal lamination.

Not surprisingly, considering the uni-axial bending configuration, the Glulam-like plate lay-up having all layers parallel to the bending direction, returns the best bending behavior. The favorable effect of rotating the transverse layers on the CLT mid-span deflection is more evident at low slenderness ratios, which are not very common in practical applications. Only thick CLT plates show increasing failure loads when rotating their transverse layers up to about 40° . After that lamination angle, plane shear stresses within cross layers increase drastically and lead to a failure load drop. Unless dealing with a thick panel and a dimensioning criterion driven by deflection, the low gains when varying transverse layer orientation make these configurations awkward to exploit. The predicted behavior of these innovative configurations of crosslam are qualitatively in agreement with the experimental results of Buck et al (2016).

2.6 Conclusion and perspectives

In the present Chapter, the bending behavior of CLT panels has been modeled by means of an equivalent layer model combined with a 3D elastic solution and a failure criterion. The heterogeneities at layer scale are taken into account by means of a homogeneous and equivalent layer whose mechanical properties change whether or not the narrow boards are glued to each other. Concerning the heterogeneities at the structure's scale, the exact 3D solution for layered plates in bending provides an

2. BENDING BEHAVIOR OF STANDARD CLT: MODELING AND PARAMETER STUDIES

accurate description of stresses, especially under concentrated loads. Moreover, such a solution leads to the analysis of non-orthotropic lay-ups and requires reasonable computational times. A failure criterion for wood combined with the elastic stress field has been used to identify progressive failure stages highlighted by the experimental evidence. The plate stiffnesses and failure modes predicted with the continuous and discontinuous equivalent layers are in agreement with the corresponding actual glued or unglued stages. Edge-glued layers make the panel a little stiffer but introduce also an additional failure mode at low load levels. Therefore it appears that gluing narrow boards has almost no positive effects on the mechanical response of CLT panels in bending. Moreover, clear wood mechanical properties lead to an accurate prediction, even if the tested reference panel was affected by the presence of knots. This shows that assembling lumber boards in a CLT configuration increases raw wood stiffness and strength, especially tensile one. The discontinuous equivalent-layer gives a good description of both elastic and failure response and therefore is used to study the influence of some panels' parameters on the CLT bending response. The trend of failure load and shear deflection as a function of the panel's slenderness ratio clearly quantify the influence of shear effects in CLT in bending. However, this shear weakness does not only depend on the panel's slenderness, but also on the CLT lay-up. Concerning the variation in the number of layers for a fixed total thickness, the more the number of layers increases, the more the mid-span deflection increases and the failure load decreases. This means that "homogenizing" CLT panels in uni-axial bending yields a worse mechanical behavior from a deterministic point of view. Finally, CLT shear weakness can be mitigated by varying the lamination of cross layers, especially in terms of deflection and dealing with thick plates. The predicted variation of stiffness, failure load and failure mode are very similar to the experimental behavior found by Buck et al (2016). However, the small gains in terms of uni-axial bending performance make these further CLT configurations not really interesting.

Note that the discontinuous equivalent layer suggested in this study involves simplified hypotheses on the layer's in-plane shear stiffness (G_{LN}) and Young's modulus (E_N). The actual reduction of in-plane stiffnesses of a non edge-glued CLT panel can be significant, as pointed out by theoretical (Moosbrugger et al 2006; Silly 2010) and experimental (Brandner et al 2015) studies, but it is difficult to predict with simplified approaches. Therefore the hypotheses on the discontinuous layer's in-plane properties will be further investigated with a model currently in development (Lebé and Sab 2012; 2013). This model can also predict the influence of stronger heterogeneities like periodic voids within the panel and filled by insulating material, in order to obtain lighter and more acoustically efficient floors for mid-rise and high-rise timber buildings.

Chapter 3

Experimental investigation

Note: Parts of this Chapter have been published in the proceeding of the conference *World Conference on Timber Engineering 2016, Vienna (AUT)* with the title *Bending behavior of regularly spaced CLT panels*

Abstract. This Chapter presents the experimental behavior of regularly spaced CLT panels. 4-points bending tests on standard and innovative full-size floors as well as small-scale tests on raw timber were performed and discussions on obtained results are presented. Moreover, an existing experimental test on in-plane behavior of crosslam panels having short spacing is presented as well.

Résumé. Ce Chapitre présente la campagne expérimentale réalisée dans le cadre de ce travail. Cette campagne comprend des essais de flexion 4-points sur planchers standard et innovants ainsi que les essais de caractérisation du bois composant les panneaux. Les résultats obtenus sont ensuite commentés. Enfin, la dernière partie de ce Chapitre présente une étude expérimentale de la littérature portant sur le comportement dans le plan des CLT avec petits espacements.

3.1 Introduction

Among the main outcomes of Chapter 2, the low influence of small gaps between lateral boards on the global bending behavior and the moderate influence on the failure load and failure modes can be identified. However, the modeling developed up to now is not capable to quantify the actual influence of lateral spacing on the panel's behavior. Additionally, the simplified equivalent behavior of a laterally unglued CLT layer cannot reproduce the behavior of innovative panels having large spacings. In particular, introducing large spaces may modify the CLT "system effect" of the massive orthogonal structure described in Section 2.4.2.3 which increase raw material's stiffness and strength. Moreover, the influence of large spaces on the (rolling) shear effects is unknown both regarding shear deflection and shear failure. Therefore, experiments of CLT panels having short and large spaces are needed in order to set a reference ex-

3. EXPERIMENTAL INVESTIGATION

perimental behavior of spaced CLT. The results will be subsequently compared with simplified and refined modeling in Chapter 4. Furthermore, the material characterization of the raw timber of tested panels ensures more reliable input values of wood properties for the modeling step than choosing values of the literature. Hence, small-scale test of tension, compression and shear on small specimens of timber have been performed.

Since the out-of-plane behavior of spaced CLT is the main topic of this work and due to equipment limitations, it was not possible to perform in-plane tests of spaced crosslam. However, the influence of short spaces on the in-plane shear stiffness of standard CLT has been quantified by a recent experimental investigation of Brandner et al (2015). The results of this experimental campaign are considered the experimental reference of standard spaced CLT diaphragms.

In this Chapter, 4-points bending tests on spaced CLT floors are first presented. Both standard panels having small gaps between lamellas and innovative timber products with large voids have been tested. Then, the mechanical properties of the tested panels' raw wood estimated by means of small-scale tests of tension, compression and shear are showed. Finally, the results of recently performed in-plane shear tests by Brandner et al (2015) are presented as well.

3.2 4-points bending tests on full scale floors

3.2.1 Materials and methods

4-points bending on shortly and largely spaced crosslam floors were performed. Figure 3.1 shows a cross section of a regularly spaced CLT panel. The standard configura-

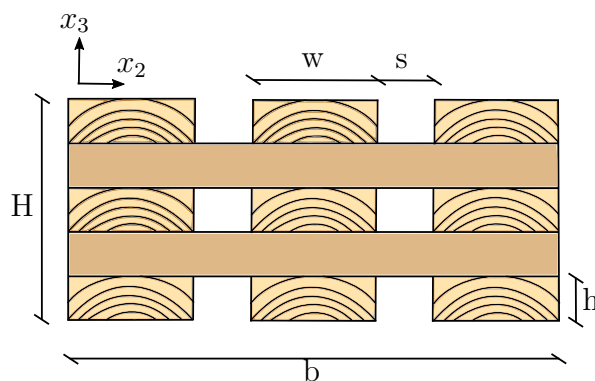


Figure 3.1: Scheme of a cross section of a regularly spaced CLT

tion had gaps of $s = 5$ mm in average between narrow boards, while two configurations of innovative panels were tested: having $s = 150$ mm and $s = 300$ mm spacing between boards. Such spacings of 150 and 300 mm correspond respectively to volume fractions λ of 0.4 and 0.25, where $\lambda = w/(w+s)$. In total, six panels of standard and innovative CLT were tested, with two specimens for each spacing of 5, 150 and 300

3.2 4-points bending tests on full scale floors

mm. Table 3.1 presents the geometrical properties of the tested specimens. Before testing, the moisture content of each panel was verified to be in the acceptable range of 8-14% with handheld moisture meter. The voids of innovative panels were filled by insulating material (glass wool) having no mechanical properties.

	s=5 mm	s=150 mm	s=300 mm
L [m]	4.65	5.9	5.9
H [mm]	100	210	210
layers	5	7	7
h [mm]	20	30	30
w [mm]	140	100	100
λ	0.95	0.4	0.25

Table 3.1: Geometrical properties of the tested panels

The measuring system was based on vertical LVDTs (displacement transducers) in order to measure the panel's curvature and horizontal LVDTs to determine the absolute rotation at supports. The vertical displacement at supports was measured as well, in order to determine the actual mid-span deflection without the contribution of settlement at supports. Figure 3.2 shows a schematic representation of the experimental set-up.

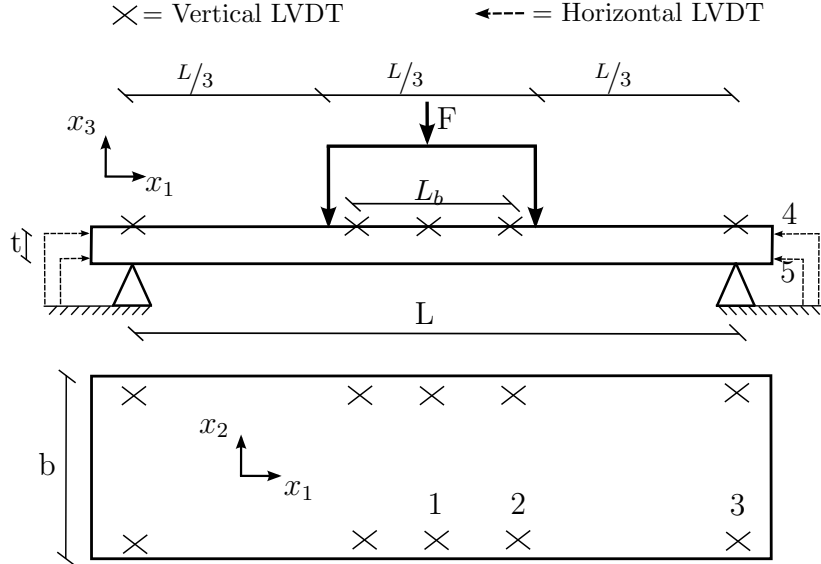


Figure 3.2: 4-points bending test set-up and position of LVDTs

A first cycle of load/unload until about the 20% of the expected failure load was performed, with a following load until the panel's failure. The panel's bending stiffness EI_{11} can be derived either from the measured curvature or from the rotation at supports following the following expressions:

3. EXPERIMENTAL INVESTIGATION

$$EI_{11} = \frac{L \cdot L_b^2 \cdot F}{48 \cdot U_b} \quad \text{or} \quad EI_{11} = \frac{L^2 \cdot F}{18 \cdot \phi} \quad (3.1)$$

where, with respect to fig. 3.2, $U_b = U_g - |u_2|$ is the local deflection in the pure bending region, u_x is a measured displacement by the x LVDT, $U_g = |u_1| - |u_3|$ is the mid-span deflection and $\phi = \frac{u_5 - u_4}{t}$ is the absolute rotation at supports. t is the distance between the measuring points of horizontal LVDTs for the absolute rotation at supports. Then, knowing the bending stiffness and the global mid-span deflection, the shear stiffness GA_{13} and the ratio between shear deflection and bending deflection $\alpha = \frac{u_{shear}}{u_{bending}}$ can be also obtained with:

$$GA_{13} = \frac{216 \cdot L \cdot EI_{11}}{1296 \cdot EI_{11} \cdot U_g/F - 23 \cdot L^2} \quad \text{and} \quad \alpha = \frac{216 \cdot EI_{11}}{23 \cdot GA_{13} \cdot L^2} \quad (3.2)$$

3.2.2 Results

Figure 3.3 shows the obtained load/displacement curves, where the displacement is the mid-span deflection, while Table 3.2 summarizes the main results of the experimental investigation on spaced floors. The presented results are the mean between the two specimens for each configuration. The relative difference of measured stiffnesses and failure load between the two specimens of each configuration was very small, in the range of 5-10%. Dealing with failure modes, the abbreviation TL stands for longitudinal tensile failure of bottom layer while RS means rolling shear failure in transverse boards.

	s=5 mm	s=150 mm	s=300 mm
F_{max} [kN]	80	68	34
Failure mode	TL	TL	RS
EI_{11} [kN · m ²]	895	3500	1980
GA_{13} [kN]	12530	5750	1850
$\alpha = U_{shear}/U_{bending}$	0.03	0.16	0.28

Table 3.2: Main results of 4-points bending tests. TL= tensile failure in longitudinal direction of bottom layer; RS= rolling shear failure in middle layer

Dealing with failure modes, the standard crosslam failed due to bending stresses with a brittle tensile failure of bottom layer (Figure 3.4a). However, before tensile failure, longitudinal compressive cracks appeared on the top layer (Figure 3.4b), even if such cracks are hardly identifiable on the load-displacement curve of Figure 3.3. On the contrary, the 150 mm spaced floor failed in tension of bottom boards without ductile behavior of top layers (Figure 3.5a). This is mainly due to the presence of larger knots in this innovative panel (Figure 3.5) with respect to standard configuration which decrease significantly the tensile strength. The most spaced configuration with 300 mm spacing failed brittly with shear in cross layers and consequent delamination at supports (Figure 3.6a) and rotation of transverse boards (Figure 3.6b).

3.2 4-points bending tests on full scale floors

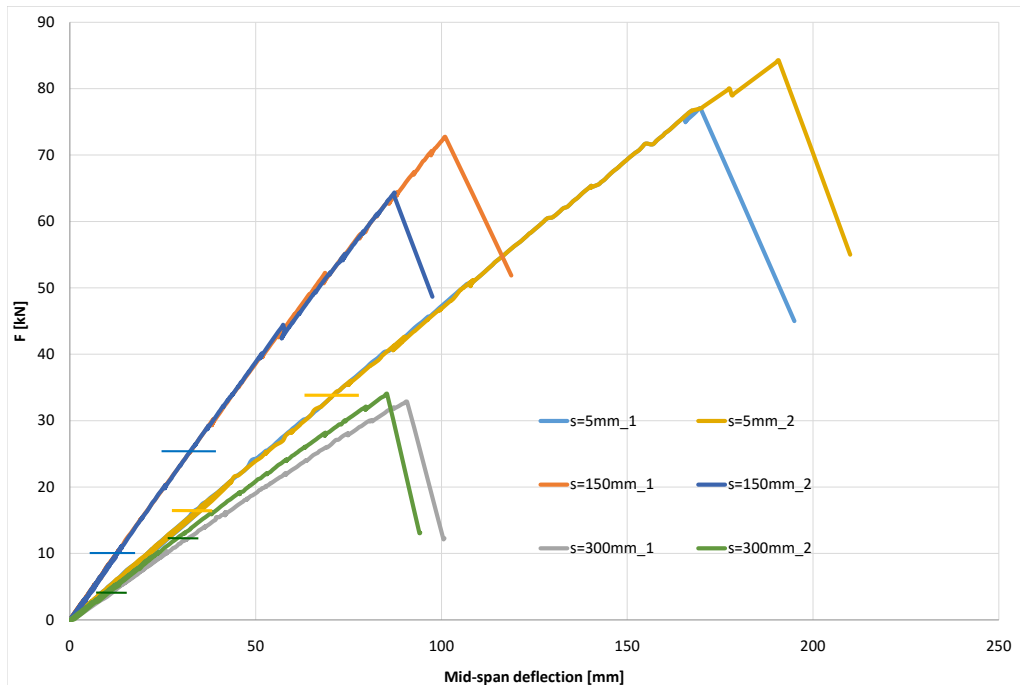


Figure 3.3: Load/displacement curves of the tested floors out-of-plane. The solid horizontal lines show the considered elastic range for stiffness estimation



Figure 3.4: Tensile failure of standard CLT panel (a) and longitudinal compressive cracks (b)

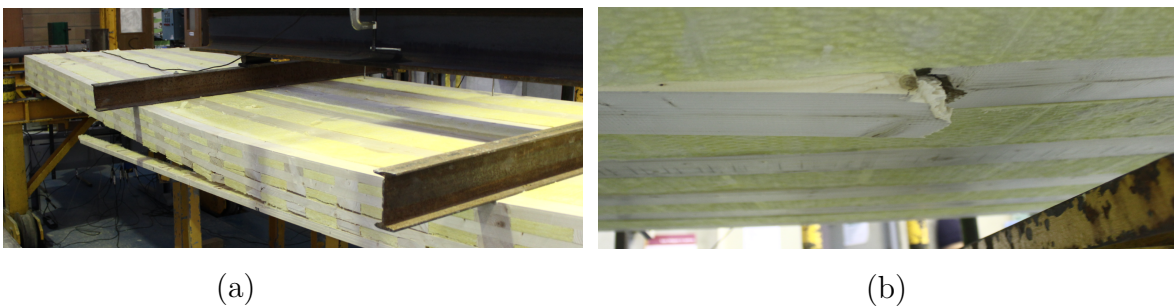


Figure 3.5: Tensile failure of s=150 mm panel (a) and detail of failure due to a local knot (b)

3. EXPERIMENTAL INVESTIGATION



Figure 3.6: Shear failure of $s=300$ mm panel (a) and detail of failure of transverse boards (b)

3.2.3 Discussion

Due to its high slenderness, the standard crosslam failed as expected due to bending stresses, with ductile compressive cracks on upper layer before the final tensile brittle failure of bottom layer. Increasing the spacing between lateral boards increases the influence of shear effects on elastic and failure behavior. Indeed the contribution to shear deflection increased from 15% to about 30% for floors having respectively 150 mm and 300 mm spacing. At volume fraction $\lambda = 0.4$ the failure derives from bending stresses due to presence of isolated knots in bottom boards. This shows the lost of CLT “system effect” (see Section 2.4.2.3) by the presence of large spaces. A more detailed analysis involving stress prediction at failure point of the tested specimens will be presented in Chapter 4. When decreasing the wood volume fraction down to $\lambda = 0.25$, there are few transverse lamellas bearing shear forces, leading to rolling shear failure of the central transverse lamellas. The rotation of lamellas within this kind of failure may derive from an interaction between rolling shear stress and stresses perpendicular to grain, as will be discussed more in detail in Chapter 4. As Figure 3.3 shows, both bending and shear failures of the tested floors were brittle failure modes, preceded by an almost perfectly elastic behavior. Therefore it is worth modeling the failure of the tested panels as the reach of a defined strength by elastic stresses, as presented in the following Chapter.

3.3 Small-scale tests on raw timber

In order to obtain material properties for the modeling step, the timber lamellas of panels has been tested with small-scale tests of tension, compression and shear.

3.3.1 Materials and methods

The standard and innovative panels were supplied by two different producers and the raw timber were graded following two different grading systems. The standard CLT was made by Norway spruce strength graded as S10 following the German standard (DIN 2012), while innovative panels were made up of C24 Norway spruce according

3.3 Small-scale tests on raw timber

to European strength classes (EN 2009). Hence, the two timber populations were separated.

Instead of respecting wood's orthotropic coordinates L , T and R , the simplified board's reference frame L , N and Z introduced in Chapter 2 is considered when testing the raw wood. The small-scale tests were tensile and compressive tests in L direction, compression tests along N and Z directions (Figure 3.8) and symmetric double-lap shear tests (Figure 3.7) in ZN and LZ planes. Preliminary FE simulations were performed to check the suitability of specimens' geometry. The width to thickness ratio of shear specimens was set equal to the ratio of the boards of the tested innovative floors which showed rolling shear failures. The Young's modulus E_L is the mean between tensile and compressive moduli. Due to material and equipments limitations, it was not possible to measure tensile properties perpendicular to grain and shear in LN plane. Therefore the Young's modulus in N and Z directions was derived from only compressive tests and the LN shear modulus is supposed to equal the LZ , according to the hypotheses made in Chapter 2.

According to full-scale panels failure modes found during testing, at least the longitudinal tensile strength and the rolling shear strength of the raw wood should be estimated. However, the tensile specimens were fabricated ensuring a defect-free central zone in tension, and consequently it was expected to find very high tensile- L strength values of "clear" wood. Dealing with shear tests, only the rolling shear tests in ZN plane were destructive in order to find the rolling shear strength.

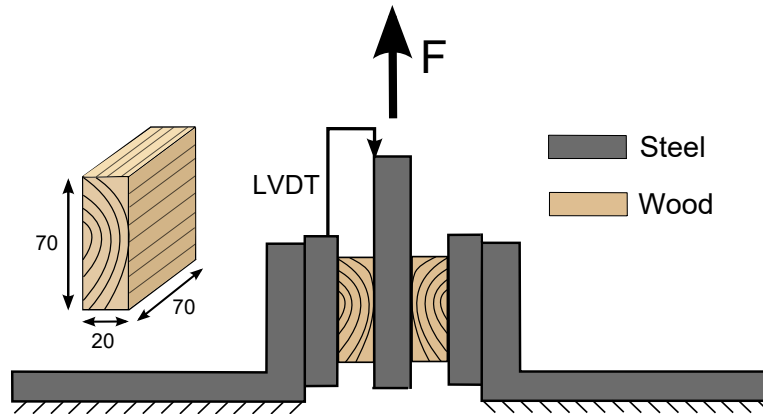


Figure 3.7: Symmetric double-lap shear test for raw timber of panels. Dimensions in mm

All specimens were stored in a conditioning room with 20° and 50% RH for one month. Dealing with axial tests, the elastic strains were measured by means of uni-axial strain gages, while Poisson's ratios were determined thanks to bi-axial strain gages in compressive tests. During shear tests, the vertical uplift of central steel plate was measured by a LVDT (Figure 3.7), leading to a single mean value of shear modulus between the two symmetric specimens.

3. EXPERIMENTAL INVESTIGATION

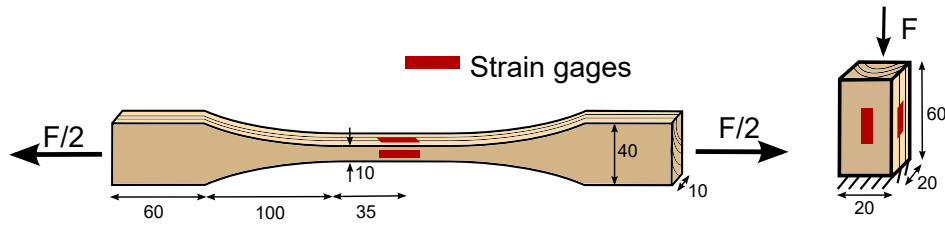


Figure 3.8: Specimens for axial tensile and compressive tests on raw timber of panels. Dimensions in mm

3.3.2 Results

Typical obtained stress/strain curves within the elastic range for compressive axial test are plotted in Figure 3.9 and Figure 3.10, while Figure 3.11 shows typical stress/strain curve for the shear test. The solid horizontal lines show the considered elastic range for stiffness estimation.

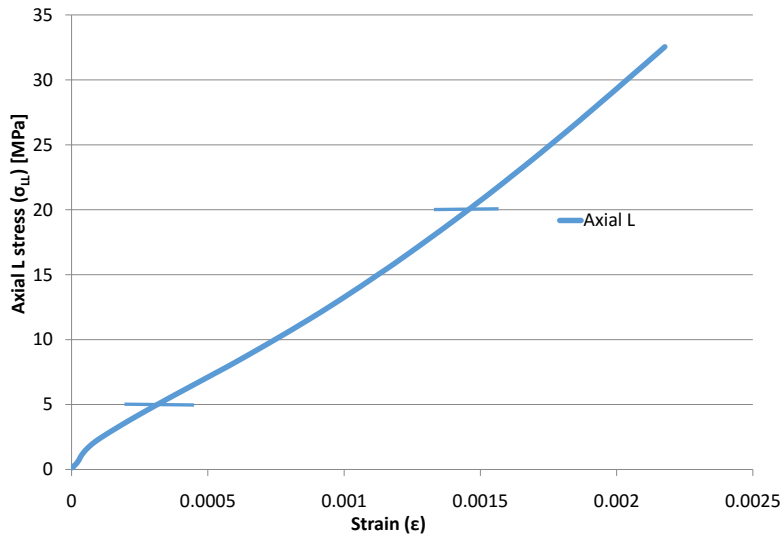


Figure 3.9: Typical stress/strain curve of compressive axial tests on wood specimens along L direction

Table 3.3 shows the derived values of derived stiffnesses for the raw wood of the tested standard and innovative floors, fitting the linear trend of stress/strain curves. The E_L Young's modulus is the mean between tensile and compressive tests.

As expected, the measured mean tensile- L strength of specimens without knots was found to be very high, in the range of 80 MPa. Since such value do not represent the actual timber strength, mean values of tensile- L strength from the literature will be considered later on. Only the shear tests in ZN -plane (rolling shear) were conducted until failure of specimens, that showed the typical cracking patterns following growth

3.3 Small-scale tests on raw timber

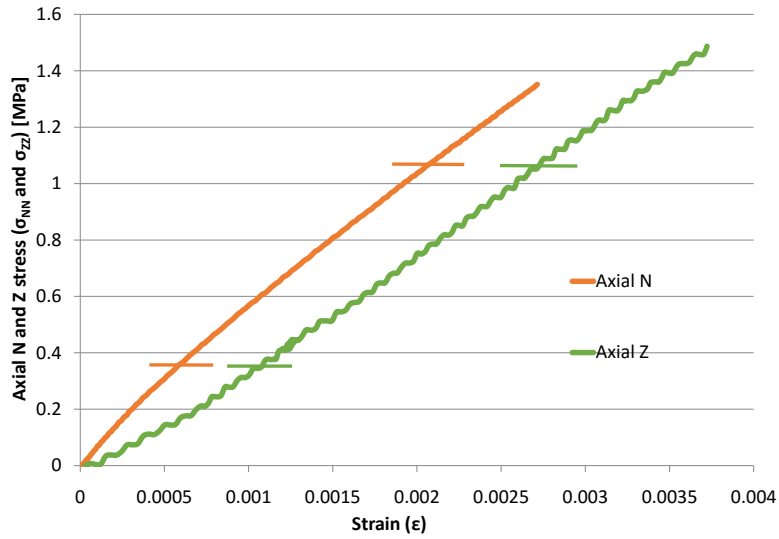


Figure 3.10: Typical stress/strain curves of compressive axial tests on wood specimens along N and Z directions

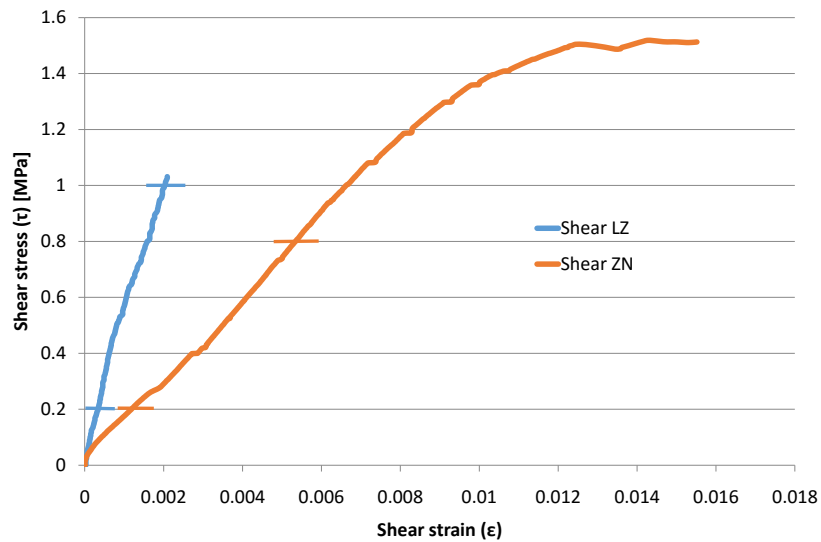


Figure 3.11: Typical stress/strain curves of shear tests on wood specimens in ZN and LZ planes. Note that the LZ test was stopped before the failure of the specimen

3. EXPERIMENTAL INVESTIGATION

	E_L	E_N	E_Z	G_{ZN}	G_{LZ}	ν_{ZN}	ν_{LZ}	ν_{LN}
Innovative panels								
n	21	6	5	10	6	5	8	8
Mean	12500	530	400	110	580	0.71	0.35	0.51
COV [%]	16	25	7	27	14	6	16	12
Standard panels								
n	17	6	5	8	-	5	8	8
Mean	9900	620	440	75	-	0.69	0.38	0.49
COV [%]	11	28	6	25	-	10	14	6

Table 3.3: Obtained elastic properties of the raw wood. Stiffness in MPa

rings (Figure 3.12-left) and a mean rolling shear strength of 1.3 MPa for S10 lamellas and 1.6 MPa for C24 lamellas. Moreover, exactly as in case of 4-points bending tests, cracking pattern due to tensile stresses perpendicular to grains was visible (Figure 3.12-right).

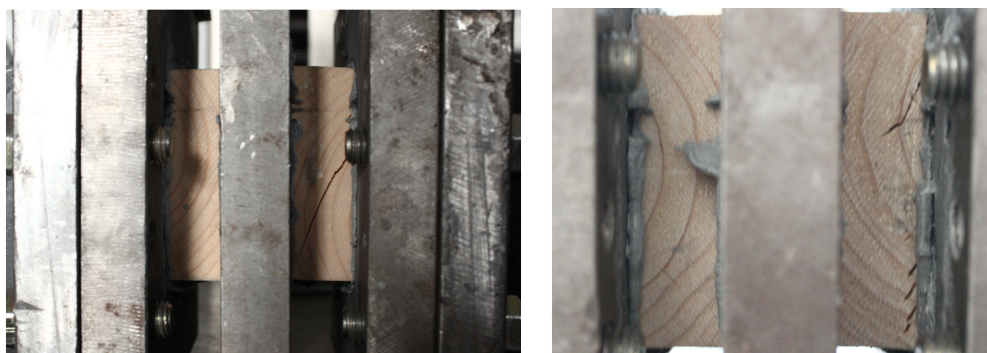


Figure 3.12: Typical rolling shear cracking pattern in softwoods (left) and presence of tensile perpendicular to grain cracks (right) close to free edges

3.3.3 Discussion

The obtained values of C24 spruce stiffnesses are in agreement with several studies of literature (Keunecke et al 2008; WoodHandbook 2010; Ehrhart et al 2015) on spruce axial and shear mechanical behavior. The mean value of rolling shear strength is very similar to values obtained in the framework of the comprehensive testing of Ehrhart et al (2015). Additionally, Ehrhart et al (2015) observed a tensile perpendicular to grain cracking pattern that appear in several specimens exactly as found during the present experiments. Such stress concentrations are very localized in a small region close to free edges, and therefore their influence on the rolling shear stiffness can be considered to be low. On the contrary, a non-negligible influence of tensile perpendicular to grain stresses on the rolling shear failure of lamellas may occur. Such stress concentrations decrease the rolling shear strength the more the aspect ratio w/h increases (Ehrhart et al

3.4 CLT in-plane shear tests of literature

2015). Hence, the tested small-scale specimens in shear having the same ratio w/h of lamellas within the tested panels should return a realistic value. This because also the lamellas of the full-scale tests show free edges and consequently stress concentrations when submitted to shear force.

The derived elastic properties are the input to model timber in the next Chapter in order to reproduce the experimental behavior of tested floors. Moreover, the measured rolling shear strength will be compared to predicted shear stress under 4-points failure loads of tested specimens.

3.4 CLT in-plane shear tests of literature

The in-plane behavior of CLT has been object of many recent experimental campaigns. In particular, Brandner et al (2015) investigated on a new in-plane shear test configuration based on compression tests on 45° rotated CLT panels in order to obtain a stress state close to pure in-plane shear (Figure 3.13).

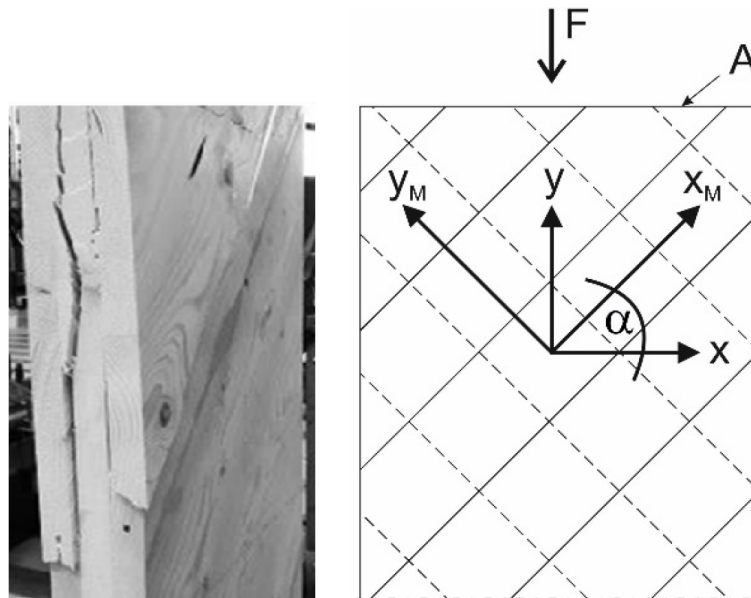


Figure 3.13: In-plane shear test set-up of Brandner et al (2015)

During their investigation on the new test configuration, Brandner et al (2015) studied the influence of several panel's parameters on in-plane behavior such as the lay-up, the board width and the gap execution. The latter turned out to be the parameter that mostly decrease crosslam in-plane shear behavior. Indeed, the reduction of the in-plane shear stiffness when passing from glued boards to unglued boards was about 30% and reduced up to 50% for a 5 mm gap between boards. Table 3.4 shows the properties of the so-called "series A" tested by Brandner et al (2015) and the obtained in-plane shear stiffnesses.

The results of such experimental campaign will be used as reference in-plane shear

3. EXPERIMENTAL INVESTIGATION

	A1	A2	A3
h [mm]	30	30	30
w [mm]	160	160	160
layers	3	3	3
s [mm]	glued	0	5
In-plane shear stiffness [MPa]	650	475	310

Table 3.4: Properties of the tested specimen and measured in-plane shear stiffness by Brandner et al (2015)

behavior of standard panels having short spacing. Unfortunately, there are no in-plane shear tests on crosslam panels having larger spacings between boards in the literature.

3.5 Conclusion

In this Chapter, the experimental behavior of spaced CLT panels was investigated. The 4-point bending tests on standard and innovative floors highlighted the increasing shear effects on elastic and failure behavior together with the increasing voids within the panel. Results of bending tests on standard and innovative floors will be the reference out-of-plane behavior of spaced CLT for the modeling presented in Chapter 5 and 6. The material properties for the modeling will be the stiffness derived with the small-scale tests on raw timber of the tested panels. Moreover, the derived rolling shear strength of lumber boards will serve as a comparison value for predicted shear stress under 4-points failure loads of tested specimens. The in-plane shear tests on standard panels by Brandner et al (2015) showed sharp drop of in-plane shear stiffness when small gaps between boards of CLT appear. Results from such in-plane shear tests will be considered as reference in-plane behavior of shortly spaced CLT panels.

Chapter 4

Homogenization of regularly spaced CLT panels

Note: Part of this Chapter has been submitted for publication with the title *Thick-plate modeling of regularly spaced CLT panels*

Abstract. This Chapter deals with the modeling of regularly spaced CLT panels in order to predict their mechanical response. The Bending-Gradient theory (Lebée and Sab 2011a) for thick laminates has been applied to the geometry of spaced crosslam by means a periodic homogenization scheme (Lebée and Sab 2012). Existing closed-form methods have been compared to the homogenization results and experimental data. Only the homogenization approach can well predict the in-plane and transverse shear behavior of spaced CLT. Moreover, the predicted bending and rolling shear stresses at failure point of the tested panels are in agreement with strength values of the literature.

Résumé. Ce Chapitre concerne la modélisation des panneaux CLT espacés pour pouvoir prédire leur comportement mécanique. La théorie du Bending-Gradient (Lebée and Sab 2011a) pour les stratifiés épais est appliquée à la géométrie des CLT espacés grâce à un schéma d'homogénéisation périodique (Lebée and Sab 2012). Des méthodes analytiques existantes ont été comparées avec les résultats de l'homogénéisation et avec des données expérimentales. Seule la méthode d'homogénéisation permet de prédire correctement le comportement de cisaillement plan et de cisaillement transverse des panneaux CLT espacés. De plus, les valeurs des contraintes de flexion et de cisaillement roulant à la rupture des panneaux calculées à l'aide de notre modèle sont en accord avec les valeurs de résistance données dans la littérature.

4.1 Introduction

The experimental investigation of Chapter 3 highlighted the reduction of mechanical performance of spaced CLT while increasing the spaces within the panel. In order to predict the reduced mechanical behavior of spaced CLT and to point out which

4. HOMOGENIZATION OF REGULARLY SPACED CLT PANELS

panel's properties mostly influence such reduction, a robust modeling tool is needed. As introduced in Chapter 1, a first simplified approach for predicting the out-of-plane behavior may be using a method for massive crosslam combined with reduced properties of wood by the volume fraction within the floor. This method is common in engineering approaches and has been already applied by Blass and Gorglacher (2000) to spaced timber floors. The shear analogy method (Kreuzinger 1999) for massive crosslam is combined in this thesis with volume fraction in order to predict spaced CLT panels bending and transverse shear stiffnesses. Dealing with the in-plane shear stiffness of spaced CLT diaphragms, the closed-form solution derived by Moosbrugger et al (2006) presented in Chapter 1 is the existing simplified method and will be compared to the available experimental results. However, these simplified approaches for estimating the mechanical behavior of spaced CLT have to be compared with a more refined modeling in order to check their suitability.

Due to the increasing influence of shear effects when enlarging the spaces between lamellas observed during the experimental investigation, a method which can take into account spaced crosslam shear compliance is required. The 3D analytical solution for laminates (Pagano 1969) applied in Chapter 2 demonstrated to well catch the standard CLT mechanics, but cannot be extended to the discontinuous geometry of largely spaced panels. There are very few models in literature that can predict the mechanical behavior of spaced panels with voids. For instance, Takabatake et al (1996) derived a closed-form approach for predicting the bending and transverse shear behavior of cellular plates based on a Reissner-Mindlin kinematics combined with Dirac functions in order to take into account the presence of voids. However this methods requires a precise geometry of the panel which cannot be, for instance, a laminated member. Recently, a thick plate theory has been developed (Lebée and Sab 2011a) in order to obtain a good estimation of transverse shear effects in thick layered plates. This model, called the Bending-Gradient plate theory, is an extension of the Reissner-Mindlin theory to layered plates, for which sometimes it is necessary to consider the whole gradient of the bending moment as shear variable instead of the divergence originally considered by Reissner. Considering the gradient of the bending moment yields additional shear variables that is necessary to consider in some situations in order to predict the shear force stiffness of strongly anisotropic laminates (Lebée and Sab 2011b). The Bending-Gradient plate theory is appropriate for modeling regularly spaced CLT panels since it can be extended to in-plane periodic plates thanks to a homogenization scheme. Indeed, the Bending-Gradient model has been applied to periodic sandwich panels by means of a periodic homogenization scheme (Lebée and Sab 2012) and good agreement between the predicted and the reference numerical mechanical response has been pointed out. The homogenization principle is based on energy equivalence with a periodic unit-cell submitted to unit membrane, bending and shear strains in order to predict the homogenized plate moduli. In this thesis, the Bending-Gradient homogenization scheme is therefore chosen as refined modeling of spaced CLT panels to compare with test results and simplified methods.

In the present Chapter, the application of the Bending-Gradient homogenization scheme to regularly spaced CLT panels is presented, as well as the predicted mechanical behavior of the panel. The plate homogenization is capable of predicting the membrane, bending and shear force stiffnesses of the panel. Moreover, the homogenization scheme is based on FE computation and therefore also the stresses acting on the panel can be estimated. The Chapter is organized as follows: first, in Section 4.2, the Bending-Gradient plate theory, its related homogenization scheme and their application to regularly spaced crosslam are summarized. Then, Section 4.3 presents the comparison between the predicted and experimental behavior of spaced CLT presented in Chapter 3. Within this Section, the bending and shear force stiffnesses predicted with the plate homogenization and volume fraction approach are compared with the 4-points bending test results. Then, the in-plane shear stiffness estimated with the existing closed-form solution and plate homogenization are compared to the experimental in-plane shear behavior of the literature. Finally, the stresses at failure point acting on the tested spaced panels in 4-points bending are predicted with the plate homogenization and compared to tensile strength values of the literature and derived rolling shear strength.

4.2 Modeling of spaced CLT

In this section, we first briefly introduce the Bending-Gradient plate theory. Full details about this theory can be found in (Sab and Lebée 2016; Lebée and Sab 2011a;b). Then, the application of the plate theory to a periodic geometry is presented as well, with focus on regularly spaced CLT panels.

4.2.1 Summary of the Bending-Gradient model

CLT with small gaps as well as aerated CLT may be considered as in-plane periodic structures since they are made of a repetitive pattern. Finite element modeling of such structures requires a very fine mesh. Hence, in order to spare computational burden, it is convenient to seek an equivalent membrane and plate model for these 3D structures by means of a homogenization scheme. Additionally, according to the significant shear effects found during the experimental investigations (see Table 3.2), knowing the deflection related to transverse shear effects is also necessary for engineering applications of spaced CLT. This suggests to apply the Bending-Gradient theory which is an extension of the well known Reissner-Mindlin thick plate theory to the case of heterogeneous plates.

Let us recall that the usual generalized stresses for Reissner-Mindlin plate are the membrane stress $N_{\alpha\beta}$, the bending moment $M_{\alpha\beta}$, and the shear force Q_α . These generalized stresses are respectively in duality with the membrane strain $e_{\alpha\beta}$, the curvature $\chi_{\alpha\beta}$, and the transverse shear distortion γ_α . Assuming the plate is symmetric with respect to its mid-plane, these variables are related through the following constitutive

4. HOMOGENIZATION OF REGULARLY SPACED CLT PANELS

equations:

$$\begin{cases} \mathbf{N} = \mathbf{A} : \mathbf{e} & (4.1a) \\ \mathbf{M} = \mathbf{D} : \boldsymbol{\chi} & (4.1b) \\ \mathbf{Q} = \mathbf{F}^{\text{RM}} \cdot \boldsymbol{\gamma} & (4.1c) \end{cases}$$

where \mathbf{A} is the membrane fourth order stiffness tensor, \mathbf{D} is the bending fourth order stiffness tensor and \mathbf{F}^{RM} is the shear force sixth order stiffness tensor. The simple, double and triple contraction products are hereinafter defined as follows: $\mathbf{X} \cdot \mathbf{Y} = X_\alpha Y_\alpha$, $\mathbf{X} : \mathbf{Y} = X_{\alpha\beta} Y_{\beta\alpha}$ and $\mathbf{X} \vdash \mathbf{Y} = X_{\alpha\beta\gamma} Y_{\gamma\beta\alpha}$, with Greek letters that stand for 2D plane coordinates.

Whereas the derivation of \mathbf{A} and \mathbf{D} is well established in the literature for laminated plates (Classical Lamination Theory) as well as for periodic plates (Caillerie 1984; Kohn and Vogelius 1984); the derivation of \mathbf{F}^{RM} raised many difficulties. Indeed, when the plate is heterogeneous, additional variables are required to describe accurately transverse shear deformations.

In the Bending-Gradient theory, the conventional shear force \mathbf{Q} with two degrees of freedom is replaced by the generalized shear force \mathbf{R} with six degrees of freedom. The generalized shear force is a third order tensor. With this new set of variables, the constitutive equation becomes:

$$\begin{cases} \mathbf{N} = \mathbf{A} : \mathbf{e} & (4.2a) \\ \mathbf{M} = \mathbf{D} : \boldsymbol{\chi} & (4.2b) \\ \mathbf{R} = \mathbf{F}^{\text{BG}} \vdash \boldsymbol{\Gamma} & (4.2c) \end{cases}$$

where $\boldsymbol{\Gamma}$ is the generalized shear distortion and \mathbf{F}^{BG} the generalized shear force sixth order stiffness tensor. In case \mathbf{F}^{BG} is not invertible, \mathbf{R} and $\boldsymbol{\Gamma}$ are restricted to a specific vector space detailed in (Lebée and Sab 2015a;b).

Depending on the plate micro-structure, the Bending-Gradient theory may be turned into the Reissner-Mindlin plate theory. For instance, this is the case when the plate is homogeneous. In (Lebée and Sab 2011a), the relative distance between both plate theories was introduced as $0 \leq \Delta^{\text{RM/BG}} < 1$. When $\Delta^{\text{RM/BG}} = 0$ the Bending-Gradient theory exactly reduces to a Reissner-Mindlin theory and we have the following direct estimation of Reissner-Mindlin shear force stiffness moduli as function of the Bending-Gradient ones:

$$F_{111111}^{\text{BG}} = F_{11}^{\text{RM}} \quad \text{and} \quad F_{222222}^{\text{BG}} = F_{22}^{\text{RM}} \quad (4.3)$$

When dealing with laminated plates it is possible to derive \mathbf{A} , \mathbf{D} and \mathbf{F}^{BG} directly from the constitutive material behavior. However, with periodic plates this requires a homogenization procedure which is detailed in the next section.

4.2.2 Homogenization scheme

Let us consider a plate generated by periodicity of a unit-cell Y according to the in-plane Directions 1 and 2 (Figure 4.1). The upper face ∂Y_3^+ and the lower face ∂Y_3^-

4.2 Modeling of spaced CLT

are traction free and the lateral faces ∂Y_l connect adjacent unit-cells. A_Y is the area of the unit-cell cross section with the plate mid-plane. $\mathbf{x} = (x_1, x_2, x_3)$ is the set of coordinates in the unit-cell reference frame.

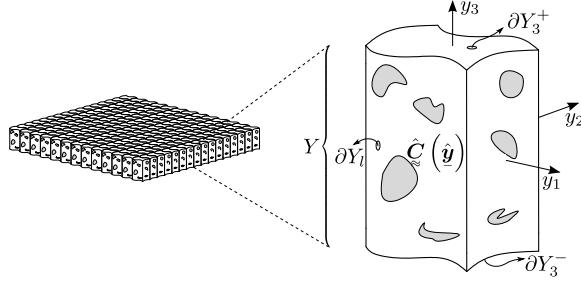


Figure 4.1: The plate unit-cell

Finding \mathbf{A} , \mathbf{D} and \mathbf{F}^{BG} requires the resolution of unit-cell problems. The membrane \mathbf{A} and bending \mathbf{D} stiffness tensors are derived by means of a first unit-cell problem which also gives the corresponding stress states. Then solving a second unit-cell problem is necessary for deriving \mathbf{F}^{BG} .

4.2.2.1 Membrane and thin plate unit-cell problem

Homogenization of periodic plates at leading order was first established by Caillerie (1984). The unit-cell problem is stated as follows:

$$\mathcal{P}^{(e,\chi)} \begin{cases} \operatorname{div} \boldsymbol{\sigma}^{(e,\chi)} = 0 & (4.4a) \\ \boldsymbol{\sigma}^{(e,\chi)} = \mathbf{C}(\mathbf{x}) : \boldsymbol{\varepsilon}^{(e,\chi)} & (4.4b) \\ \boldsymbol{\varepsilon}^{(e,\chi)} = \hat{\mathbf{e}} + x_3 \hat{\boldsymbol{\chi}} + \operatorname{grad}^s \mathbf{u}^{\text{per}} & (4.4c) \\ \boldsymbol{\sigma} \cdot \mathbf{e}_3 = 0 \text{ on free faces } \partial Y_3^\pm & (4.4d) \\ \boldsymbol{\sigma} \cdot \mathbf{n} \text{ skew-periodic on lateral boundaries } \partial Y_l & (4.4e) \\ \mathbf{u}^{\text{per}}(x_1, x_2, x_3) \text{ } (x_1, x_2)\text{-periodic on lateral boundaries } \partial Y_l & (4.4f) \end{cases}$$

where grad^s is the symmetric part of the gradient operator and \mathbf{n} is the outer normal to the unit-cell. This problem basically enforces the membrane strains \mathbf{e} and the curvatures $\boldsymbol{\chi}$ on average on the unit-cell while taking into account periodicity in the (x_1, x_2) -plane and traction-free conditions on the upper and lower faces of the plate. In Equation 4.4c, $\hat{\mathbf{e}}$ and $\hat{\boldsymbol{\chi}}$ denote the out-of-plane extension of the in-plane tensors \mathbf{e} and $\boldsymbol{\chi}$:

$$\mathbf{e} = \begin{pmatrix} e_{11} & e_{12} & 0 \\ e_{21} & e_{22} & 0 \\ 0 & 0 & 0 \end{pmatrix} \quad \text{and} \quad \boldsymbol{\chi} = \begin{pmatrix} \chi_{11} & \chi_{12} & 0 \\ \chi_{21} & \chi_{22} & 0 \\ 0 & 0 & 0 \end{pmatrix} \quad (4.5)$$

Solving the problem for each individual component of \mathbf{e} and $\boldsymbol{\chi}$ leads to the localization stress fields $\mathbf{s}^{(e)}$ and $\mathbf{s}^{(\chi)}$ such that the total stress $\boldsymbol{\sigma}^{(e,\chi)}$ solution of the problem $\mathcal{P}^{(e,\chi)}$

4. HOMOGENIZATION OF REGULARLY SPACED CLT PANELS

is recovered by linear combinations:

$$\sigma_{ij}^{(e,\chi)} = s_{ij\alpha\beta}^{(e)}(\mathbf{x})e_{\beta\alpha} + s_{ij\alpha\beta}^{(\chi)}(\mathbf{x})\chi_{\beta\alpha} \quad (4.6)$$

Hence, $\boldsymbol{\sigma}^{(e,\chi)}$ is the stress state inside any unit-cell when the periodic plate is subjected to given uniform membrane strain and curvature.

The membrane and thin plate stiffness tensors are then evaluated as follows:

$$\mathbf{A} = \langle {}^T \mathbf{s}^{(e)} : \mathbf{C}^{-1} : \mathbf{s}^{(e)} \rangle, \quad \mathbf{D} = \langle {}^T \mathbf{s}^{(\chi)} : \mathbf{C}^{-1} : \mathbf{s}^{(\chi)} \rangle \quad (4.7)$$

where

$$\langle f \rangle = \frac{1}{A_Y} \int_Y f(\mathbf{x}) dY \quad (4.8)$$

is the normalized average (surface average) on the unit-cell and the superscript T stands for the transpose operator. Finally, using the inverted plate constitutive law of Equation 4.1a and Equation 4.1b and localization tensors $\mathbf{s}^{(e)}$ and $\mathbf{s}^{(\chi)}$, it is possible to write the local stress field generated by membrane stress and bending moment as:

$$\boldsymbol{\sigma}^{(N)} = \mathbf{s}^{(N)} : \mathbf{N} = (\mathbf{s}^{(e)} : \mathbf{a}) : \mathbf{N} \quad \text{and} \quad \boldsymbol{\sigma}^{(M)} = \mathbf{s}^{(M)} : \mathbf{M} = (\mathbf{s}^{(\chi)} : \mathbf{d}) : \mathbf{M} \quad (4.9)$$

where \mathbf{a} and \mathbf{d} are respectively the membrane and thin plate compliance tensors (reciprocals of \mathbf{A} and \mathbf{D}).

4.2.2.2 The generalized shear unit-cell problem

Dealing with in-plane periodic plates, the bending moment can be assumed to vary linearly in the (x_1, x_2) -plane, and therefore can be expressed as a function of the generalize shear force as $\mathbf{M} = \mathbf{R} \cdot \mathbf{x}$ (Lebée and Sab 2012). Inserting this in Equation 4.9 and applying the 3D divergence of the bending stress field $\boldsymbol{\sigma}^{(M)}$ leads to the body force in the unit-cell generated by a uniform gradient of the bending moment \mathbf{R} :

$$f_i^{(R)} = s_{i\gamma\epsilon\eta}^{(\chi)}(\mathbf{x}) d_{\eta\epsilon\beta\alpha} R_{\alpha\beta\gamma} \quad (4.10)$$

This body force has to be equilibrated by the Bending-Gradient stress $\boldsymbol{\sigma}^{(R)}$, and therefore the generalized shear auxiliary problem on the unit-cell is defined as:

$$\mathcal{P}^{(R)} \begin{cases} \operatorname{div} \boldsymbol{\sigma}^{(R)} + \mathbf{f}^{(R)}(\mathbf{x}) = 0 & (4.11a) \\ \boldsymbol{\sigma}^{(R)} = \mathbf{C}(\mathbf{x}) : (\operatorname{grad} \mathbf{u}^{(R)}) & (4.11b) \\ \boldsymbol{\sigma}^{(R)} \cdot \mathbf{e}_3 = 0 \text{ on free faces } \partial Y_3^\pm & (4.11c) \\ \boldsymbol{\sigma}^{(R)} \cdot \mathbf{n} \text{ skew-periodic on lateral boundaries } \partial Y_l & (4.11d) \\ \mathbf{u}^{(R)}(x_1, x_2, x_3) \text{ } (x_1, x_2)\text{-periodic on lateral boundaries } \partial Y_l & (4.11e) \end{cases}$$

Solving $\mathcal{P}^{(R)}$ for each component of \mathbf{R} leads to the localization stress field $s_{ij\alpha\beta\gamma}^{(R)}$ associated to \mathbf{R} . The overall stress is obtained by linear combination:

$$\sigma_{ij}^{(R)} = s_{ij\alpha\beta\gamma}^{(R)}(\mathbf{y}) R_{\gamma\beta\alpha} \quad (4.12)$$

It is then possible to identify the Bending-Gradient compliance tensor as:

$$\mathbf{f}^{\text{BG}} = \left\langle {}^T(\mathbf{s}^{(R)}) : \mathbf{C}^{-1}(\mathbf{x}) : \mathbf{s}^{(R)} \right\rangle \quad (4.13)$$

Finally \mathbf{F}^{BG} is obtained taking the pseudo inverse: $\mathbf{F}^{\text{BG}} = (\mathbf{f}^{\text{BG}})^{-1}$.

4.2.3 Application to a regularly spaced CLT panel

A unit-cell of a 5-ply regularly spaced CLT panel is showed in Figure 4.2. The lateral faces are periodic along x_1 and x_2 directions, while the upper and lower faces are free. Perfect connections between layers are considered. The investigated lay-ups in this study are 3, 5 and 7-ply panels. Moreover, the studies of Moosbrugger et al (2006) and Silly (2010) highlighted the great influence of lamellas' aspect-ratio width to thickness w/h on the in-plane behavior of CLT panels with gaps in each layer. Therefore two different lamella's aspect-ratios w/h are also analyzed: $w/h = 3.33$ and $w/h = 10$. This is achieved fixing the width at 100 mm, while the considered thicknesses are 30 or 10 mm (Figure 4.2) which is within the standard range from 6 to 45 mm for CLT layers' thickness established in EN-16351 (2016).

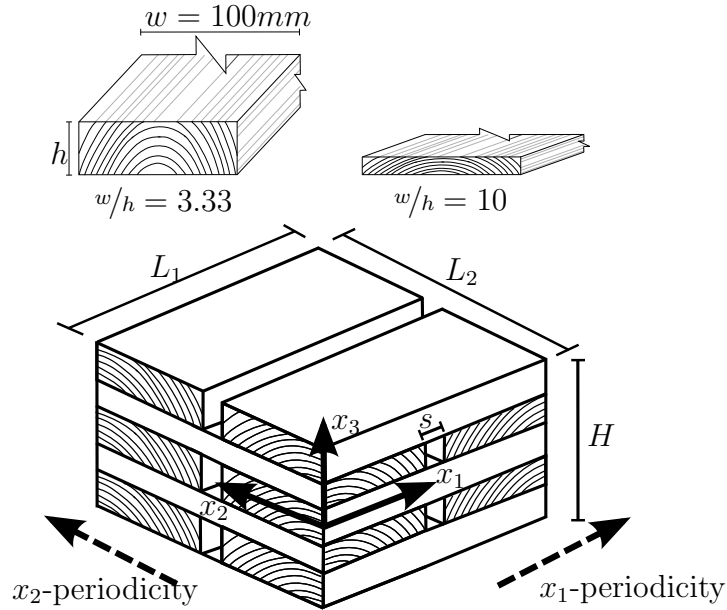


Figure 4.2: Unit-cell of spaced 5-ply CLT with investigated ratios w/h of lamellas

In this thesis, unit-cell of regularly spaced CLT panels having three planes of symmetry are considered. It is possible to study only one fourth of the unit-cell and only symmetric or skew-symmetric boundary conditions apply. Moreover, the mirror symmetry on the panel mid-plane allows analyzing only one eighth of the unit-cell as showed in Figure 4.3, reducing further computational costs.

The symmetries of regularly spaced CLT lead to simplifications also on the constitutive equation. When the unit-cell is unchanged through a π angle rotation with

4. HOMOGENIZATION OF REGULARLY SPACED CLT PANELS

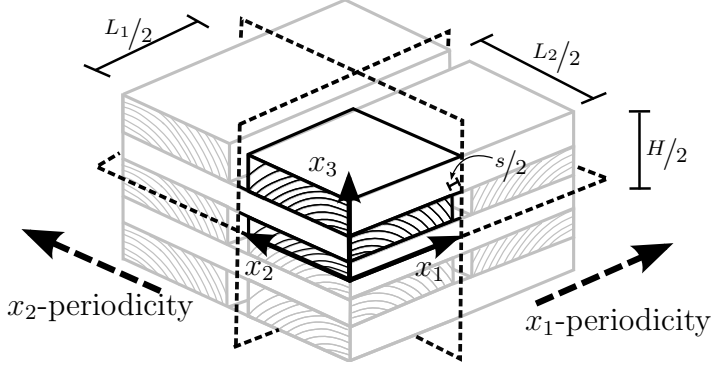


Figure 4.3: One eight of the CLT unit-cell when considering the three major symmetries

respect to a vertical axis, then the membrane and thin-plate stresses (\mathbf{N} , \mathbf{M}) are uncoupled from \mathbf{R} . When the unit-cell follows the mirror symmetry with respect to the mid-plane, membrane stress are uncoupled from bending moments. Finally, the plate is orthotropic when the unit-cell is invariant through a vertical plane symmetry. When all these symmetries occurs, there remain 4 moduli for membrane stress, 4 moduli for bending moments and 12 moduli for the bending gradient (Lebée and Sab 2011b). The plate moduli \mathbf{A} and \mathbf{D} have the following form:

$$\mathbf{A} = \begin{pmatrix} A_{11} & A_{12} & 0 \\ & A_{22} & 0 \\ sym & & A_{33} \end{pmatrix} \quad \mathbf{D} = \begin{pmatrix} D_{11} & D_{12} & 0 \\ & D_{22} & 0 \\ sym & & D_{33} \end{pmatrix} \quad (4.14)$$

Introducing the following notation

$$\begin{pmatrix} R_{111} \\ R_{221} \\ \sqrt{2}R_{121} \\ R_{112} \\ R_{22} \\ \sqrt{2}R_{122} \end{pmatrix} = \begin{pmatrix} R_1 \\ R_2 \\ R_3 \\ R_4 \\ R_5 \\ R_6 \end{pmatrix} \quad (4.15)$$

leads writing the Bending-Gradient shear force stiffness \mathbf{F}^{BG} as:

$$\mathbf{F}^{BG} = \begin{pmatrix} F_{11}^{BG} & F_{12}^{BG} & 0 & 0 & 0 & F_{16}^{BG} \\ & F_{22}^{BG} & 0 & 0 & 0 & F_{26}^{BG} \\ & & F_{33}^{BG} & F_{34}^{BG} & F_{35}^{BG} & 0 \\ & & & F_{44}^{BG} & F_{45}^{BG} & 0 \\ & sym & & & F_{55}^{BG} & 0 \\ & & & & & F_{66}^{BG} \end{pmatrix} \quad (4.16)$$

The auxiliary problems of thin and thick plate homogenization are solved by means of a finite elements software in order to obtain the elastic strain energy of the unit-cell. Solid C3D8 linear elements in ABAQUS are chosen. When the spaces are very short, the size of single elements should be smaller than the gap length. A convergence study,

not detailed here, led to a mesh of minimum six elements per gap's edge, as showed in detail of Figure 4.4, and of minimum six elements per layer's thickness. The timber elastic engineering constants for the FEM modeling are taken from Table 3.3.

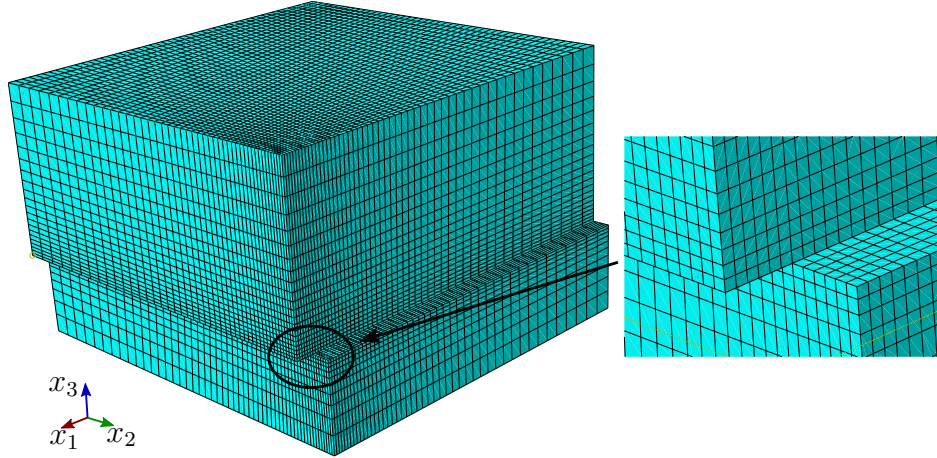


Figure 4.4: FE mesh of one eighth 3-ply unit-cell with zoom on gap (5 mm) mesh

In the following, the applied loads and boundary conditions within the unit-cell problems are presented.

4.2.3.1 Boundary conditions and loads for the thin-plate and membrane unit-cell problem

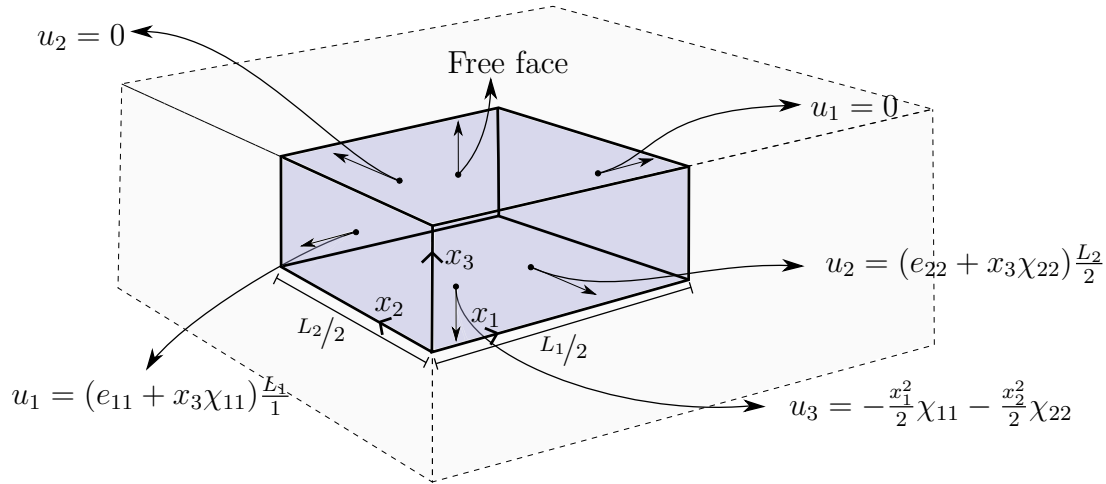
The orthotropy of the unit-cell allows to apply only symmetric or skew-symmetric boundary conditions on periodic lateral faces, while periodic boundary conditions vanish. The load of the thin-plate and membrane homogenization are imposed membrane (e_{11}, e_{22}, e_{12}) and curvature ($\chi_{11}, \chi_{22}, \chi_{12}$) strains on the boundaries. Since the auxiliary problems are implemented with solid 3D elements in ABAQUS, displacements boundary conditions apply. Figure 4.5 shows the applied boundary condition of symmetry, skew-symmetry and imposed loadings. e_{11} and e_{22} are unit axial membrane strains along directions x_1 and x_2 respectively, while χ_{11} and χ_{22} are unit out-of-plane bending strains in x_1 and x_2 directions. Finally e_{12} and χ_{12} are respectively the skew-symmetric in-plane shear and in-plane bending (or torsional) strains.

4.2.3.2 Boundary conditions and loads for the thick-plate unit-cell problem

According to Equation (4.10), the load for the Bending-Gradient auxiliary problem is the body force $\mathbf{f}^{(R)}$ deriving from a uniform gradient of the bending moment. Such body force is a volume force that has six components, and each one produces a uniform generalized shear force ($R_1, R_2, R_3, R_4, R_5, R_6$). The user subroutine DLOAD in ABAQUS is implemented in order to apply each component of $\mathbf{f}^{(R)}$ at the integration points. Finally, the boundary conditions for the Bending-Gradient homogenization are presented in Figure 4.6. The boundary conditions for the thick plate homogenization

4. HOMOGENIZATION OF REGULARLY SPACED CLT PANELS

(a) Symmetric loadings e_{11} , e_{22} , χ_{11} , χ_{22}



(b) Skew-symmetric loadings e_{12} , χ_{12}

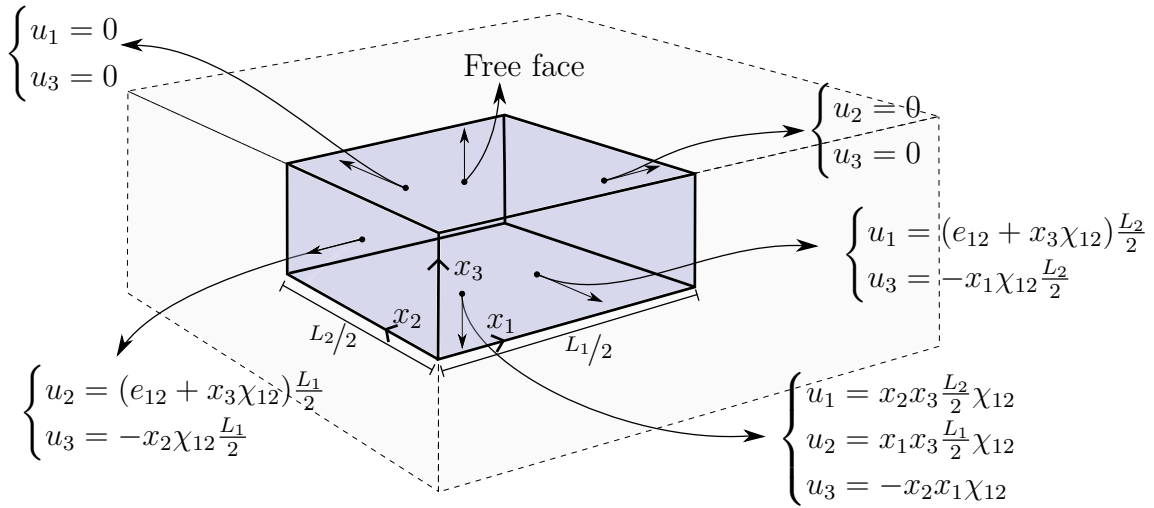


Figure 4.5: Applied boundary conditions and loadings for the symmetric (a) and skew-symmetric (b) loadings of the thin plate and membrane unit-cell problem

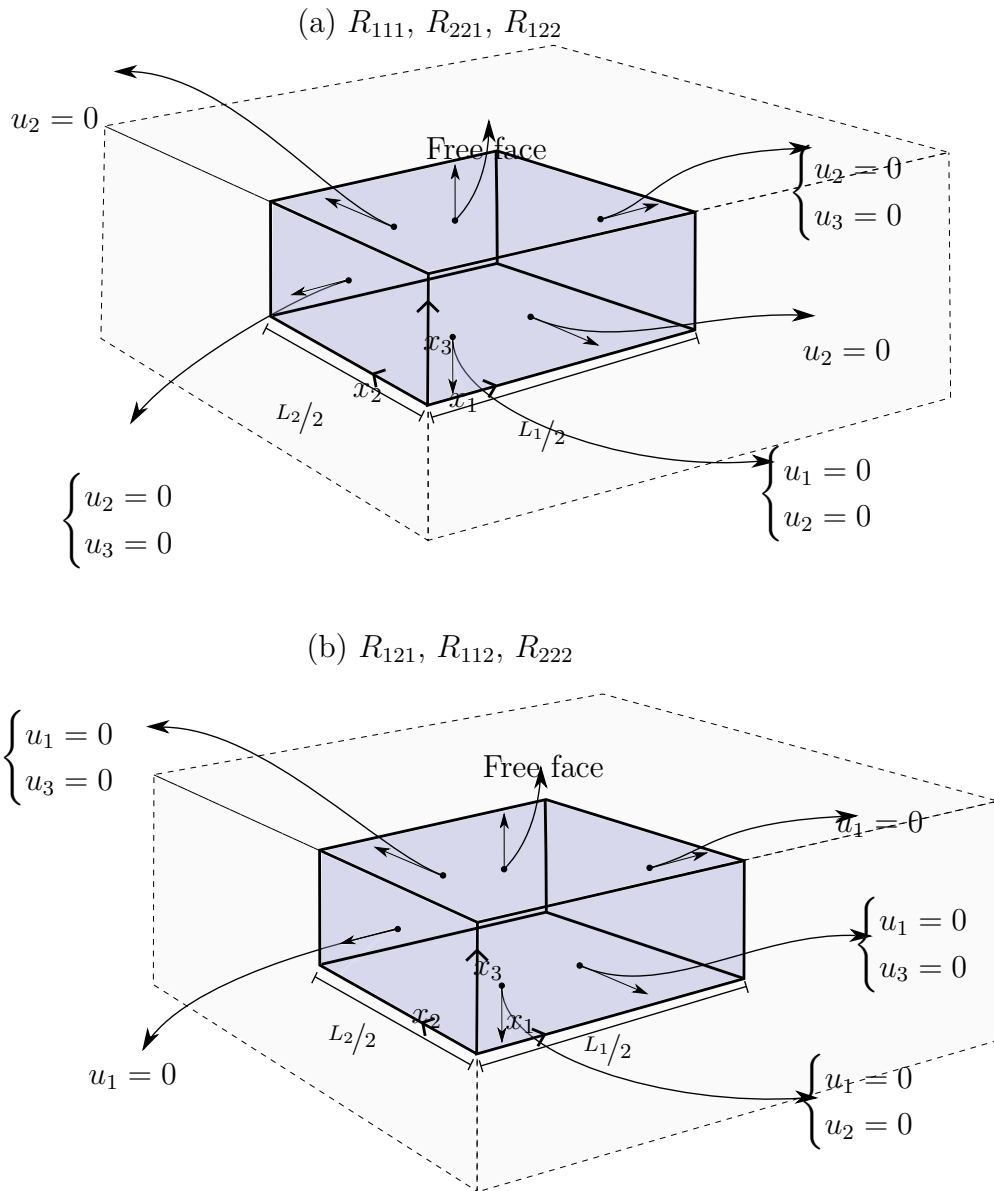


Figure 4.6: Applied boundary conditions for the R_1, R_2, R_6 (a) and R_3, R_4, R_5 (b) loadings of the thick plate unit-cell problem

4. HOMOGENIZATION OF REGULARLY SPACED CLT PANELS

can be divided into two main groups: the first one concerning generalized shear forces in the (x_1, x_3) -plane (R_1, R_2, R_6) and the second group which deals with shear forces in (x_2, x_3) -plane (R_3, R_4, R_5) .

4.3 Results

In this section, results from the thin and thick plate homogenization are presented and compared to simplified approaches as well as to available experimental data. First, the variation of plate moduli is plotted as a function of the length of spaces within the panel. For each investigated value of spaces s , the corresponding experimental or predicted value of plate modulus K is normalized over the predicted modulus of a continuous panel having the lateral lamellas glued K^* . Then, the predicted variation of longitudinal and transverse shear stresses as a function of spaces is compared to the experimental results of 4-points bending tests.

4.3.1 Bending stiffness

Figure 4.7 shows the deformed one eighth of a regularly spaced CLT unit-cell under the unit curvature χ_{11} , while Figure 4.8 plots the variation of the homogenized stiffness D_{11} as a function of spaces.

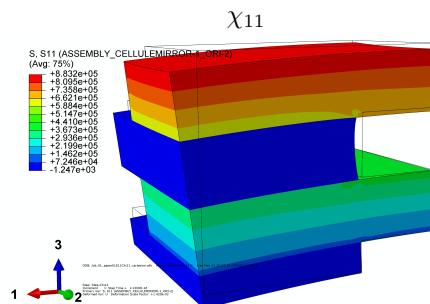


Figure 4.7: Deformed one-eighth unit-cell of a 7-ply submitted to the unit curvature χ_{11} . $w=100$, $s=50$, $h=20$. The contour plot shows the longitudinal stress σ_{11}

There is no dependency from the aspect ratio w/h of lamellas, while there is a slight influence of the number of layers on the variation of normalized stiffness $\frac{D_{11}}{D_{11}^*}$ as a function of spaces. As Figure 4.8 shows, the bending stress σ_{11} is significant only in longitudinal layers parallel to x_1 direction. Therefore, only longitudinal layers contribute to the bending stiffness of the panel while the contribution of transverse layers is negligible, exactly like CLT without gaps. Similar results have been found for the membrane stiffness A_{11} and A_{22} and also for the bending stiffness along x_2 direction D_{22} . The simplified approach to determine the bending stiffness of spaced CLT is the Classical Lamination Theory combined with reduced properties of wood by the volume fraction coefficient λ . For instance, the shear analogy method (Kreuzinger 1999), a commonly used design approach for massive crosslam, is based on the Classical

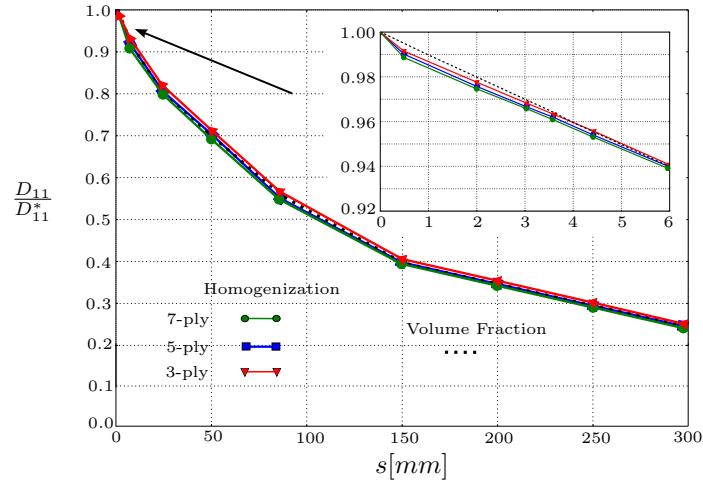


Figure 4.8: Variation of the normalized stiffness $\frac{D_{11}}{D_{11}^*}$ as a function of spaces between lamellas

Lamination Theory. The comparison between predicted and experimental bending stiffness of regularly spaced crosslam panels is plotted in Figure 4.9 and detailed in Table 4.1, where good agreement is found dealing with both homogenization and closed-form approach.

D_{11}/D_{11}^*	$s=5\text{mm}, \lambda=0.95$	$s=150\text{mm}, \lambda=0.4$	$s=300\text{mm}, \lambda=0.25$
Test result	0.97	0.38	0.23
Homogenization	0.95	0.40	0.25
Lamination Theory (λ)	0.95	0.40	0.25

Table 4.1: Comparison between the experimental and predicted normalized bending stiffness D_{11}/D_{11}^* of spaced CLT

4.3.2 In-plane shear and torsional stiffnesses

Deformed unit-cells of a panel having small and large spaces under in-plane shear strain e_{12} and in-plane bending (or torsional) strain χ_{12} are respectively showed in Figure 4.10 and Figure 4.11.

When dealing with these generalized strains, all layers contribute to the stiffness of the panel. In the case of laterally glued crosslam, global in-plane shearing or torsion of the panel occur and the continuous geometry ensures the stress transmission through all the thickness. In the case of discontinuous CLT panels with spaces within each layer, the presence of free edges prevents the direct transmission of stresses between lamellas, leading to stress singularities (Figure 4.10). As a consequence, the stresses increase due the decrease of the net cross section (as also highlighted by Brandner et al (2013) and Bogensperger et al (2010)) and the global stiffness decreases. Such decrease of stiffness is also due to an additional compliance mechanism of rotation between upper

4. HOMOGENIZATION OF REGULARLY SPACED CLT PANELS

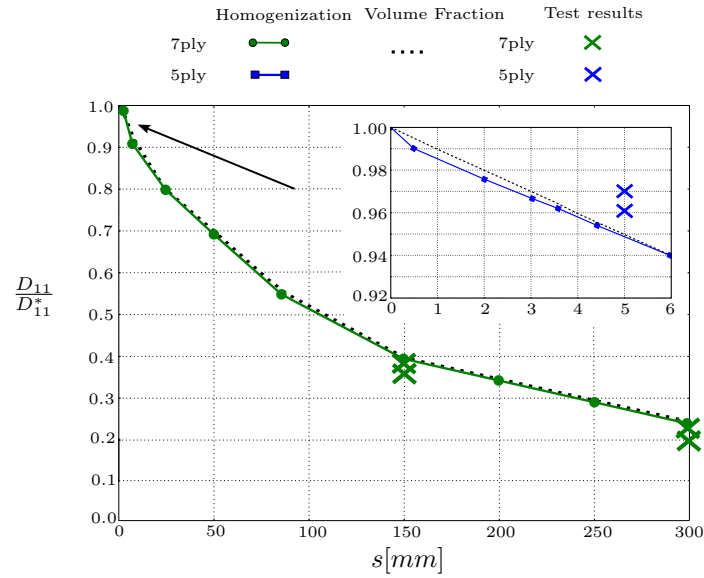


Figure 4.9: Comparison between the experimental and predicted bending stiffness D_{11} of spaced CLT

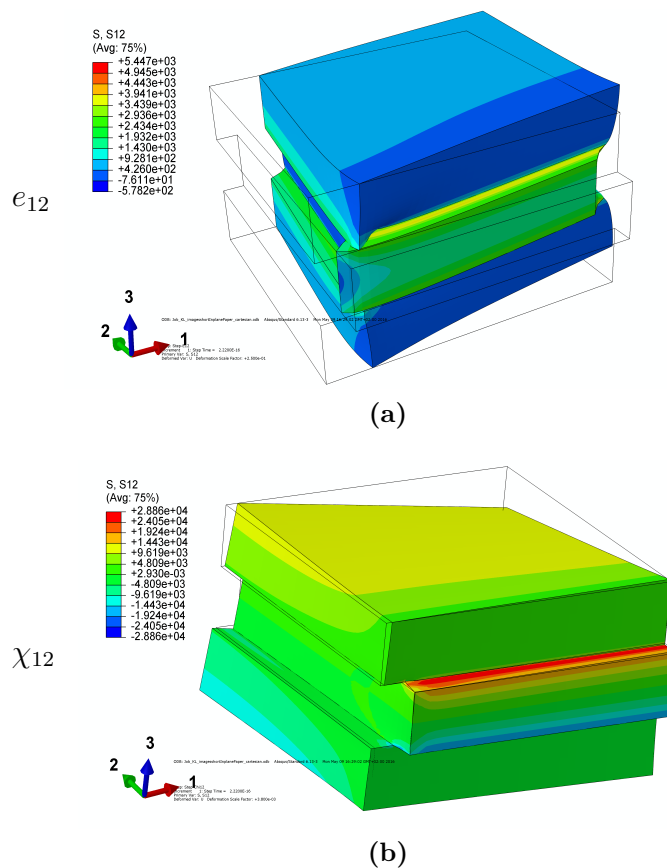


Figure 4.10: One fourth of a 3-ply unit-cell having small spaces under in-plane shear (a) and torsion (b) unit strains. $w=100$, $h=10$, $s=6$. The contour plot shows the in-plane shear stress σ_{12}

4. HOMOGENIZATION OF REGULARLY SPACED CLT PANELS

and lower lamellas that appears when the lateral edges are not glued. The reduction of in-plane stiffness becomes more significant in the case of large spaces, where all spaced lamellas are submitted to bending in their plane due to their slenderness (Figure 4.11).

Moosbrugger et al (2006) derived a simplified closed-form solution for predicting the in-plane shear stiffness of crosslam panels having short gaps. According to this method, the in-plane shear stiffness of a glued panel is reduced by a “torsion-like” mechanism, dependent on the ratio w/h , that appears when the lamellas are not laterally glued each other. This in order to take into account the additional mechanisms of relative rotation under in-plane shear described above. The derivation of this simplified method is based on a CLT representative volume element (RVE) composed by two lamellas and therefore the reduction of in-plane shear stiffness is independent from the number of layers. Moreover, Moosbrugger et al (2006) considered the gaps to be short beams and their bending and shear compliance are taken into account. The three mechanisms acting on a spaced CLT under in-plane shear according to Moosbrugger et al (2006) are showed in Figure 4.12. Since increasing the spaces means increasing the span of

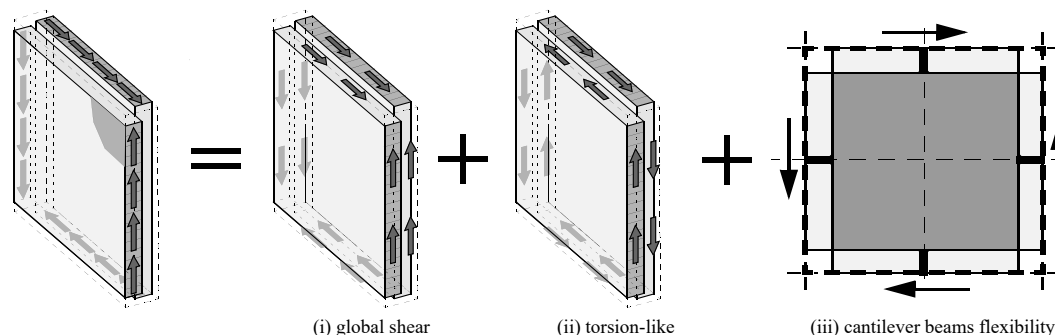


Figure 4.12: Mechanisms acting on spaced CLT under in-plane shear according to Moosbrugger et al (2006)

beams represented by gaps, such simplified approach may also predict the stiffness for large spaces within the panel. The closed-form solution returns directly the reduction G/G^* , where G is the reduced stiffness of spaced CLT and G^* is the in-plane shear stiffness of solid wood (G_{LN}) that equals the stiffness of a continuous laterally glued CLT. This closed-form solution is compared in this section with the predicted A_{33} and D_{33} moduli normalized over the stiffnesses of a continuous crosslam panel.

In Figure 4.13, the comparison between the experimental results of Brandner et al (2015) on the in-plane shear behavior of spaced crosslam and the predicted reduction of the modulus A_{33} is presented. Both results from thin-plate homogenization and from the closed-form solution are showed.

When the lateral edges are not anymore glued each other, the mechanism of relative in-plane rotation of lamellas yields a sharp drop of in-plane shear stiffness that can be well predicted by the homogenization approach, while the closed-form approach underestimates the reduction of the stiffness of about 25%.

As the study of Silly (2010) showed, the in-plane shear and torsional stiffness of

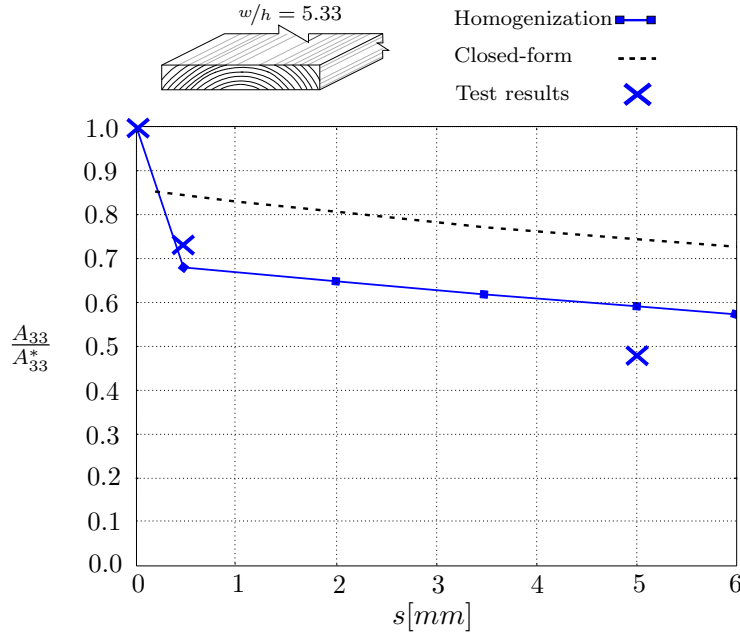


Figure 4.13: Comparison between test results and in-plane shear stiffness reduction $\frac{A_{33}}{A_{33}^*}$ predicted with homogenization and closed-form solution

spaced CLT are influenced by the aspect ratio w/h . Therefore from Figure 4.14 to Figure 4.17 are plotted the variation of normalized in-plane shear stiffness A_{33} and torsional stiffness D_{33} as a function of spaces for crosslam made up of lamellas having aspect ratio $w/h = 3.33$ and $w/h = 10$. Within each plot, the influence of the number of layers is highlighted as well.

Both the aspect ratio w/h and the number of layers influence the in-plane shear and torsional stiffness of spaced CLT. Indeed, increasing the number of layers and the value of the ratio w/h yields a lower drop of in-plane shear stiffnesses. The worst case of a 3-ply panel having lamellas with $w/h = 3.33$ shows a 40% reduction of A_{33} when the panel is not laterally glued and a 50% reduction for 6 mm gaps. For small spaces, the torsional stiffness D_{33} shows higher reduction than the in-plane shear stiffness and the same dependency on the number of layers. Interestingly, this trend is reversed when enlarging the spaces, where higher values of D_{33} are found for 3-ply lay-ups and especially for high values of ratio w/h .

4.3.3 Thick-plate homogenization

The relative distance between the Reissner-Mindlin and the Bending-Gradient plate theories is plotted in Figure 4.18 as a function of the increasing spaces and for different lay-ups. This distance is not always small and is strongly influenced by the lay-up of the panel. For very large spaces all relative distances tend to $\frac{2\sqrt{2}}{3}$ (Lebée and Sab 2013), and it is the 3-ply configuration that goes more rapidly to this limit value. Additionally, thick lamellas ($w/h = 3.33$) yield lower values of the relative distance than thin lamellas ($w/h = 10$). However, except for the 3-ply lay-up, the relative distance

4. HOMOGENIZATION OF REGULARLY SPACED CLT PANELS

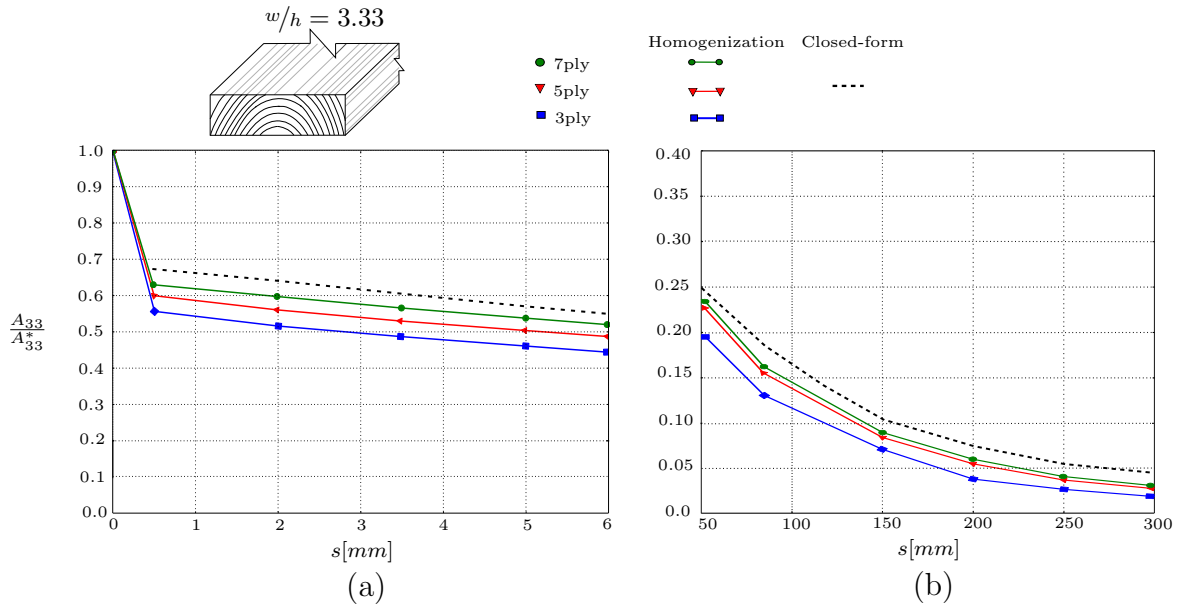


Figure 4.14: Variation of normalized in-plane shear stiffness $\frac{A_{333}}{A_{33}^*}$ for (a) small and (b) large spaces for ratio $w/h = 3.33$ of lamellas and for 3, 5 and 7 layers

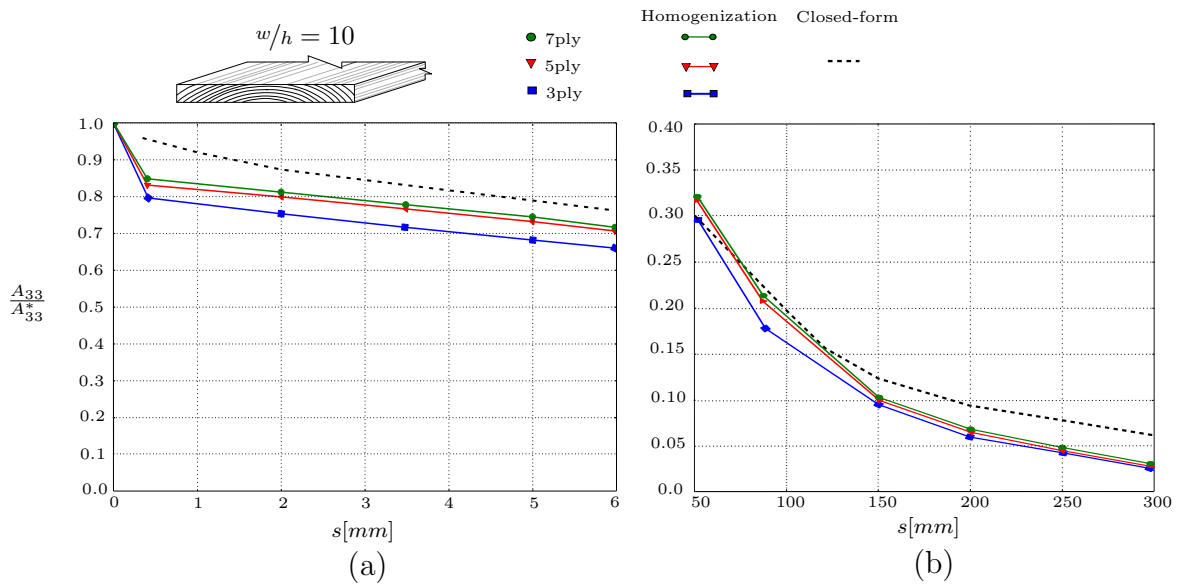


Figure 4.15: Variation of normalized in-plane shear stiffness $\frac{A_{333}}{A_{33}^*}$ for (a) small and (b) large spaces for ratio $w/h = 10$ of lamellas and for 3, 5 and 7 layers

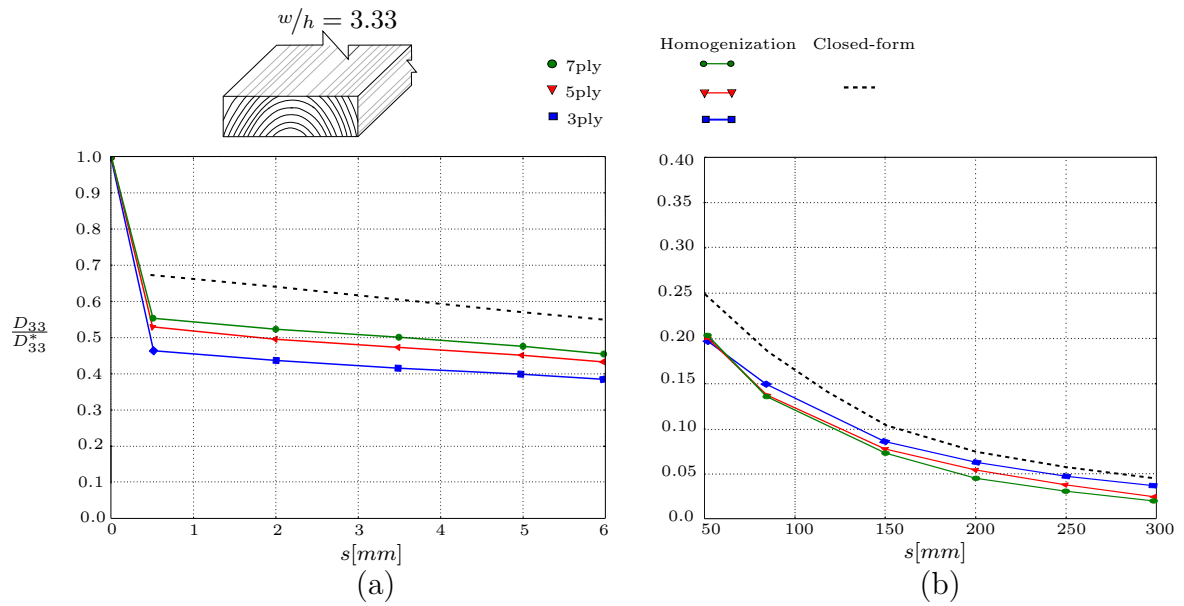


Figure 4.16: Variation of normalized torsional stiffness $\frac{D_{33}}{D_{33}^*}$ for (a) small and (b) large spaces for ratio $w/h = 3.33$ of lamellas and for 3, 5 and 7 layers

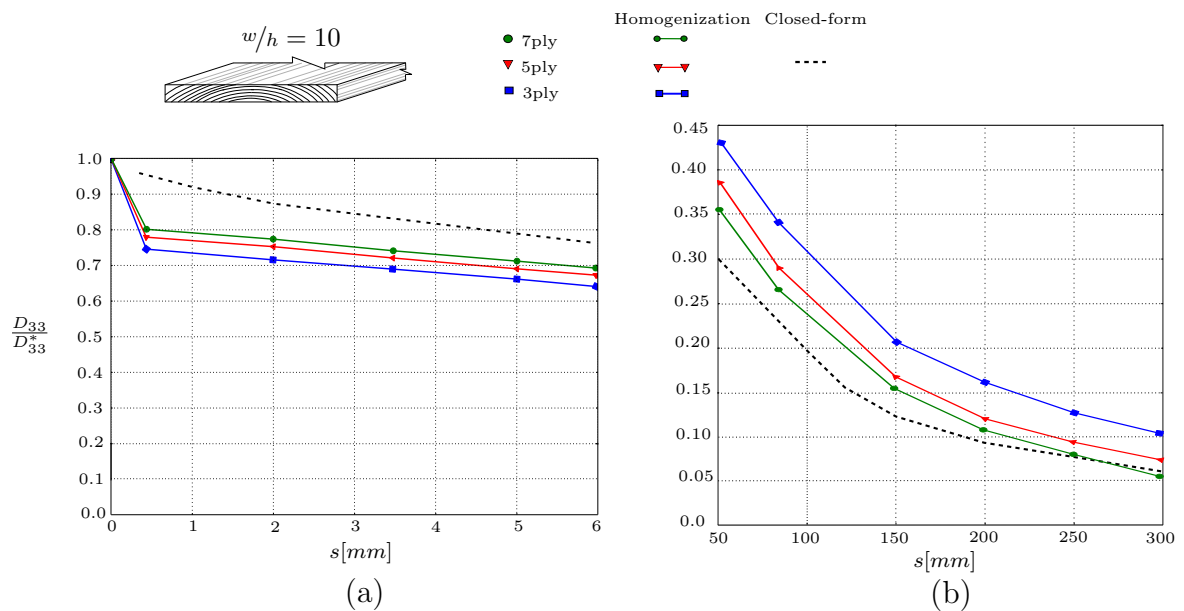


Figure 4.17: Variation of normalized torsional stiffness $\frac{D_{33}}{D_{33}^*}$ for (a) small and (b) large spaces for ratio $w/h = 10$ of lamellas and for 3, 5 and 7 layers

4. HOMOGENIZATION OF REGULARLY SPACED CLT PANELS

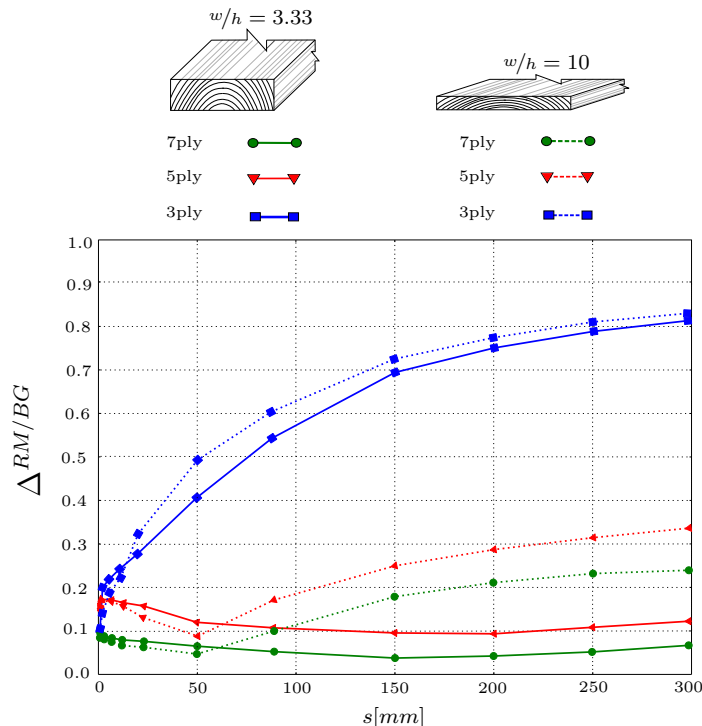


Figure 4.18: Distance between Reissner-Mindlin and Bending-Gradient plate model as a function of the spaces and for different lay-ups

remains moderate for the range of spaces interesting for practical applications plotted in Figure 4.18. This allows the use of the more conventional Reissner-Mindlin plate theory.

Finally, CLT floors are commonly simply supported on two sides with the longitudinal layers aligned to the bending direction, which is also called a *cylindrical* bending configuration. The results of (Lebée and Sab 2015b) pointed out that the cylindrical part of the Bending-Gradient shear force compliance f_{11}^{BG} (see Equation 4.13) is sufficient to well describe the shear force compliance of a layered plate under cylindrical bending, even if $\Delta^{RM/BG}$ is not small. Hence, only the term f_{11}^{BG} of the Bending-Gradient shear force compliance is discussed in this section.

Deformed unit-cells of spaced CLT panels under the cylindrical part of the generalized shear force R_1 are showed in Figure 4.19 for both small and large spaces. In both cases, the free edges lead to stress singularities in the discontinuities at interfaces. Further analyses revealed that an interaction between rolling shear stresses (σ_{13}) and perpendicular to grain stresses (σ_{22} and σ_{33}) is present in the discontinuous interface between upper and lower lamellas. Such interaction between perpendicular to grain and transverse shear stresses has been proved by recent experimental and numerical studies (Hochreiner et al 2013; Ehrhart et al 2015) to reduce the strength of spaced crosslam transverse lamellas. However, being a very localized phenomenon, the contribution of stress concentrations to the shear force stiffness is low.

In this Section, the chosen simplified method for the prediction of the shear force

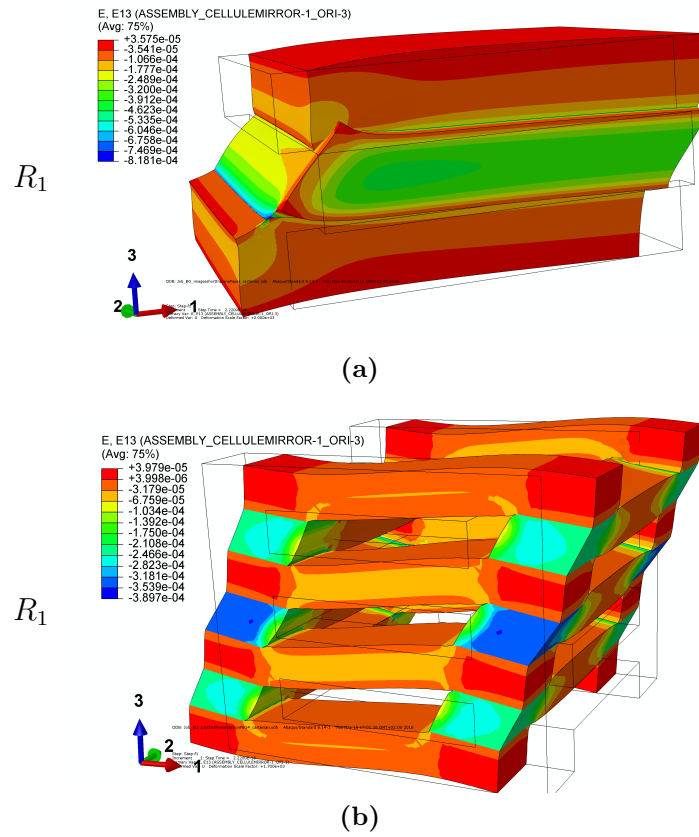


Figure 4.19: Deformed unit-cell under R_1 generalized shear force in the case of short spaces (a) ($w=100, h=10, s=6$) and large spaces (b) ($w=100, h=30, s=150$). The contour plot shows the transverse shear strain ϵ_{13} .

4. HOMOGENIZATION OF REGULARLY SPACED CLT PANELS

stiffness of spaced CLT is the shear analogy method derived by Kreuzinger (1999) combined with reduced properties by the wood volume fraction λ . According to this method, the shear stress across the panel's thickness has a trapezoidal distribution and the global shear compliance is determined as the sum of layers' compliance weighted by the thickness of each layer. Figure 4.19a shows that when the spaces are short, the dominant contribution to the shear strain energy still derives from the rolling shear of transverse layers, exactly as in the case of laterally glued crosslam. When the voids between narrow lamellas increase, the longitudinal lamellas behave as beams under simple bending connected to transverse lamellas (Figure 4.19b) and this additional mechanism (like a Verendeel beam) increases the transverse shear compliance. The shear force stiffness prediction with the shear analogy method combined with the volume fraction cannot take into account this additional compliance mechanism and therefore overestimates the shear force stiffness $\frac{1}{f_{11}}$, as Figure 4.20 and Figure 4.21 show, while homogenization results are in good agreement with test results. Table 4.2 presents as well the comparison between experimental and predicted reduction of normalized shear force stiffness.

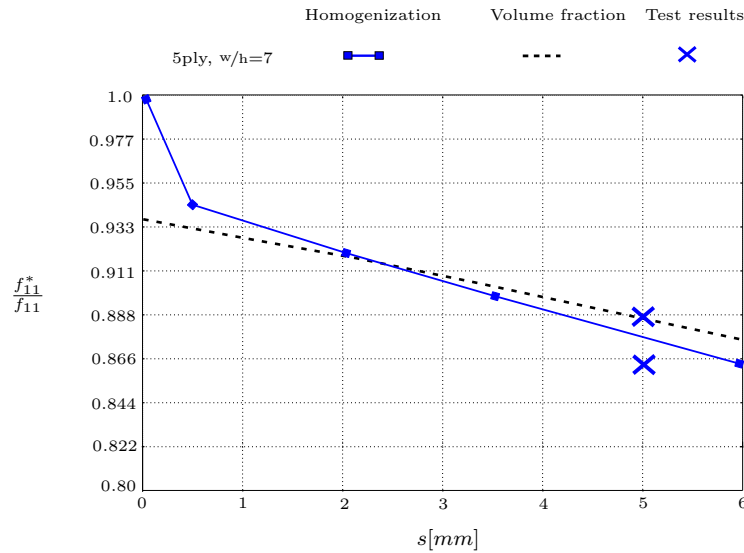


Figure 4.20: Variation of normalized shear force stiffness $\frac{f_{11}^*}{f_{11}}$ for short spaces and comparison with test results

f_{11}^*/f_{11}	s=5mm, $\lambda=0.95$	s=150mm, $\lambda=0.4$	s=300mm, $\lambda=0.25$
Test result	0.8723	0.1261	0.0386
Homogenization	0.8768	0.1321	0.0397
Kreuzinger (1999) (λ)	0.8874	0.3925	0.2453

Table 4.2: Variation of normalized shear force stiffness f_{11}^*/f_{11} for short and large spaces and comparison with test results

In Figure 4.22 is plotted the variation of shear force stiffness as a function of in-

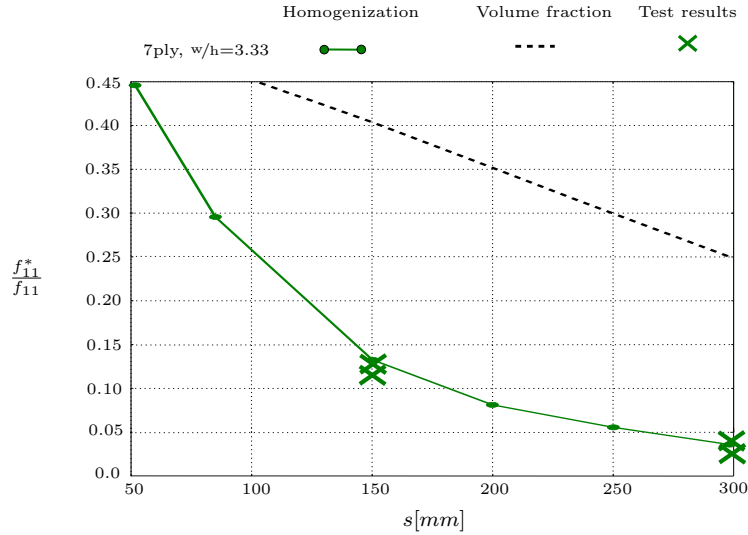


Figure 4.21: Variation of normalized shear force stiffness $\frac{f_{11}^*}{f_{11}}$ for large spaces and comparison with test results

creasing space and for two different aspect ratios w/h . The influence of the number of layers on the normalized stiffness has been found to be very small exactly as in the case of the bending stiffness D_{11} , and therefore only the case of a 7-ply is plotted. As Figure 4.22a shows, already at short spaces there is a small drop of normalized shear force stiffness because of the free edges. This effect cannot be predicted by the volume fraction approach.

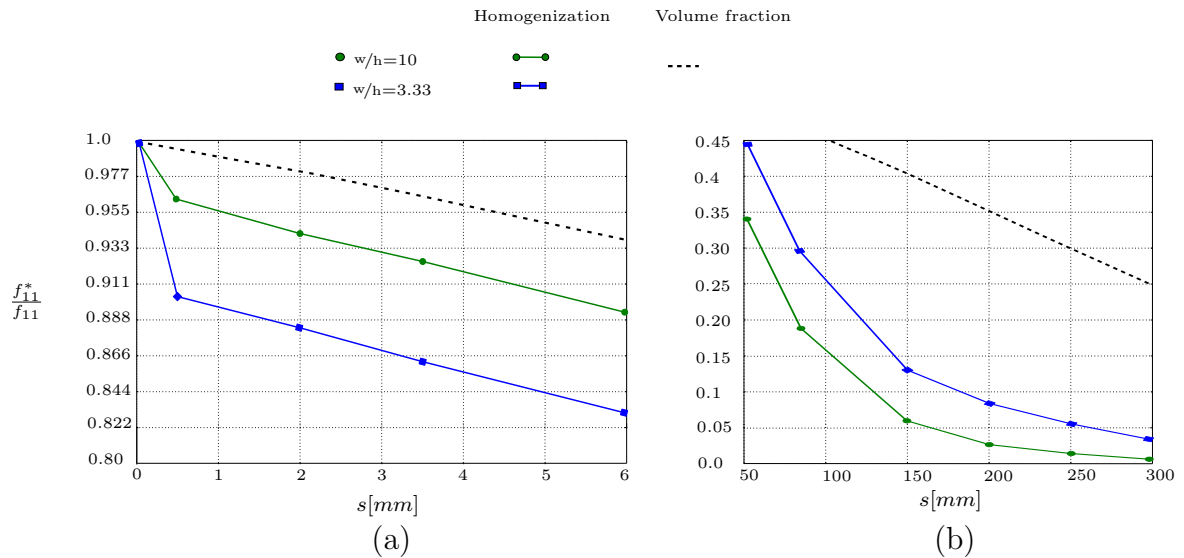


Figure 4.22: Variation of the normalized shear force stiffness $\frac{f_{11}^*}{f_{11}}$ for (a) large and (b) short spaces for different lamella ratio w/h

More precisely, in this case the number of free edges per unit length increases with the aspect ratio w/h . Hence, a higher drop of stiffness is observed with $w/h=3.33$ than with $w/h=10$ in Figure 4.22a. Enlarging the spaces means increasing the span of the longitudinal beams connected to transverse lamellas. When such beams have

4. HOMOGENIZATION OF REGULARLY SPACED CLT PANELS

small thickness, their slenderness further increases and their bending stiffness decreases. Therefore, as highlighted in Figure 4.22b and contrary to the small spaces case, panels having large spaces and made of lamellas having high values of w/h present lower shear force stiffness than panels with thicker lamellas.

4.3.4 Influence of predicted stresses on variation of failure modes

The results presented in the previous sections concerned the variations of plate elastic moduli as a function of spaces between lamellas. The presence of lateral spaces influences also the failure modes of regularly spaced CLT, as test results of Chapter 4 show. In addition to the global elastic energy stored in the unit-cell, the homogenization scheme predicts the 3D stress field acting on the unit-cell. The actual stress field generated by bending moment or shear force can be rebuilt according to Equation 4.9 and Equation 4.12. The predicted stress fields on a unit-cell have been successfully compared to a complete 3D FE simulation of the whole panels submitted to 4-points bending but not reported in this work. When computing the stress field generated on the unit-cell by the failure bending moment or shear force found experimentally, the failure stresses σ_{11}^{max} and σ_{13}^{max} presented in Figure 4.23 can be found, since the shear force (R_1) is dominant close to supports and there is pure bending (M_{11}) between loading forces.

Figure 4.23 shows that with the increasing spaces within lateral lamellas, the failure bending stress decreases while the failure transverse shear stress increases. The 4-points bending tests on spaced floors pointed out the transition between tensile parallel to grain failure of longitudinal layers to shear failure of transverse lamellas when enlarging the spaces. Therefore, the predicted longitudinal and shear failure stresses have to be compared to tensile parallel to grain and rolling shear strength values of spruce. The mean tensile strength parallel to grain has been found to be approximately 30 MPa by means of tensile tests on thousands of spruce specimens by Stapel and van de Kuilen (2014); Ranta-Maunus et al (2011). Timber natural variability has a great influence on tensile strength, leading to a great sample size in order to attain a consistent strength value. On the contrary, rolling shear strength is considered to be independent from timber natural variability (Blass and Fellmoser 2004a; Grandvuiet and Muszynski 2016), and mean rolling shear strength of spruce has been found to be 1.6 MPa in Chapter 3 with symmetric double-lap shear test and 1.8 MPa with two-plates shear test by Ehrhart et al (2015).

Table 4.3 summarizes the predicted longitudinal and transverse shear stresses at failure for the three tested configurations of spaced panels.

Dealing with the standard crosslam, the predicted σ_{11}^{max} stress is close to the mean tensile strength of spruce, while the rolling shear failure stress is lower than the respective strength. This is in agreement with the experimental tensile failure of bottom layer. The $s = 150mm$ configuration failed in tension on bottom layer, even if the

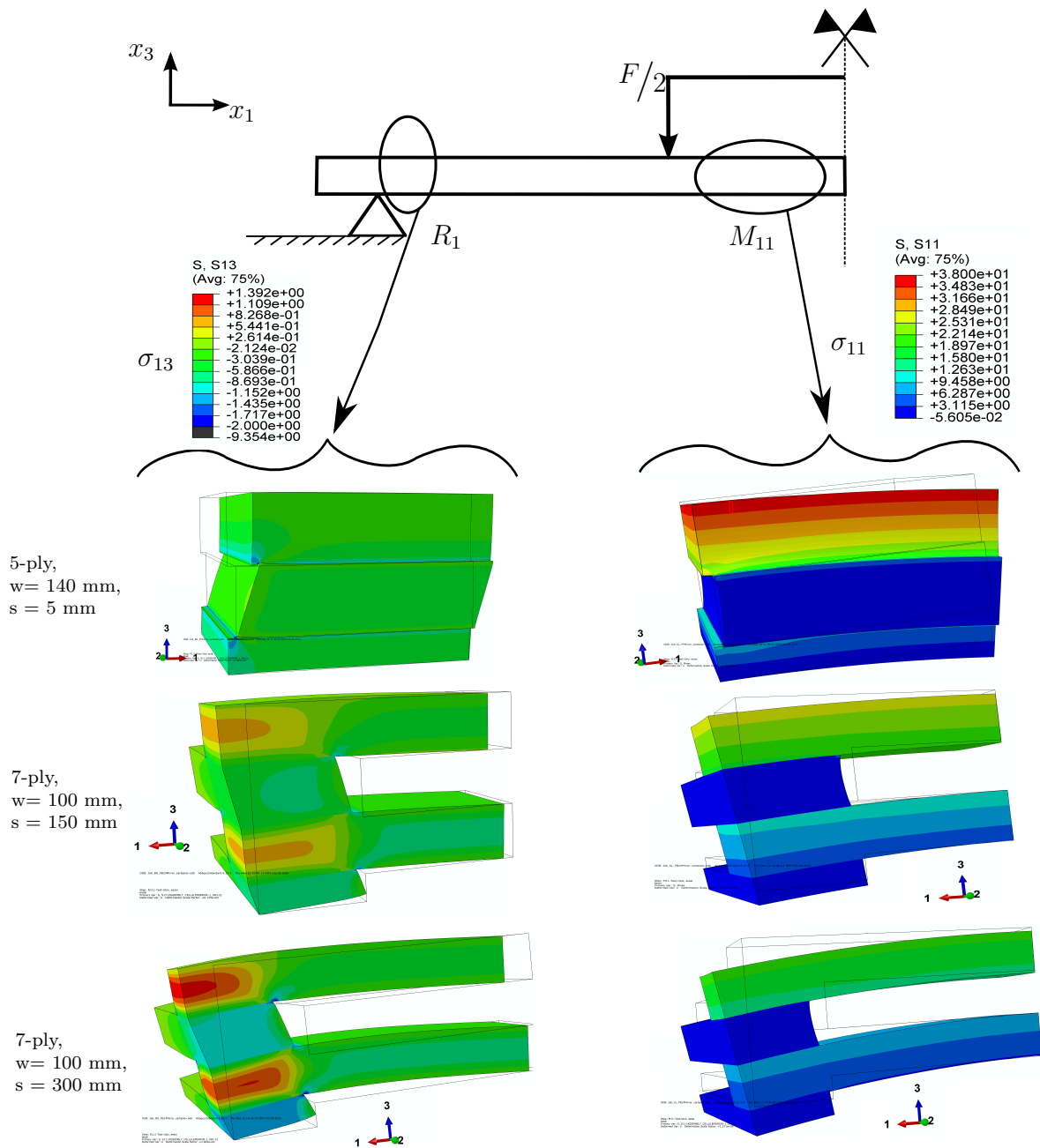


Figure 4.23: Variation of longitudinal σ_{11}^{max} (right) and rolling shear σ_{13}^{max} (left) stresses under experimental failure bending moment M_{11}^{max} and shear force R_1^{max} for the three tested spaces

4. HOMOGENIZATION OF REGULARLY SPACED CLT PANELS

	Predicted σ_{11}^{max} [MPa]	Predicted σ_{13}^{max} [MPa]	Failure mode in tests
$s = 5mm$	38	0.5	TL
$s = 150mm$	25	0.9	TL
$s = 300mm$	18	1.4	RS

Table 4.3: Variation of predicted longitudinal and shear stresses at failure of tested panels and comparison with strength values of literature [MPa]. TL = tensile longitudinal, RS = rolling shear

predicted σ_{11}^{max} decreases and σ_{13}^{max} increases, compared to the standard configuration. This is because of the greater size of knots that led to tensile failure the $s = 150mm$ panel (see Figure 3.5b) compared to the smaller size of knots of standard CLT. Furthermore, standard crosslam is characterized by a “system” effect that increases timber strength thanks to the glued surfaces between upper and lower lamellas, limiting so the propagation of cracks due to local defects (Chapter 2) (Flaig and Blass 2014). This effect is progressively reduced when enlarging the spaces, due to the increasing free unglued parts of upper and lower lamellas, where the cracking of isolated knots is not anymore mitigated. Finally, rolling shear stress predicted at failure of $s = 300mm$ panel in transverse lamellas are very close to rolling shear strength, while the predicted σ_{11}^{max} is lower than the tensile strength. This is in agreement with the experimental shear failure of transverse lamellas of the $s = 300mm$ spaced panel.

4.4 Conclusion

In the present Chapter, the elastic mechanical response of regularly spaced CLT panels has been investigated by means of thin and thick plate homogenization schemes and compared to experimental data and simplified closed-form solutions. Both cases of small gaps allowed in standard panels and large spaces of innovative timber products have been analyzed.

The experimental investigation pointed out the increasing influence of elastic and failure shear effects while enlarging the spaces between lamellas. This motivates the choice of the Bending-Gradient thick plate theory for a precise estimation of shear effects. The plate theory has been applied to the geometry of spaced CLT by means of a periodic homogenization scheme.

When increasing the spaces between lateral lamellas, the reduction of bending stiffness follows exactly the wood volume fraction within the panel. As consequence, the influence of small gaps is very low and the mechanical behavior can be well predicted, even at large spaces, with the Classical Lamination Theory combined with reduced properties by the volume fraction. On the contrary, for in-plane shear and torsion, the reduction of stiffness does not follows the volume fraction and yet at small spaces the reduction of stiffness is significant. This is due to the presence of free edges that

prevents the direct transmission of shear stress and introduces a mechanism of relative rotation between upper and lower lamellas. In some cases, the closed-form solution derived by Moosbrugger et al (2006) cannot precisely reproduce such complex mechanism and therefore the predicted in-plane shear stiffness deviates from the experimental results. However, the plate homogenization returned a good comparison with the in-plane shear test results of Brandner et al (2015). While the investigated parameters of number of layers and lamella's aspect ratio w/h have a negligible influence on the normalized bending stiffness, their influence on normalized in-plane shear and torsional stiffnesses is significant. Indeed, increasing the number of layers and the aspect ratio w/h leads to spaced CLT panels with higher values of in-plane shear and torsional stiffness.

Dealing with transverse shear behavior, the reduction of shear force stiffness while enlarging the spaces cannot be predicted with the volume fraction approach due to an additional compliance mechanism related to simple bending of longitudinal lamellas. Therefore only the homogenization method can well predict the experimental results, while the volume fraction approach strongly overestimates the shear force stiffness. The presence of free edges in spaced crosslam introduces an interaction between rolling shear stress and traction perpendicular to grain, leading to potential mixed failure modes in transverse lamellas, as highlighted by the conducted 4-points bending tests. The influence of the number of layers on the variation of normalized shear force stiffness as a function of spaces is negligible. In standard CLT with small gaps the governing effect is rolling shear of transverse layers and, therefore, the thicker are the lamellas, the more shear compliant the panel is. On the contrary, concerning innovative panels with large spaces, the simple bending of longitudinal layers due to shear force yields stiffer panels when the lamellas are thick.

In addition to the global stiffness of the panel, the homogenization approach can well predict the 3D stress field within the panel. The predicted values of longitudinal and rolling shear failure stresses are in agreement with the experimental variation of failure modes and strength values of literature, even if the natural variability of raw wood has not been taken into account and may be the object of a more accurate modeling.

In some cases, the existing closed-form approaches for predicting spaced CLT mechanical behavior are not appropriate. Nevertheless, the periodic homogenization presented in this Chapter requires the numerical solution of auxiliary problems by means of a FE software, that limits its implementation in practical applications. Hence, the derivation of closed-form solutions for predicting the elastic behavior of spaced CLT panels is the object of the next Chapter.

4. HOMOGENIZATION OF REGULARLY SPACED CLT PANELS

Chapter 5

Closed-form solutions for spaced CLT

Abstract. In this Chapter, closed-form solutions for predicting the elastic behavior of spaced CLT panels are derived. Regularly spaced CLT are modeled as a frame of beams connected each other by means of deformable blocks. Thin and thick plate moduli are then derived based on energy equivalence with a periodic unit-cell. The obtained closed-form solutions return a better agreement with the reference behavior than existing closed-form approaches for in-plane and transverse shear stiffness. Moreover, closed-form expressions for predicting the governing bending and rolling shear stresses in spaced CLT are derived as well.

Résumé. Ce Chapitre présente les formules analytiques qui ont été établies pour prédire le comportement élastique de panneaux CLT espacés. Les CLT espacés sont modélisés comme un réseau de poutres connectées entre elles avec des blocs déformables. Les modules des plaques mince et épaisse sont prédits en s'appuyant sur le principe d'équivalence énergétique avec une cellule élémentaire périodique. Les formules obtenues donnent une meilleure comparaison avec le comportement de référence par rapport à des approches analytiques existantes, en ce qui concerne les raideurs en cisaillement plan et transverse. Enfin, des formules analytiques sont établies pour prédire les contraintes dominantes en flexion et en cisaillement.

5.1 Introduction

The thick-plate homogenization scheme applied in Chapter 5 to regularly spaced CLT returned good agreement with the reference experimental behavior. However, within this method, the resolution of auxiliary problems by means of FE computation is required. This limits the extension of this method to practical applications. Therefore, this Chapter presents the derivation of closed-form solutions to predict the elastic behavior of spaced CLT.

The spaced CLT panel is modeled as a 3D space frame of beams connected each

5. CLOSED-FORM SOLUTIONS FOR SPACED CLT

other with deformable blocks. Following the approach from Lebée and Sab (2013), such space frame can be viewed as a thick plate, and plate moduli can be derived based on energy equivalence with a periodic unit-cell. This is a procedure very similar to the one of Chapter 5, but in this case the simplified geometry of connected beams allows a closed-form derivation of the elastic energy. Indeed, the beam equations can be integrated since they depend only on one coordinate. The loads for the thin space frame analysis are beam displacements and rotations, while the gradient of the bending moment is the load for predicting the shear force stiffness of a thick space frame.

First, the geometry of the space frame and the related notation are presented. Then, thin and thick space frame computations are performed, leading to the derivation of spaced CLT elastic moduli with closed-form expressions. The following section concerns the derivation of simplified closed-form expressions for predicting the bending and rolling shear stresses in spaced CLT. Finally, the elastic behavior estimated with the closed-form solutions is compared to the reference results of homogenization modeling presented in Chapter 5 and existing methods.

5.2 Spaced CLT as beam space frame

Regularly spaced CLT panels can be viewed as a 3D space frame of Timoshenko beams connected each other with deformable blocks (Figure 5.1). The blocks represent the glued parts of upper and lower lamellas, while the beams are the unglued/free parts of lamellas. The space frame of Figure 5.1 is a reproduction along the two directions

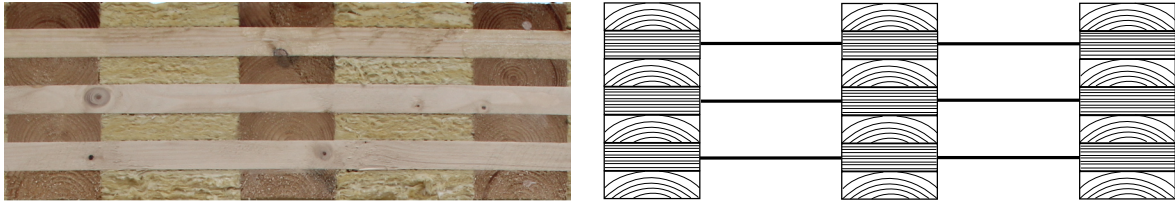


Figure 5.1: Cross section of spaced CLT panel modeled as beam space frame

of elementary unit-cells like the one in Figure 5.2. Each unit-cell is made of N beams connected each others with wooden blocks, where N is the number of CLT layers. There are N_L longitudinal (L) beams and N_T transverse (T) beams, with $N = N_L + N_T$ and $N_L = \frac{N+1}{2}$, $N_T = \frac{N-1}{2}$. The position of each beam with respect to the reference frame of Figure 5.2 is denoted z^i , with $i \in [-\frac{N-1}{2}; \frac{N-1}{2}]$ and the top and bottom beams are always oriented in the longitudinal x_1 direction. The unit-cell has all lamellas with the same thickness h and width w , while the length of the unit-cell is b . The mirror symmetry of beams with respect to the mid-plane is respected, so that $z^i = -z^{-i}$. Each wooden block is defined as the volume $h \cdot w^2$, with respect to Figure 5.3.

The spaced CLT stiffnesses are derived averaging over the surface the strain energy stored in the unit-cell under imposed loads while taking into account its periodicity

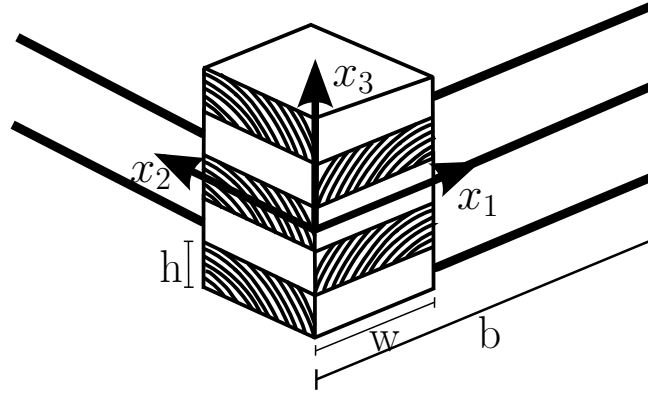


Figure 5.2: Periodic unit-cell of spaced CLT modeled as a space frame of beams connected with wooden blocks

along x_1 and x_2 directions. There are two contributions to the elastic energy of the unit-cell: the energy associated to beams and to the deformable blocks. For thin and thick space frame analyses, both contributions of beams and blocks energy have to be estimated.

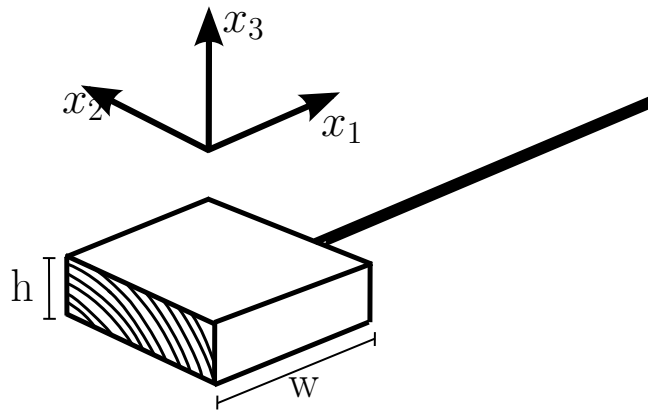


Figure 5.3: Longitudinal layer of a spaced CLT modeled as a wooden block connected to a beam

5.3 Thin space frame

In this section, closed-form solutions for predicting the membrane and bending stiffnesses of spaced CLT are derived. The wooden blocks of the unit-cell in Figure 5.2 are modeled as springs connecting upper and lower beams, deformable only under in-plane rotations and with a rotational stiffness K_θ (Figure 5.4). This in order to reproduce the torsion-like mechanism discussed in Section 4.3.3 that yields relative in-plane rotation of blocks when spaced CLT are submitted to in-plane shear. The modeling of such mechanism as a rotational spring submitted to in-plane rotation is of course a simplification, but it follows the approach of several existing experimental and theoretical approaches (Joebstl et al 2004; Moosbrugger et al 2006).

5. CLOSED-FORM SOLUTIONS FOR SPACED CLT

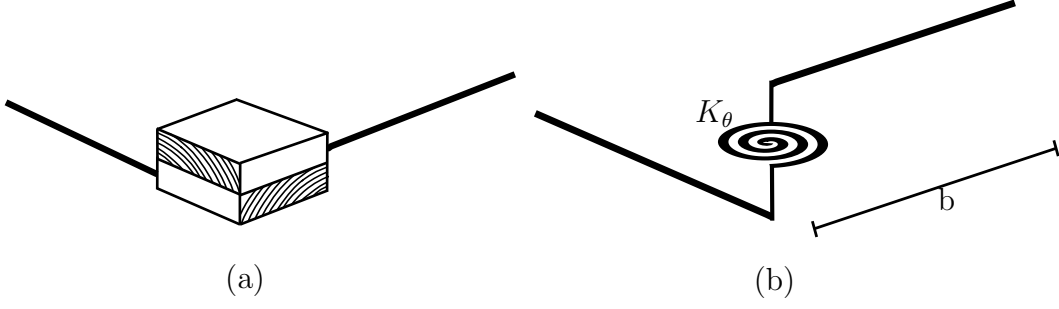


Figure 5.4: Blocks connecting beams (a) and modeled as rotational spring deformable under in-plane rotation (b)

In this case the loads are the relative displacements $\mathbf{u}^{i,ext}$ and the relative rotations $\boldsymbol{\theta}^{ext}$ applied to beams as periodicity conditions:

$$L_{\mathbf{u}}^{b,i} - L_{\mathbf{u}}^{0,i} = L_{\mathbf{u}}^{i,ext} = \begin{pmatrix} b(e_{11} + z^i \chi_{11}) \\ b(e_{12} + z^i \chi_{12}) \\ -b^2 \chi_{11}/2 \end{pmatrix} \quad T_{\mathbf{u}}^{b,i} - T_{\mathbf{u}}^{0,i} = T_{\mathbf{u}}^{i,ext} = \begin{pmatrix} b(e_{12} + z^i \chi_{12}) \\ b(e_{22} + z^i \chi_{22}) \\ -b^2 \chi_{22}/2 \end{pmatrix} \quad (5.1)$$

where L and T stand for the longitudinal and transverse layers. e_{11} and e_{22} are axial membrane strains, χ_{11} and χ_{22} are out-of-plane curvatures, e_{12} is the in-plane shear strain and χ_{12} is the in-plane bending (or torsional) curvature. The superscripts 0 and b in Equation 5.1 stand for the displacement field evaluated respectively at the beginning and the end of beams. These relative displacements are equivalent to those applied in the 3D case on lateral faces of the unit-cell (see Figure 4.5). When dealing with beams, the energy is also carried by the 3D rotation field defined as the skew-symmetric part of the gradient of displacements. Following the approach of (Lebée and Sab 2013), the rotation field must comply with the following periodicity conditions:

$$L_{\boldsymbol{\theta}}^{b,i} - L_{\boldsymbol{\theta}}^{0,i} = L_{\boldsymbol{\theta}}^{i,ext} = \begin{pmatrix} -b\chi_{12} \\ b\chi_{11} \\ 0 \end{pmatrix} \quad T_{\boldsymbol{\theta}}^{b,i} - T_{\boldsymbol{\theta}}^{0,i} = T_{\boldsymbol{\theta}}^{i,ext} = \begin{pmatrix} -b\chi_{22} \\ b\chi_{12} \\ 0 \end{pmatrix} \quad (5.2)$$

Figure 5.5 shows the applied loads for the thin space frame analysis.

5.3.1 Energy of connected beams

In Chapter 5, the elastic energy of a 3D unit-cell has been predicted with FE computation. Such 3D energy can be written as:

$$W^{3D} = \frac{1}{2} \int_{\Omega} (\boldsymbol{\epsilon}^{3D} : \mathbf{C} : \boldsymbol{\epsilon}^{3D}) d\Omega \quad (5.3)$$

where $\boldsymbol{\epsilon}^{3D}$ are the 3D strains, \mathbf{C} is the material stiffness tensor and Ω is volume of the unit-cell. Dealing with a unit-cell made of connected beams, if $(\mathbf{t}, \mathbf{n}, \mathbf{v})$ is the local reference frame of each beam associated to the coordinate (s_1, s_2, s_3) , the contribution

5.3 Thin space frame

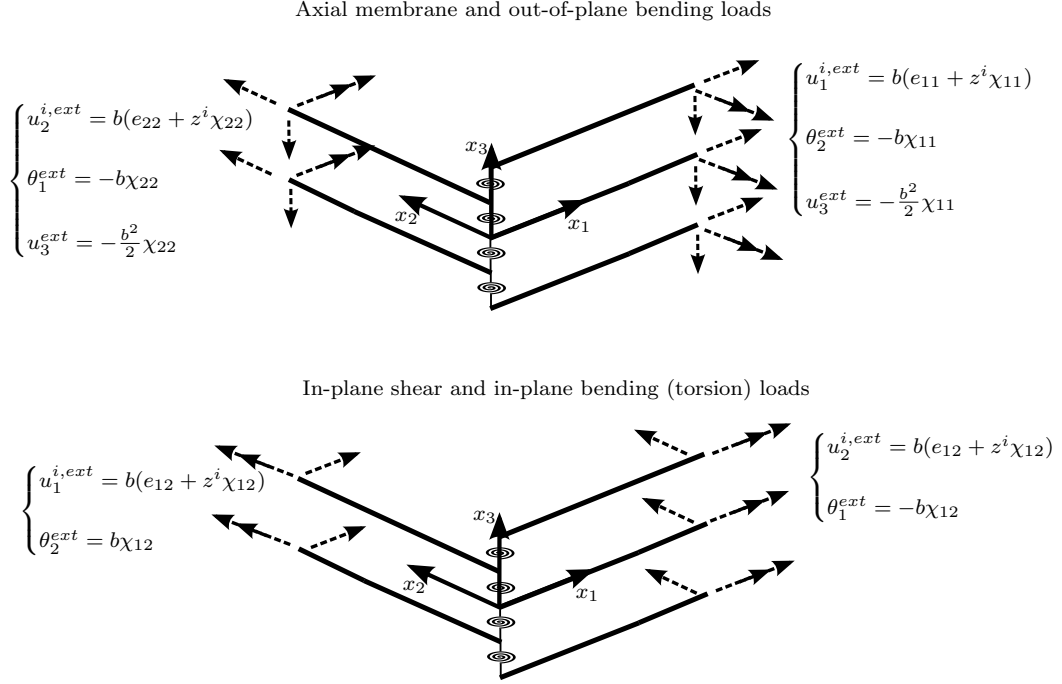


Figure 5.5: Unit loads for the thin space frame analysis on a 5-ply unit-cell of spaced CLT imposed as displacement and rotation boundary conditions

of each beam to the elastic energy of the unit-cell can be written as:

$$W^i(\mathbf{u}^i, \boldsymbol{\theta}^i) = \int_0^b \frac{1}{2} (\boldsymbol{\gamma}^i \cdot \mathbf{F}^i \cdot \boldsymbol{\gamma}^i + \boldsymbol{\kappa}^i \cdot \mathbf{H}^i \cdot \boldsymbol{\kappa}^i) ds_1 \quad (5.4)$$

where \mathbf{u}^i and $\boldsymbol{\theta}^i$ are respectively the displacement and rotation fields of each beam, $\boldsymbol{\gamma}^i = (\mathbf{u}^{i'} + \mathbf{t}^i \times \boldsymbol{\theta}^i)$ is the vector containing the axial strain and shear distortions of the beam and $\boldsymbol{\kappa}^i = \boldsymbol{\theta}^{i'}$ is the beam's curvature. Here $'$ denotes the derivative with the respect to s_1 coordinate and \times is the cross product. In the beam local reference frame, the beam stiffness tensors \mathbf{F}^i and \mathbf{H}^i are defined as:

$$\mathbf{F} = \begin{bmatrix} ES & 0 & 0 \\ 0 & GS_2 & 0 \\ 0 & 0 & GS_3 \end{bmatrix} \quad (5.5)$$

$$\mathbf{H} = \begin{bmatrix} GJ & 0 & 0 \\ 0 & EI_2 & 0 \\ 0 & 0 & EI_3 \end{bmatrix} \quad (5.6)$$

where E is the longitudinal Young's modulus (E_L), G the longitudinal shear modulus ($G_{LZ}=G_{LN}$), $S = w \cdot h$ is the section area, $S_2 = S_3 = 5/6 \cdot w \cdot h$ are the shear areas and $I_2 = \frac{h^3 \cdot w}{12}$ and $I_3 = \frac{w^3 \cdot h}{12}$ are the second moments of inertia. J is the torsion constant defined as

$$J = w/2 \cdot (h/2)^3 \cdot (16/3 - 3.36 \cdot (h/w) \cdot (1 - (h/w)^4/12))$$

5. CLOSED-FORM SOLUTIONS FOR SPACED CLT

. Since the beam constitutive equations for translations and rotations are:

$$\begin{cases} \mathbf{r}^i = \mathbf{F}^i \cdot (\mathbf{u}^{i'} + \mathbf{t}^i \times \boldsymbol{\theta}^i) \\ \mathbf{m}^i = \mathbf{H}^i \cdot \boldsymbol{\theta}^{i'} \end{cases} \quad (5.7)$$

where \mathbf{r}^i and \mathbf{m}^i are respectively beams' resultant forces and bending moments, it is possible to rewrite Equation 5.4 as:

$$W^i(\mathbf{u}^i, \boldsymbol{\theta}^i) = \int_0^b \frac{1}{2} ({}^t\mathbf{r}^i \cdot \mathbf{F}^{i-1} \cdot \mathbf{r}^i + {}^t\mathbf{m}^i \cdot \mathbf{H}^{i-1} \cdot \mathbf{m}^i) ds_1 \quad (5.8)$$

with $\mathbf{r}^i(\mathbf{u}^i, \boldsymbol{\theta}^i)$ and $\mathbf{m}^i(\mathbf{u}^i, \boldsymbol{\theta}^i)$. Now the stress state of beams will be exactly derived in order to evaluate the contribution of each beam expressed by Equation 5.8. The beam equilibrium equations are:

$$\begin{cases} \mathbf{r}^{i'} = 0 \\ \mathbf{m}^{i'} + \mathbf{t}^i \times \mathbf{r}^i = 0 \end{cases} \quad (5.9)$$

Integrating equations 5.9 leads to constant resultants and linear moments:

$$\mathbf{r}^i = \mathbf{r}^{0,i} \quad \mathbf{m}^i = \mathbf{m}^{b/2,i} - \mathbf{t} \times \mathbf{r}^{0,i}(s_1 - b/2) \quad (5.10)$$

where $\mathbf{r}^{0,i} = \mathbf{r}^i(s_1 = 0)$ and $\mathbf{m}^{b/2,i} = \mathbf{m}^i(s_1 = b/2)$ are integration constants taken at $s_1 = 0$ and $s_1 = b/2$ respectively. Therefore finding $\mathbf{r}^{0,i}$ and $\mathbf{m}^{b/2,i}$ leads the complete stress state of beams. Substituting equations 5.10 into the constitutive equations 5.7 and integrating at $s_1 = 0$ yields:

$$\boldsymbol{\theta}^i - \boldsymbol{\theta}^{0,i} = \mathbf{H}^{i-1} \left(\mathbf{m}^{b/2,i} s_1 + \mathbf{t} \times \mathbf{r}^{0,i} \frac{s_1(s_1 - b)}{2} \right) \quad (5.11)$$

Rewriting the above expression for $s_1 = b$ yields the left term equal to $\boldsymbol{\theta}^i(b) - \boldsymbol{\theta}^i(0)$. This difference is equal to the imposed rotation field $\boldsymbol{\theta}^{ext}$ (Equation 5.2). Therefore $\mathbf{m}^{b/2,i}$ is:

$$\mathbf{m}^{b/2,i} = \frac{\mathbf{H}^i \cdot \boldsymbol{\theta}^{ext,i}}{b} \quad (5.12)$$

The same procedure can be done substituting the expression of $\boldsymbol{\theta}^i$ found in Equation 5.11 into the constitutive equation of displacements, leading to the following expression of $\mathbf{r}^{0,i}$:

$$\mathbf{r}^{0,i} = \mathbf{P}^i \cdot [\mathbf{u}^{ext,i} + \mathbf{t}^i \times (\boldsymbol{\theta}^{0,i} b + \frac{b}{2} \boldsymbol{\theta}^{ext,i})] \quad (5.13)$$

where the operator \mathbf{P}^i is, in the local reference frame:

$$\mathbf{P}^i = \begin{pmatrix} ES^{-1} & 0 & 0 \\ 0 & \alpha_2 & 0 \\ 0 & 0 & \alpha_3 \end{pmatrix} \quad (5.14)$$

with $\alpha_2 = \frac{b}{GS_2} + \frac{b^3}{12EI_3}$ and $\alpha_3 = \frac{b}{GS_3} + \frac{b^3}{12EI_2}$. Now that the resultant forces and moments of beams are determined, it is possible to write the contribution of each beam "i" to

the potential energy of the unit-cell as:

$$W^{i,thin} = \frac{1}{2} \left[{}^t \left[\mathbf{u}^{i,ext} + \mathbf{t}^i \times \left(\boldsymbol{\theta}^{0,i} b + \frac{b}{2} \boldsymbol{\theta}^{ext,i} \right) \right] \cdot \mathbf{P}^i \cdot \left[\mathbf{u}^{i,ext} + \mathbf{t}^i \times \left(\boldsymbol{\theta}^{0,i} b + \frac{b}{2} \boldsymbol{\theta}^{ext,i} \right) \right] + \right. \\ \left. + \frac{1}{b} {}^t \boldsymbol{\theta}^{ext,i} \cdot \mathbf{H}^i \cdot \boldsymbol{\theta}^{ext,i} \right] \quad (5.15)$$

in which the unknowns are the rotation constants $\boldsymbol{\theta}^{0,i}$.

5.3.2 Derivation of the spaced CLT stiffnesses

The unknown kinematic variables are derived minimizing the total potential energy of the unit-cell, leading to the explicit closed-form expression of the unit-cell elastic energy. In order to obtain the unit-cell total potential energy, the contribution of deformable wooden blocks modeled as rotational springs has to be added to the contribution of beams:

$$W^{total,thin}(\mathbf{u}^{0,i}, \boldsymbol{\theta}^{0,i}) = \sum_{i=-(N-1)/2}^{(N-1)/2} W^{i,thin} + \frac{1}{2} \sum_{j=-(N-1)/2}^{(N-3)/2} K_{\theta} (\theta_3^{0,j+1} - \theta_3^{0,j})^2 \quad (5.16)$$

where K_{θ} is the rotational stiffness of the springs and $(\theta_3^{0,j+1} - \theta_3^{0,j})$ is the relative in-plane rotation of beams at their interface that corresponds to the relative in-plane rotation between upper and lower blocks. Since the connection between beams has been modeled as a spring deformable only under in-plane rotations (Figure 5.4a), the beam displacements $\mathbf{u}^{0,i}$ and out-of-plane rotations $\theta_1^{0,i}$ and $\theta_2^{0,i}$ at beams' interfaces $s_1 = 0$ are equal for all beams. This means that such kinematic variables represent rigid translations and rotations of the whole unit-cell that do not contribute to the potential energy. Therefore these variables can be set to zero when minimizing the potential energy. This means that the only kinematic variable that is unknown is the in-plane rotation $\theta_3^{0,i}$. Hence, the minimization problem can be written as:

$$\min_{\theta_3^{0,i} \in \mathbb{R}^N} W^{total, thin}(\theta_3^{0,i}) \quad (5.17)$$

The N in-plane rotations of beams at their interfaces are the only unknown variables to find with the minimization problem 5.17 in order to obtain a closed-form expression of the unit-cell elastic energy. Finally, membrane \mathbf{A} and bending \mathbf{D} moduli of spaced CLT as thin space frame are evaluated averaging over the unit-cell surface the energy associated to membrane strains and curvatures:

$$\frac{1}{2} ({}^t \mathbf{e} : \mathbf{A} : \mathbf{e}) = \frac{1}{b^2} W^{(e)total, thin} \quad \frac{1}{2} ({}^t \boldsymbol{\chi} : \mathbf{D} : \boldsymbol{\chi}) = \frac{1}{b^2} W^{(\chi)total, thin} \quad (5.18)$$

where \mathbf{e} are the imposed membrane strains and $\boldsymbol{\chi}$ the imposed curvatures.

5. CLOSED-FORM SOLUTIONS FOR SPACED CLT

5.3.3 Membrane and bending stiffness of spaced CLT

Substituting the imposed displacement and rotation fields into Equations 5.13, 5.12 and 5.10, the stress state of beams under symmetric membrane e_{11} e_{22} strains and out-of-plane curvatures χ_{11} χ_{22} strains can be directly derived, since it does not depend on the unknown in-plane rotations $\theta_3^{0,i}$. The only non zero axial resultant force r_1^i and out-of-plane moment m_2^i of L and T beams write, in the local reference frame of beams:

$$\text{L beams} \begin{cases} r_1^i = ES(e_{11} + z^i \chi_{11}) \\ m_2^i = EI_2 \chi_{11} \end{cases} \quad (5.19)$$

$$\text{T beams} \begin{cases} r_1^i = ES(e_{22} + z^i \chi_{22}) \\ m_2^i = EI_2 \chi_{22} \end{cases} \quad (5.20)$$

which are very similar to those found in (Lebée and Sab 2013). Applying Equation 5.18 separately to the contribution of membrane strains and curvatures leads the following closed-form expressions for spaced CLT membrane A_{11} and out-of-plane bending D_{11} stiffnesses along the x_1 direction:

$$A_{11} = N_L \frac{ES}{b} \quad (5.21)$$

$$D_{11} = N_L \frac{EI_2}{b} + \frac{ES}{b} \sum_L z_i^2 = \frac{Eh^3 w}{24b} (N+1)(N^2 + 2N - 2) \quad (5.22)$$

where the sum \sum_L operates only on longitudinal beams. The result is rather intuitive: the bending stiffness D_{11} is a contribution of the N_L longitudinal beams bending stiffness EI_2 and the transport term related to the position of each longitudinal beam with respect to the neutral axis. This is also the principle of the Classical Lamination Theory, upon which many design methods are based (for instance, the shear analogy method (Kreuzinger 1999) or the gamma method (EN1995-1-1 2004)). The contribution of transverse beams to spaced CLT bending stiffness is not taken into account by Equation 5.22, due to the negligible influence of transverse layers on CLT bending behavior. In the same way, only the longitudinal beams contribute to the membrane stiffness A_{11} . The derived closed-form expressions for bending and membrane stiffness are divided by the unit-cell length b , which is equivalent of applying volume fraction to the stiffness of a massive CLT panel. Indeed, when $b = w$, Equations 5.21 and 5.22 return the bending stiffnesses of a massive crosslam panel. Therefore, the derived closed-form solutions for spaced CLT bending and membrane stiffness are exactly the volume fraction approach that was found to return the same homogenization results (see Section 4.3.1). The same procedure can be applied for the membrane and out-of-plane bending stiffness along x_2 direction (A_{22} and D_{22}), leading to similar expressions of Equations 5.21 and 5.22 considering the T transverse beams instead of the longitudinal beams:

$$A_{22} = N_T \frac{ES}{b} \quad D_{22} = \frac{Eh^3 N}{24b} (N-1)(N^2 - 2N - 2) \quad (5.23)$$

Finally, the in-plane A_{12} and out-of-plane D_{12} Poisson's effects predicted with the obtained closed-form solutions are null: $A_{12} = D_{12} = 0$.

5.3.4 In-plane shear and torsional stiffness of spaced CLT

The stress state of L and T beams associated to skew-symmetric loads of in-plane shear e_{12} strain and in-plane bending (or torsional) curvature χ_{12} from Equation 5.13 depends on the unknown in-plane rotations $\theta_3^{0,i}$. In the local reference frame of L and T beams the stress state is written:

$$\text{L beams} \begin{cases} r_2^i = \frac{b}{\alpha_2} [(e_{12} + z^i \chi_{12}) - \theta_3^{0,i}] \\ m_1^i = -GJ\chi_{12} \\ m_3^i = r_2^i (s_1 - \frac{b}{2}) \end{cases} \quad (5.24)$$

$$\text{T beams} \begin{cases} r_2^i = \frac{b}{\alpha_2} [-(e_{12} + z^i \chi_{12}) - \theta_3^{0,i}] \\ m_1^i = -GJ\chi_{12} \\ m_3^i = r_2^i (s_1 - \frac{b}{2}) \end{cases} \quad (5.25)$$

Therefore, the unit-cell potential energy associated to in-plane shear and torsional loads also depends on the unknown rotations $\theta_3^{0,i}$. Minimizing the functional 5.16 with respect to the unknowns $\theta_3^{0,i}$ leads to the identification of a linear system of N equations that can be solved. However, solving such system with a closed-form approach is not straightforward. Nevertheless, for 3-ply and 5-ply configurations there are few variables and closed-form expressions of $\theta_3^{0,i}$ and therefore of the in-plane shear A_{33} and torsional D_{33} stiffnesses can be found. For a 3-ply we have:

$$A_{33}^{3ply} = \frac{4K_\theta}{3\alpha_2 K_\theta + b^2} \quad D_{33}^{3ply} = \frac{3GJ}{2b} + \frac{h^2 K_\theta}{\alpha_2 K_\theta + b^2} \quad (5.26)$$

and for a 5ply:

$$A_{33}^{5ply} = \frac{4}{\alpha_2} \left[\frac{(28\beta^2 + 40\beta + 15) + 2\beta(8\beta^2 + 12\beta + 5)}{(4\beta^2 + 10\beta + 5)^2} \right] \quad (5.27)$$

$$D_{33}^{5ply} = \frac{5GJ}{2b} + \frac{5h^2}{\alpha_2} \left[\frac{(20\beta^2 + 8\beta + 1) + 2\beta(8\beta^2 + 4\beta + 1)}{(4\beta^2 + 6\beta + 1)^2} \right] \quad (5.28)$$

where $\beta = \frac{b^2}{2\alpha_2 K_\theta}$.

Simplified general expressions of spaced CLT in-plane shear and torsional stiffnesses can be derived as the sum of compliances of the two limit cases when the dominant regime is either the spring or the beam regime. For instance, substituting $K_\theta \gg 1/\alpha_2$ in the expression of stiffnesses found for 3-ply and 5-ply means finding the limit case when the interfaces between beams are clamped connections ($\theta_3^{0,i+1} - \theta_3^{0,i} = 0$) and there is no contribution of blocks. This represents the case when the spaces are very large and the deformation energy of the blocks can be neglected (Figure 5.6a) compared to the contribution of beams. In the same way, when the beam stiffness $1/\alpha_2$ is large

5. CLOSED-FORM SOLUTIONS FOR SPACED CLT

compared to K_θ , the contribution of beams is neglected, that corresponds to the case of small spaces where the short beams can be considered to be rigid (Figure 5.6b) and only the blocks contribute to the energy. Under the conditions $K_\theta \gg 1/\alpha_2$ or

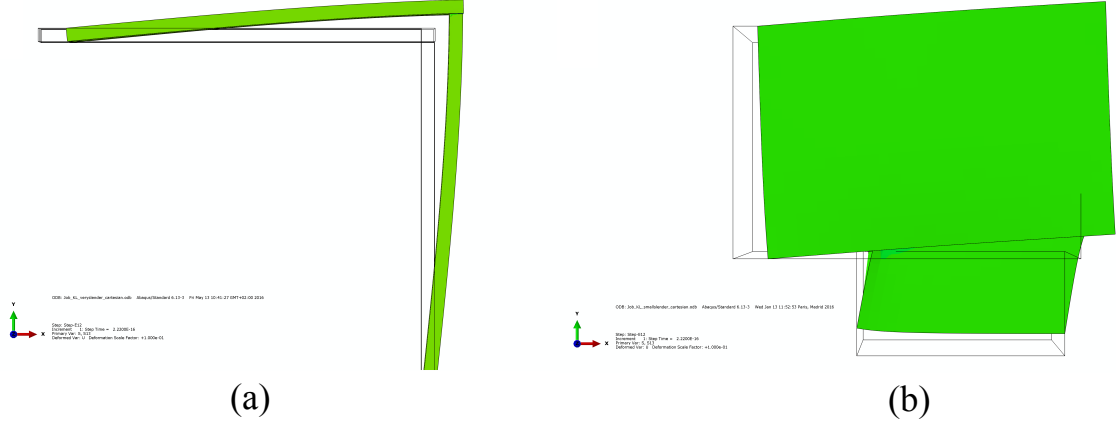


Figure 5.6: FE deformed of limit cases of a spaced CLT unit-cell under in-plane shear: (a) beam regime at large spaces ($K_\theta = \infty$) and (b) blocks regime at short spaces ($\alpha = 0$)

$K_\theta \ll 1/\alpha_2$, the minimization of problem 5.17 with respect to $\theta_3^{0,i}$ is straightforward and leads to:

$$A_{33} = \begin{cases} \frac{N^2-1}{2N\alpha_2} & \text{if } K_\theta \gg 1/\alpha_2 \\ \frac{2(N-1)K_\theta}{b^2} & \text{if } K_\theta \ll 1/\alpha_2 \end{cases} \quad (5.29)$$

$$D_{33} = \begin{cases} \frac{24\alpha_2}{Nh^2(N^2-1)} & \text{if } K_\theta \gg 1/\alpha_2 \\ \frac{6b^2}{NK_\theta h^2(N-2)(N-1)} & \text{if } K_\theta \ll 1/\alpha_2 \end{cases} \quad (5.30)$$

Computing the sum of compliances of these two limit cases yields the following simplified closed-form solutions for in-plane shear stiffness of spaced CLT as a function of N :

$$A_{33} = (N-1) \left(\frac{b^2}{2K_\theta} + \frac{2N\alpha}{N+1} \right)^{-1} \quad (5.31)$$

The same procedure can be applied for torsional stiffness of spaced CLT leading to:

$$D_{33} = \frac{NGJ}{2b} + \frac{Nh^2(N-1)}{6} \left(\frac{b^2}{K_\theta(N-2)} + \frac{4\alpha}{N+1} \right)^{-1} \quad (5.32)$$

In-plane shear of wooden blocks Until now, the expression of the rotational stiffness K_θ has not been yet established. As already introduced, when such stiffness is large compared to $1/\alpha_2$, the wooden blocks are modeled as clamped connections that prevent relative in-plane rotations. This situation corresponds to laterally glued panels, where the mechanism of relative in-plane rotation between upper and lower layers is not present. However, laterally glued crosslam are submitted to gross in-plane shear over all the cross section, and such mechanism is not taken into account by the rotational

5.4 Thick space frame

spring. The gross in-plane shear of wooden blocks can be taken into account introducing a correction factor on the beam length b . Indeed, when $K_\theta = \infty$ and $b = w$ Equation 5.31 should return the in-plane shear stiffness of a massive crosslam panel having glued lateral lamellas: $A_{33}^{full} = 2G_{LN}Nh$. This is possible only when introducing the beam compliance $\alpha_2^* = \frac{b-x}{GS_2} + \frac{(b-w)^3}{12EI_3}$ with a correction on the beam length. Moreover, since the term related to in-plane bending $\frac{(b-w)^3}{12EI_3}$ has to vanish when the lateral lamellas are glued ($b = w$), the beam length under in-plane bending is set at $b - w$. In order to find the correction x , the following relation has to be satisfied:

$$\left(\frac{2N \frac{w-x}{GS_2}}{N^2 - 1} \right)^{-1} = 2G_{LN}Nh \quad (5.33)$$

where the left term is Equation 5.31 substituting $K_\theta = \infty$ and $b = w$. Considering a great number of layers of spaced CLT ($N = \infty$) in order to overcome the influence of upper and lower free edges, one find that Equation 5.33 yields the correction on the beam length under in plane shear $x = 19w/24$, and therefore the corrected value $\alpha_2^* = \frac{b-19w/24}{5wh/6} + \frac{(b-w)^3}{w^3h}$ has to be used in Equations 5.31 and 5.32. The same correction can be found when applying the same procedure to the expressions of torsional stiffness of Equation 5.32.

The expression of the rotational stiffness K_θ to use with the derived equations has been found within the available literature. The mechanical behavior of two orthogonally glued wooden lamellas under relative in-plane rotation has been object of several experimental and theoretical studies (Blass and Goerlacher 2002; Joebstl et al 2004; Moosbrugger et al 2006). In particular, Moosbrugger et al (2006) considered the spaced CLT in-plane shear stiffness reduced by this compliance mechanism when the lateral lamellas are not glued (Figure 5.7) and suggested the following expression for the in-plane stiffness associated to such mechanism:

$$G_{LN}^* = \frac{G_{LN}}{3G_{eff}} \left(\frac{w}{h} \right)^2 \quad (5.34)$$

where $G_{eff} = \frac{G_{LN} + G_{ZN}}{2}$ is the mean between the plane and rolling shear moduli. Therefore, this expression is dependent on the lamella's aspect ratio and also on rolling shear modulus of wood, confirming the results of (Jeitler 2004). In order to adapt this approach to our case, expression 5.34 is modified to represent a rotational spring stiffness of a wooden block having volume $w^2 \cdot h$ with:

$$K_\theta = G_{LN}^* h w^2 = \frac{2G_{LN}w^4}{3h(G_{LN} + G_{ZN})} \quad (5.35)$$

5.4 Thick space frame

In this section, a closed-form expression for predicting the shear force compliance of spaced CLT is derived. The complete unit-cell of Figure 5.2 is considered, without any

5. CLOSED-FORM SOLUTIONS FOR SPACED CLT

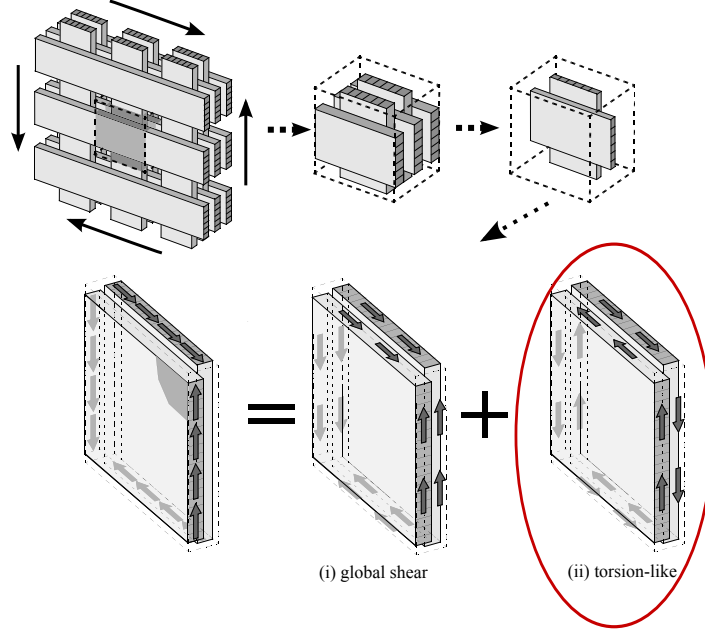


Figure 5.7: Torsion-like mechanism of glued lamellas in spaced CLT (Moosbrugger et al 2006)

simplified modeling of wooden blocks. This leads to impose a 3D shear kinematics to the whole block and deriving its contribution to the strain energy. In this section, the Bending-Gradient plate theory already presented in Chapter 4 is applied, considering the space frame as a thick plate. Therefore, as in Chapter 4, the imposed load is a body force deriving from a uniform gradient of the bending moment. In the case of beam space frame, this body force defined in Equation 4.10 has to be transformed in beam loadings. The unit bending stress $\mathbf{s}^{(\chi)}$ of Equation 4.10 has been derived in terms of beam resultant forces and moments by Equations 5.19 and 5.24, when applying unit curvature ($\chi = 1$) and unit membrane strains ($\mathbf{e} = 1$). Applying Equation 4.9 with such stress field yields the unit stress field $\mathbf{r}^{(M)}, \mathbf{m}^{(M)}$ generated by a uniform bending moment \mathbf{M} . As in Chapter 4, such bending moment is considered to vary linearly in the (x_1, x_2) -plane $\mathbf{M} = \mathbf{R} \cdot \mathbf{x}$ and therefore the Bending-Gradient stress field can be expressed in terms of beam resultant forces and moments as a function of \mathbf{R} and \mathbf{x} . The generalized shear force \mathbf{R} is a third-order tensor having six components ($R_1, R_2, R_3, R_4, R_5, R_6$) (see Section 4.2.3). As suggested by Lebée and Sab (2013), inserting the Bending-Gradient beam stress field in the beam equilibrium equations 5.9 points out that beam distributed loadings \mathbf{q} and \mathbf{l} appear in order to ensure the equilibrium.

The following beam distributed forces \mathbf{q} for L and T beams can be found, expressed in the local beam reference frame:

$${}^L \mathbf{q}^i = \begin{pmatrix} z^i E S D_{11}^{-1} R_1 \\ \rho^i (\sqrt{2} D_{33})^{-1} R_3 \\ 0 \end{pmatrix} \quad (5.36)$$

$${}^T \mathbf{q}^i = \begin{pmatrix} z^i E S D_{22}^{-1} R_5 \\ \rho^i (\sqrt{2} D_{33})^{-1} R_6 \\ 0 \end{pmatrix} \quad (5.37)$$

where ρ^i are the resultant forces of beams associated to a unit torsional curvature $\chi_{12} = 1$ (see Equations 5.24 and 5.25). Moreover, the distributed torques \mathbf{l}^i acting on each beam having length $d = b - w$ are derived as $\mathbf{l}^i = \mathbf{l}^{d/2,i} + \mathbf{t}^i \times \mathbf{q}^i (s_1 - d/2)$, where

$$L \mathbf{l}^{d/2,i} = \begin{pmatrix} -GJ(\sqrt{2} D_{33})^{-1} R_3 \\ EI_2 D_{11}^{-1} R_1 \\ 0 \end{pmatrix} \quad (5.38)$$

$$T \mathbf{l}^{d/2,i} = \begin{pmatrix} GJ(\sqrt{2} D_{33})^{-1} R_6 \\ EI_2 D_{22}^{-1} R_5 \\ 0 \end{pmatrix} \quad (5.39)$$

in the beam local reference frame. Figure 5.8 shows the applied loads to a unit-cell of spaced CLT, considering the whole wooden blocks that connects the beams, leading to set the beam's length d as $d = b - w$.

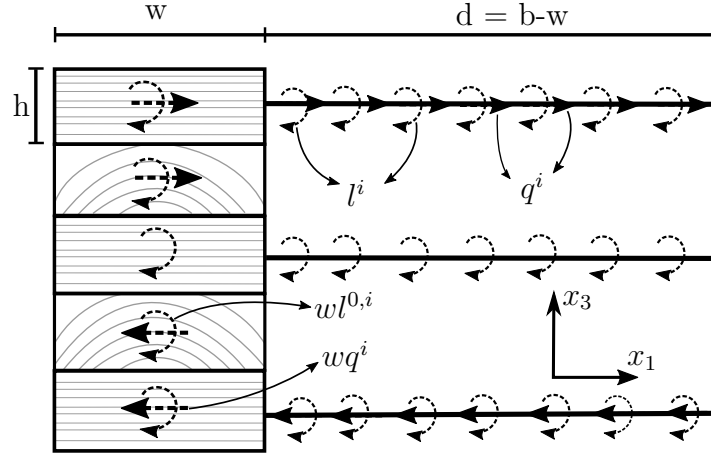


Figure 5.8: Unit loads for the thick space frame analysis on a 5-ply unit-cell of spaced CLT

5.4.1 Transverse shear kinematics of blocks and related energy

In order to derive the contribution of wooden blocks to the shear force compliance of spaced CLT, a transverse shear kinematics is imposed to the blocks and presented in Figure 5.9 for the “1-3” shear direction (plane $x_2 = 0$), where half of upper and lower blocks are showed. Basically the shear kinematics is a superposition of horizontal and vertical slips of wooden blocks. The displacement field associated to such kinematic showed in Figure 5.9 is:

$${}^T \mathbf{u} \begin{cases} u_1^{i+1} = U_1^{0,i+1} + {}^T k_1^{i,i+1} x_3 \\ u_3^{i+1} = U_3^{0,i+1} - \varphi_2^{i+1} x_1 \end{cases} \quad (5.40)$$

5. CLOSED-FORM SOLUTIONS FOR SPACED CLT

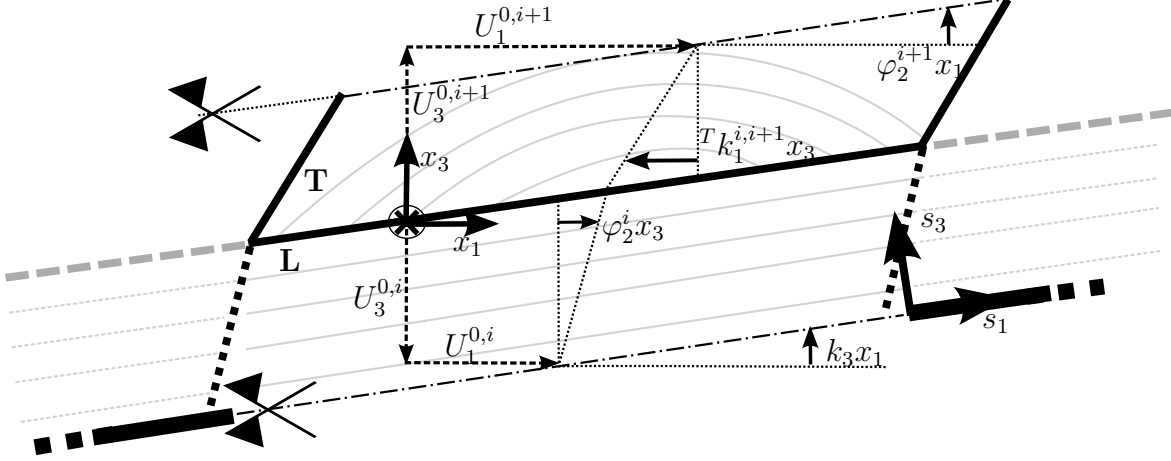


Figure 5.9: Transverse shear kinematic in plane $x_2=0$ of the interface made by half upper and lower blocks

$${}^L \mathbf{u} \begin{cases} u_1^i = U_1^{0,i} + \varphi_2^i x_3 \\ u_3^i = U_3^{0,i} - k_3 x_1 \end{cases} \quad (5.41)$$

where $\mathbf{U}^{0,i}$ are the displacements of the blocks' center of gravity. The transverse shear strain of each block can be obtained as $2\varepsilon_{13}^i = \frac{\partial u_1^i}{\partial x_3} + \frac{\partial u_3^i}{\partial x_1}$. The slip coefficient ${}^T k_1^{i,i+1}$ in Figure 5.9 is to be determined and k_3 is a slip coefficient representing the inclination of all blocks. Imposing the continuity of vertical displacements u_3^i at the interface enforces

$$U_3^{0,i} = U_3^{0,i+1} \quad \text{and} \quad \varphi_2^{i+1} = k_3 \quad (5.42)$$

meaning that a relative out-of-plane displacement between blocks is not permitted and that all transverse blocks rotate equally to the inclination of all blocks $\varphi_2^{i+1} \hat{=} {}^T \varphi_2$. The same occurs for the longitudinal blocks dealing with the shear direction “2-3”, leading to:

$$\begin{cases} \varphi_2^i \hat{=} {}^T \varphi_2 & \text{if } i \in \text{T blocks} \\ \varphi_1^i \hat{=} {}^L \varphi_1 & \text{if } i \in \text{L blocks} \end{cases} \quad (5.43)$$

Imposing the continuity of horizontal displacement field $u_1^i = u_1^{i+1}$ at blocks interface, yields the derivation of the unknown slip coefficient ${}^T k_1^{i,i+1}$:

$$\frac{h}{2} \varphi_2^i + U_1^{0,i} = \frac{h}{2} {}^T k_1^{i,i+1} + U_1^{0,i+1} \quad (5.44)$$

and therefore:

$${}^T k_1^{i,i+1} = \frac{2}{h} (U_1^{0,i+1} - U_1^{0,i}) - \varphi_2^i \quad (5.45)$$

Now the transverse shear strain $2 {}^L \varepsilon_{13}^{i,i+1}$ of L blocks at interfaces can be evaluated as:

$$2 {}^L \varepsilon_{13}^{i,i+1} = \frac{\partial {}^L u_1^i}{\partial x_3} + \frac{\partial {}^L u_3^i}{\partial x_1} = \varphi_2^{i+1} - \varphi_2^i \quad (5.46)$$

and, in the same way, for the T blocks:

$$2 {}^T \varepsilon_{13}^{i,i+1} = {}^T k_1^{i,i+1} - \varphi_2^{i+1} = \frac{2}{h} (U_1^{0,i+1} - U_1^{0,i}) - \varphi_2^{i+1} - \varphi_2^i \quad (5.47)$$

5.4 Thick space frame

When the positions of longitudinal and transverse blocks in Figure 5.9 are switched, the sign of the term related to relative displacements at the interface in Equation 5.47 becomes negative: $-\frac{2}{h}(U_1^{0,i+1} - U_1^{0,i})$.

Once the transverse shear strains along shear direction “1-3” are estimated, the interface strain energy can be evaluated as the sum of half volume strain energy of longitudinal and transverse blocks:

$$W^{i,i+1(1-3)}(\mathbf{U}^i, \varphi_2^i) = \frac{1}{2} \frac{hw^2}{2} [G_{LZ}(2 \varepsilon_{13}^{L,i,i+1})^2 + G_{ZN}(2 \varepsilon_{13}^{T,i,i+1})^2] \quad (5.48)$$

which becomes, substituting the derived shear strains 5.47 and 5.46:

$$W^{i,i+1(1-3)}(\mathbf{U}^j, \varphi_2^i) = \frac{1}{2} \frac{hw^2}{2} [G_{LZ}(\varphi_2^{i+1} - \varphi_2^i)^2 + G_{ZN}(\frac{2}{h}(U_1^{0,i+1} - U_1^{0,i}) - \varphi_2^{i+1} - \varphi_2^i)^2] \quad (5.49)$$

The same derivation of transverse shear strain and associated energy can be performed for the shear direction “2-3”, leading to:

$$W^{i,i+1(2-3)}(\mathbf{U}^j, \varphi_1^i) = \frac{1}{2} \frac{hw^2}{2} [G_{LZ}(\varphi_1^{i+1} - \varphi_1^i)^2 + G_{ZN}(\frac{2}{h}(U_2^{0,i+1} - U_2^{0,i}) - \varphi_1^{i+1} - \varphi_1^i)^2] \quad (5.50)$$

The orthotropy symmetry of spaced CLT ensures the uncoupling between transverse shear effects occurring in the $x_2 = 0$ plane and in the $x_1 = 0$ plane, and hence it is possible to sum the shear strain energies derived for each shear plane. The contribution of blocks to the potential energy of the unit-cell involves also the work related to applied loads \mathbf{q} and torques \mathbf{l} . Integrating the beam loads of Equations 5.36 to 5.39 over the length w of the block leads to the following concentrated loads applied to the center of gravity of blocks:

$$\mathbf{q}^{i,block} = w\mathbf{q}^i \quad \text{and} \quad \mathbf{l}^{i,block} = w\mathbf{l}^{d/2,i} \quad (5.51)$$

Finally, the sum of Equations 5.49 and 5.50 over all interfaces while taking into account the contribution of external loads 5.51 yields the contribution of all blocks to the unit-cell potential energy:

$$W^{blocks,thick} = \sum_{i=-(N-1)/2}^{(N-3)/2} [W^{i,i+1(x_2=0)} + W^{i,i+1(x_1=0)}] - \sum_{i=-(N-1)/2}^{(N-1)/2} w(\mathbf{U}^{0,i} \mathbf{q}^i + \varphi^i \mathbf{l}^{d/2,i}) \quad (5.52)$$

Note that the contributions of longitudinal transverse shear strain $2 \varepsilon_{13}^{L,i,i+1}$ of top and bottom interfaces of the unit-cell are considered to be null, since they involve free edges that do not carry strain energy. Even if this hypothesis is not kinematically compatible with the kinematics of Figure 5.9, it represents the actual mechanism, which is for instance taken into account by the shear analogy method (Kreuzinger 1999).

The blocks potential energy of 5.52 is expressed in terms of blocks' displacement $\mathbf{U}^{0,i}$ and rotations φ . Therefore, in the next section, relations between blocks and beams kinematic variables will be introduced in order to ensure kinematics continuity between blocks and beams.

5. CLOSED-FORM SOLUTIONS FOR SPACED CLT

5.4.2 Energy of connected beams

In order to ensure rotation continuity between the blocks and beams, the rotation of longitudinal blocks φ_2^i (with respect to Figure 5.9) is now considered to equal the section's rotation ${}^L\theta_2^i$ of the connected beam. In the same way, the rotation of transverse block $\varphi_2^{i+1} = {}^T\varphi_2$ is now considered to equal the torsion rotation $\theta_2^{i+1} = {}^T\theta_2$ of the connected transverse beam. This means that the presence of wooden blocks ensures the continuity of rotations between beams. Therefore, the rotations of all beams evaluated at their beginning $s_1 = 0$ and end $s_1 = d$ have the same value, leading to the following periodicity condition on beams' rotations:

$$\boldsymbol{\theta}^{d,i} - \boldsymbol{\theta}^{0,i} = 0 \quad (5.53)$$

In contrast, the presence of blocks influences the transmission of displacements between beams. With Figure 5.9 as reference, the relation between block displacement $U_1^{0,i}$ and beam displacement $u_1^{0,i} = u_1^i(s_1 = 0)$ is:

$$u_1^{0,i} = U_1^{0,i} + \frac{w}{2} {}^T\theta_2 \quad (5.54)$$

which can be generalized into the following periodicity condition on beams' displacements:

$$\mathbf{u}^{d,i} - \mathbf{u}^{0,i} = w\mathbf{t}^i \times \boldsymbol{\Theta} \quad \text{with} \quad \boldsymbol{\Theta} = \begin{pmatrix} {}^L\theta_1 \\ {}^T\theta_2 \\ 0 \end{pmatrix} \quad (5.55)$$

The procedure to derive the stress state of beams is very similar to the procedure presented in Section 5.3.1. Modeling the connections between beams as the whole wooden blocks yields the periodicity conditions on displacement and rotation derived in Equations 5.55 and 5.53. Moreover, in the present case the external beam loads are not null and therefore have to be taken into account when estimating the potential energy of each beam:

$$W^i(\mathbf{u}^i, \boldsymbol{\theta}^i) = \int_0^d \frac{1}{2} ({}^t\mathbf{r}^i \cdot \mathbf{F}^{-1} \cdot \mathbf{r}^i + {}^t\mathbf{m}^i \cdot \mathbf{H}^{-1} \cdot \mathbf{m}^i) ds_1 - \mathbf{q}^i \mathbf{u}^i - \mathbf{l}^i \boldsymbol{\theta}^i \quad (5.56)$$

The beam equilibrium equations are:

$$\begin{cases} \mathbf{r}^{i'} + \mathbf{q}^i = 0 \\ \mathbf{m}^{i'} + \mathbf{t}^i \times \mathbf{r}^i + \mathbf{l}^i = 0 \end{cases} \quad (5.57)$$

where the beam distributed loadings \mathbf{q} and \mathbf{l} have been defined in Equations 5.36 to 5.39. Following the same procedure of Section 5.3.1, integrating the equilibrium equations 5.57 leads to linear resultant forces and bending moments on beams:

$$\mathbf{r}^i = \mathbf{r}^{d/2,i} - \mathbf{q}^i(s_1 - d/2) \quad \mathbf{m}^i = \mathbf{m}^{d/2,i} - (\mathbf{t}^i \times \mathbf{r}^{d/2,i} + \mathbf{l}^{0,i})(s_1 - d/2) \quad (5.58)$$

5.4 Thick space frame

where both equilibrium equations have been integrated at $s_1 = d/2$. Substituting the above expression of \mathbf{m}^i into the constitutive equations of moments in Equations 5.7 and integrating at $s_1 = 0$ yields:

$$\mathbf{H}^i(\boldsymbol{\theta}^i - \boldsymbol{\theta}^{0,i}) = \mathbf{m}^{d/2,i} - (\mathbf{t}^i \times \mathbf{r}^{d/2,i} + \mathbf{l}^{0,i}) \frac{s_1}{2}(s_1 - d) \quad (5.59)$$

Then, the periodicity of rotations $\boldsymbol{\theta}^i(d) - \boldsymbol{\theta}^i(0) = 0$ enforces $\mathbf{m}^{d/2,i} = 0$ and therefore

$$\boldsymbol{\theta}^i = \boldsymbol{\theta}^{0,i} - (\mathbf{H}^i)^{-1}(\mathbf{t}^i \times \mathbf{r}^{d/2,i} + \mathbf{l}^{0,i}) \frac{s_1}{2}(s_1 - d) \quad (5.60)$$

Substituting such expression of $\boldsymbol{\theta}^i$ into the constitutive equation of resultant forces and integrating at $s_1 = 0$ while taking into account the periodicity of displacement $\mathbf{u}^{d,i} - \mathbf{u}^{0,i} = w\mathbf{t}^i \times \boldsymbol{\Theta}$, yields the following expression of resultant forces at beam mid-span $\mathbf{r}^{d/2,i}$:

$$\mathbf{r}^{d/2,i} = \mathbf{P}^{*,i} \cdot \mathbf{t}^i \times (w\boldsymbol{\Theta} + \boldsymbol{\theta}^{0,i}d + \frac{d^3}{12}(\mathbf{H}^i)^{-1}\mathbf{l}^{0,i}) \quad (5.61)$$

where the operator $\mathbf{P}^{*,i}$ is, in the local beam reference frame:

$$\mathbf{P}^{*,i} = \begin{pmatrix} ES^{-1} & 0 & 0 \\ 0 & \alpha_2^d & 0 \\ 0 & 0 & \alpha_3^d \end{pmatrix} \quad (5.62)$$

with $\alpha_2^d = \frac{b-w}{GS_2} + \frac{(b-w)^3}{12EI_3}$ and $\alpha_3^d = \frac{b-w}{GS_3} + \frac{(b-w)^3}{12EI_2}$. Therefore, the complete stress state of beams is defined and the contribution of each beam to the potential energy of the unit-cell can be evaluated as:

$$W^{i,thick}(\mathbf{u}^{0,i}, \boldsymbol{\theta}^{0,i}) = \frac{1}{2} \left[\mathbf{r}^{d/2,i} \mathbf{P}^{*,i} {}^{-1} \mathbf{r}^{d/2,i} - \frac{d^3}{12} (\mathbf{q}^i F^{-1} \mathbf{q}^i + \mathbf{l}^{0,i} H^i {}^{-1} \mathbf{l}^{0,i}) \right] - d \mathbf{q}^i \mathbf{u}^{0,i} - d \mathbf{l}^{0,i} \boldsymbol{\theta}^{0,i} \quad (5.63)$$

where the first term is the contribution of beam's stress state using Equation 5.8 and the last two terms are the contribution of external loadings.

5.4.3 Derivation of the shear force compliance

The total potential energy of the unit-cell modeled as a thick space frame is the sum of beams and blocks energy:

$$W^{total,thick}(\mathbf{u}^{0,i}, \boldsymbol{\theta}^{0,i}) = \sum_{i=-(N-1)/2}^{(N-1)/2} W^{i,thick} + W^{blocks,thick} \quad (5.64)$$

The minimization of the total potential energy with respect to the kinematic variables yields the explicit expression of the unit-cell energy which can be used to evaluate the Bending-Gradient shear force compliance. The imposed shear kinematic of the wooden blocks connecting the beams leads to equal out-of-plane displacements for all beams ${}^L u_3 = {}^T u_3$ and null in-plane rotations $\theta_3^i = 0$. Therefore these variables do not contribute to the energy stored in the unit-cell and can be set to zero. Equation

5. CLOSED-FORM SOLUTIONS FOR SPACED CLT

5.43 enforces the same rotation of transverse blocks within each shear plane, which has been supposed to equal the torsion rotation of the connected beam in the previous paragraph, leading to:

$$\begin{cases} \theta_2^i = {}^T\theta_2 & \text{if } i \in \text{T blocks} \\ \theta_1^i = {}^L\theta_1 & \text{if } i \in \text{L blocks} \end{cases} \quad (5.65)$$

In order to further simplify the expression of potential energy to minimize, the rotations of longitudinal beams or blocks are also considered to be all equal to the same value ${}^L\theta_2$ in the $x_2 = 0$ plane and ${}^T\theta_1$ in the $x_1 = 0$ plane:

$$\begin{cases} \theta_2^i = {}^L\theta_2 & \text{if } i \in \text{L blocks} \\ \theta_1^i = {}^T\theta_1 & \text{if } i \in \text{T blocks} \end{cases} \quad (5.66)$$

Therefore all the beams and blocks of the same type (L or T) are considered to have the same rotation, leading to only four unknown rotations. FE analyses revealed that this hypothesis is a reasonable approximation of the actual complex behavior of the unit-cell under transverse shear strains. Finally, there remain four rotations for all beams and two displacements per beam, leading to the following minimization problem:

$$\min_{(u_1^{0,i}, u_2^{0,i}, {}^L\theta_1, {}^L\theta_2, {}^T\theta_1, {}^T\theta_2) \in \mathbb{R}^{2N+4}} W^{\text{total, thick}}(u_1^{0,i}, u_2^{0,i}, {}^L\theta_1, {}^L\theta_2, {}^T\theta_1, {}^T\theta_2) \quad (5.67)$$

Once the explicit expression of total potential energy of the unit-cell is obtained, the shear force compliance \mathbf{f}^{BG} is evaluated as:

$$\frac{1}{2}({}^t\mathbf{R} : \mathbf{f}^{BG} : \mathbf{R}) = -\frac{1}{b^2} W^{\text{total, thick}} \quad (5.68)$$

Minimizing the potential energy 5.67 with respect to the displacements \mathbf{u} yields the following expression of the relative displacement between upper and lower beams $\mathbf{u}^{0,i+1} - \mathbf{u}^{0,i}$:

$$\mathbf{u}^{0,i+1} - \mathbf{u}^{0,i} = -\frac{bh}{2w^2 G_{ZN}} \sum_{l=-(N-1)/2}^i \mathbf{q}^l + \frac{h}{2} \mathbf{e}_3 \times ({}^L\boldsymbol{\theta} + {}^T\boldsymbol{\theta}) \quad (5.69)$$

Setting the displacement of the central beam at zero $\mathbf{u}^{i=0} = 0$ in order to avoid a rigid translation of the unit-cell, the values of each displacement $\mathbf{u}^{0,i}$ can be found with progressive substitutions:

$$\mathbf{u}^{0,i} = \frac{bh}{2w^2 G_{ZN}} \sum_{k=0}^{i-1} \left(\sum_{l=-(N-1)/2}^k \mathbf{q}^l \right) + \frac{ih}{2} \mathbf{e}_3 \times ({}^L\boldsymbol{\theta} + {}^T\boldsymbol{\theta}) \quad \text{with } \mathbf{u}^{i=0} = 0 \quad (5.70)$$

As already introduced, the orthotropy symmetry of spaced CLT allows the resolution of the minimization problem 5.67 separately for the generalized shear force components acting along the shear direction “1-3” (R_1, R_2, R_6) and along shear direction “2-3” (R_3, R_4, R_5). In the following, the solution of the problem is detailed for the “1-3”

5.4 Thick space frame

shear direction but it is equivalent for the other direction. The kinematic variables associated to the $x_2 = 0$ plane are the displacements u_1^i and the rotations ${}^L\theta_2, {}^T\theta_2$. Hence, substituting the values of u_1^i from Equation 5.70 in the functional 5.64 leads to the expression of the potential energy as a function of the rotations ${}^L\theta_2$ and ${}^T\theta_2$. Minimizing such expression with respect to ${}^L\theta_2$ and ${}^T\theta_2$ yields the following system of linear equations:

$$\begin{cases} \frac{L}{\alpha_3^d}(w {}^T\theta_2 + d {}^L\theta_2 + \frac{c^3 R_1}{12D_{11}}) = b(R_1 + \eta_6 R_6) & (5.71a) \\ \frac{hw(N-1)G_{LZ}({}^T\theta_2 - {}^L\theta_2)}{2d} = \frac{b-2w}{2w(b-w)} \sum_{-(N-1)/2}^{(N-1)/2} (z^i q_1^i) + \frac{T {}^T l_2}{w(b-w)} - \frac{L {}^L l_2}{w(b-w)} & (5.71b) \end{cases}$$

where $\eta_6 = \frac{T G J - \sum_T z^i \rho^i}{b D_{33}}$ and \sum_T operates only on transverse beams. Solving the above system of equations and substituting the obtained values in Equations 5.64 allow the explicit expression of unit-cell potential energy under (R_1, R_2, R_6) generalized shear strains. Repeating the same procedure for the remaining shear direction 23 leads to the expression of the potential energy under (R_3, R_4, R_5) generalized shear strains. Finally, taking the sum of the two contributions of each shear plane and applying Equation 5.68, the following functional can be obtained:

$$\begin{aligned} {}^t\mathbf{R} : \mathbf{f}^{BG} : \mathbf{R} = & \alpha_3^d \left(\frac{(R_1 + \eta_6 R_6)^2}{N_L} + \frac{(R_5 + \eta_3 R_3)^2}{N_T} \right) + \\ & - \frac{(b-w)^3}{12b} \left(\frac{R_1^2 + 2\eta_6 R_1 R_6}{D_{11}} + \frac{R_5^2 + 2\eta_3 R_5 R_3}{D_{22}} - \frac{\zeta_6 R_6^2}{b D_{33}^2} - \frac{\zeta_3 R_3^2}{b D_{33}^2} \right) + \\ & + \frac{1}{2hw^2(N-1)G_{LZ}} \left[\left((b-2w)(R_1 + \eta_6 R_6) + \frac{N_T G J R_6}{D_{33}} - \frac{N_L E I_2 R_1}{D_{11}} \right)^2 + \right. \\ & \left. + \left((b-2w)(R_5 + \eta_3 R_3) - \frac{N_T E I_2 R_5}{D_{22}} + \frac{N_L G J R_3}{D_{33}} \right)^2 \right] + \\ & + \frac{h}{2w^2 G_{ZN}} \sum_{j=-(N-1)/2}^{(N-3)/2} \left(\sum_{i=-(N-1)/2}^j \mathbf{q}^i \right)^2 \end{aligned} \quad (5.72)$$

where $\eta_6 = \frac{N_T G J + \sum_T z^i \rho^i}{b D_{33}}$, $\eta_3 = \frac{N_L G J + \sum_L z^i \rho^i}{b D_{33}}$, $\zeta_6 = \frac{\sum_T (\rho^i)^2}{G S_2} + N_T G J$, $\zeta_3 = \frac{\sum_L (\rho^i)^2}{G S_2} + N_L G J$. The first and second terms are related to the bending and shear of beams, the third term is the energy associated to the longitudinal shear of blocks (G_{LZ}) and the fourth term is the energy associated to the rolling shear of blocks (G_{ZN}). In the functional 5.72, the closed-form expression of all terms of the Bending-Gradient shear force compliance can be identified. However, as already discussed in Section 4.3.3, the cylindrical part of the Bending-Gradient shear force compliance (f_{11}^{BG} in the $x_2 = 0$ plane) is sufficient to well describe the transverse shear behavior of spaced CLT under cylindrical bending configuration. Hence, only the closed-form solution of f_{11}^{BG} related to the generalized shear strain R_{111} is given in the following. Taking the terms of

5. CLOSED-FORM SOLUTIONS FOR SPACED CLT

Equation 5.72 where the quadratic shear strain R_1 is present leads to the following expression of f_{11}^{BG} :

$$f_{11}^{BG} = \frac{\alpha_3^d}{N_L} - \frac{(b-w)^3}{12bD_{11}} + \frac{(b-2w - LEI_2D_{11}^{-1})^2}{2h(N-1)w^2G_{LZ}} + \frac{h(EwhD_{11}^{-1})^2}{2w^2G_{ZN}} \sum_{j=-(N-1)/2}^{(N-3)/2} \left(\sum_{i=-(N-1)/2}^j \delta^i z^i \right)^2 \quad (5.73)$$

where

$$\delta^i = \begin{cases} 1 & \text{if } i \in \text{L beams} \\ 0 & \text{if } i \in \text{T beams} \end{cases} \quad (5.74)$$

In order to suggest a simplified closed-form expression, the term $\frac{-(b-w)^3}{12bD_{1111}}$ can be neglected in Equation 5.73, because of its negligible contribution to the compliance of the panel. Finally, the closed-form expression for the shear force compliance can be written independently from the bending stiffness D_{11} and with the double sum term simplified into a polynomial as:

$$f_{11}^{BG} = \frac{2\alpha_3^d}{N+1} + \frac{b^2}{2hw^2(N^2+2N-2)^2} \left[\frac{(1-\frac{2w}{b})((N^2+2N-2)-1)^2}{G_{LZ}N-1} + \frac{6}{5G_{ZN}} \frac{(N^5+5N^4+10N^3+10N^2-11N-15)}{(N+1)^2} \right] \quad (5.75)$$

The above expression is dependent only on geometrical and material parameters of the spaced CLT panel. When $b = w$ and the CLT has no spaces, the first term $\frac{\alpha_3^d}{L}$ related to beams vanishes and Equation 5.75 returns the shear compliance of a crosslam having glued lateral lamellas.

5.5 Closed-form prediction of longitudinal and rolling shear stresses

When dealing with the out-of-plane behavior of spaced CLT, the governing failure modes are longitudinal tensile failures of bottom layer and rolling shear failure of transverse layer. This has been observed during the experimental investigation of Chapter 4 and also confirmed by other tests of the literature on standard CLT (Czaderski et al 2007; Hochreiner et al 2014; Mestek 2011; Okabe et al 2014). In Section 4.3.4, the tensile and rolling shear stresses at failure point of the tested panels (see Chapter 4) have been predicted with the numerical homogenization procedure and were in agreement with common strength values of the literature. In this section, closed-form expressions for predicting bending and rolling shear stresses of spaced CLT are derived based on the results Section 5.3 and Section 5.4. Exactly as in Section 4.3.4, the derived stresses are function of global uniform bending moment M_{11} and shear force R_{111} applied to the panel. For instance, in a 4-point bending configuration, there is pure bending between the loading forces and governing shear force close to supports (see Figure 4.23).

5.5 Closed-form prediction of longitudinal and rolling shear stresses

5.5.1 Maximum longitudinal stress

At the beginning of Section 5.4, it was mentioned that the bending stress state of beams of Equation 5.19 can be expressed as a function of an external bending moment applying Equation 4.9 to the beam stress state. Hence, the following resultant axial force r_1^i and out-of-plane moment m_2^i of beams as a function of the external bending moment M_{11} along x_1 direction can be found:

$$\begin{cases} r_1^i = \frac{EwhM_{11}}{D_{11}} z^i \\ m_2^i = \frac{EI_2M_{11}}{D_{11}} \end{cases} \quad (5.76)$$

Note that the external bending moment M_{11} is per unit length and therefore has to be normalized over the panel's width. Since the maximum longitudinal stress is located on external layers, substituting the position of the top/bottom layer $\pm \frac{(N-1)h}{2}$ in the resultant force r_1^i and dividing by the beam's cross section leads to the stress deriving from the position of the beam with respect to panel's neutral axis $\sigma_{11,max}^r$. Moreover, the bending stresses deriving from the simple bending of the beam can be found with $\sigma_{11,max}^m = \frac{m_2^i h}{I_2 2}$. Finally the closed-form expression for the maximum bending stresses is:

$$\sigma_{11,max} = \sigma_{11,max}^r + \sigma_{11,max}^m = \pm \frac{NEM_{11}h}{2D_{11}} = \pm \frac{12bNM_{11}}{wh^2(N+1)(N^2+2N-2)} \quad (5.77)$$

5.5.2 Maximum rolling shear stress

The mean rolling shear stress in transverse blocks can be estimated as $\sigma_{13}^i = \frac{V^i}{w^2}$, where V^i is the shear force on the considered wooden block. This shear force can be obtained from the equilibrium of forces showed in Figure 5.10. The external loadings q_1^i are axial

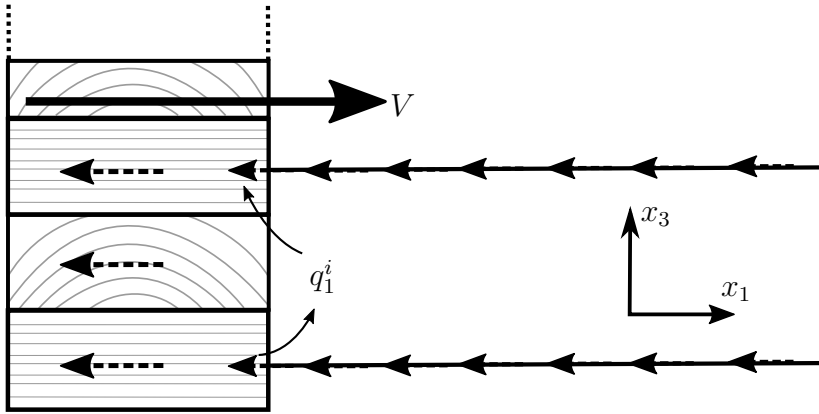


Figure 5.10: Shear force V from the equilibrium along x_1 direction

forces per unit-length and their sum $\sum_{-j=-(N-1)/2}^{i-1} q_1^i$ has to be in equilibrium with the shear force V^i , therefore substituting the closed-form expression of q_1^i from Equation

5. CLOSED-FORM SOLUTIONS FOR SPACED CLT

5.36 leads to:

$$V^i = \frac{EwhbR_1}{w^2 D_{11}} \sum_{j=-N-1/2}^{i-1} \delta^j z^j \quad (5.78)$$

where R_1 is the external shear force acting on the panel normalized over the panel's width and δ^j has been defined in Equation 5.74. Therefore the maximum shear force is obtained when i refers to the position of the transverse block closest to the mid-plane of CLT cross section, where the shear stresses reach their peak. Under the hypothesis of the same thickness h for all layers, the sum term can be simplified with ψh , where ψ is a coefficient as a function of number of layers. Finally, the closed-form expression for the maximum rolling shear stress is:

$$\sigma_{13,max} = \psi \frac{24b^2 R_1}{hw^2(N+1)(N^2+2N-2)} \quad (5.79)$$

with

$$\psi = \begin{cases} 1 & \text{for 3-ply and 5-ply} \\ 4 & \text{for 7-ply and 9-ply} \\ 9 & \text{for 11-ply and 13-ply} \end{cases} \quad (5.80)$$

5.6 Comparison

In this Section, the elastic behavior of spaced CLT predicted with closed-form solutions is compared to the reference behavior predicted with the numerical homogenization presented in Chapter 5. The predicted stiffnesses of spaced CLT are normalized over the stiffness of a full CLT having bonded lateral lamellas.

5.6.1 Bending stiffness

The derived closed-form expression for spaced CLT bending stiffness along the main direction x_1 is:

$$D_{11} = N_L \frac{EI_2}{b} + \frac{ES}{b} \sum_L z_i^2 = \frac{Eh^3w}{24b} (N+1)(N^2+2N-2) \quad (5.81)$$

As already discussed, this expression turns out to be based on the principle of the Classical Lamination Theory and volume fraction. Therefore, the volume fraction approach combined with the Classical Lamination Theory (on which the shear analogy method or the gamma method are based) returns the same results, that are in agreement with the FE homogenization results. The very slight difference is because the shear analogy or gamma method take into account the presence of transverse layers, while expression 5.81 neglects their presence.

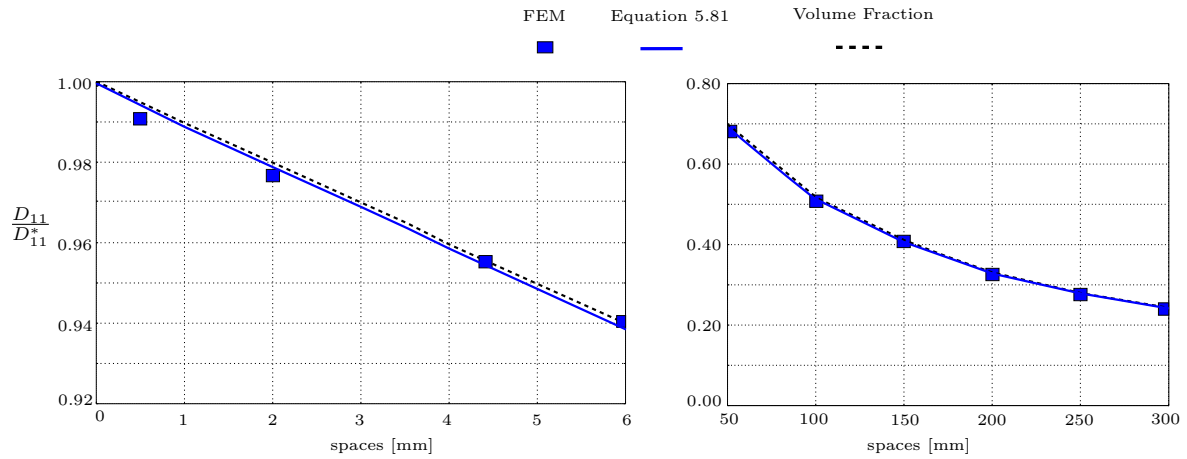


Figure 5.11: Comparison between closed-form solution, volume fraction approach and FE results for the bending stiffness D_{11} . 5ply

5.6.2 In-plane shear and torsional stiffness

In this Section, the simplified solutions 5.31 and 5.32 for predicting spaced CLT in-plane shear and torsional stiffness are compared with the FE homogenization results presented in Chapter 4. The comparison is plotted from Figure 5.12 to Figure 5.15 for different panel's lay-ups. Moreover, the closed-form solution of Moosbrugger et al (2006) and the currently adopted approach by the working draft of CLT design section in the revised Eurocode 5 1-1 (EN1995-1-1 2015) are compared as well. The latter is based on the closed-form solution of Moosbrugger et al (2006) fitted on FE simulations in order to take into account the number of layers (3, 5 and 7-ply). The simplified closed-form solutions 5.31 and 5.32 for in-plane shear and torsional stiffness give a very good approximation of the exact closed-form solution of the minimization problem 5.17. For in-plane shear stiffness, the closed-form solutions return a very good agreement with the reference behavior. The rotational stiffness that governs the in-plane rotations of spaced CLT is based on the results of Moosbrugger et al (2006), (see Section 4.3.2) who based their computations on a representative CLT element having an infinite number of layers. The resulting expression is independent from the number of layers and is in better agreement with numerical results for a large number of layers. The consequence is that for 3-ply and 5-ply such approach overestimates the actual in-plane shear stiffness, while the closed-form solutions derived in this work are in good agreement.

Dealing with the torsional stiffness, the derived closed-form expression are in good agreement with the reference behavior for spaced CLT made of thick lamellas. When the lamellas are thin, the predicted torsional stiffness with the closed-form expressions deviates from the numerical results. This is probably due to complex mechanisms difficult to take into account with a simple rotational spring that connects the beams. For small gaps the overestimation of the stiffness remains acceptable, while at large spaces the torsional stiffness is significantly underestimated. A possible explanation of this

5. CLOSED-FORM SOLUTIONS FOR SPACED CLT

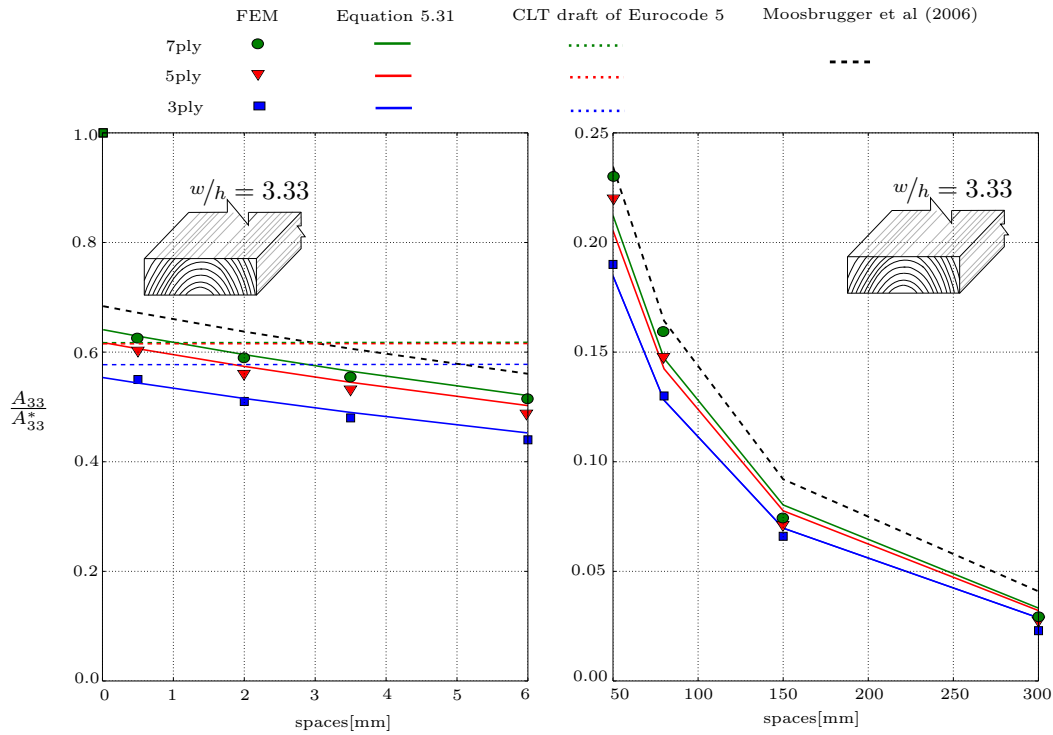


Figure 5.12: Comparison between closed-form solution, FE results and existing approaches for the in-plane shear stiffness A_{33} . $w/h = 3.33$

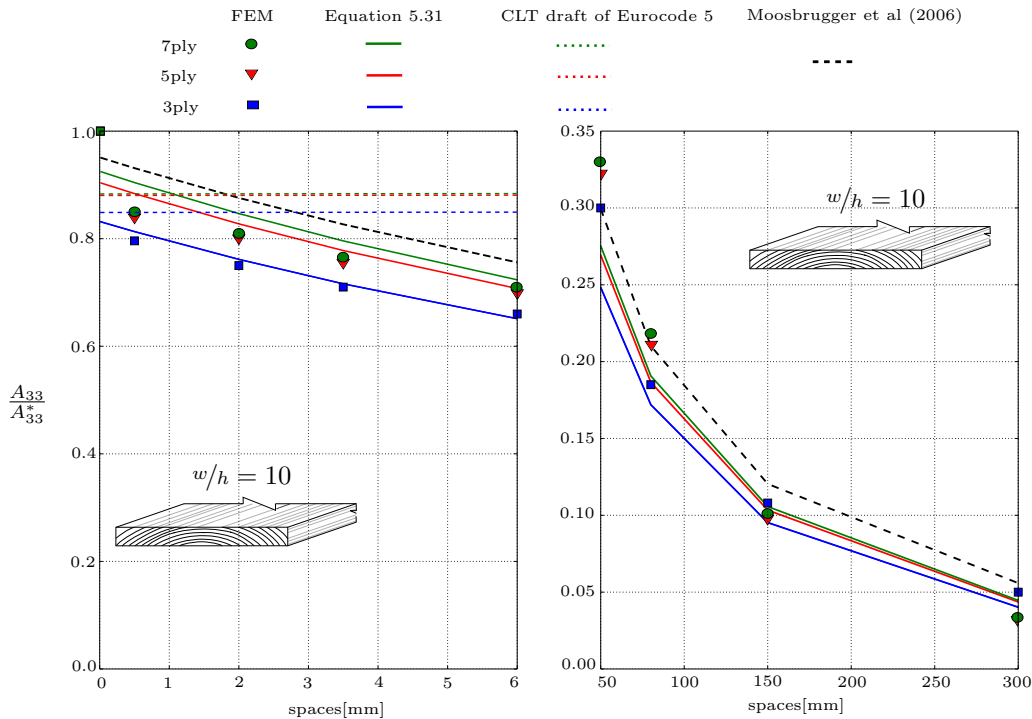


Figure 5.13: Comparison between closed-form solution, FE results and existing approaches for the in-plane shear stiffness A_{33} . $w/h = 10$

5.6 Comparison

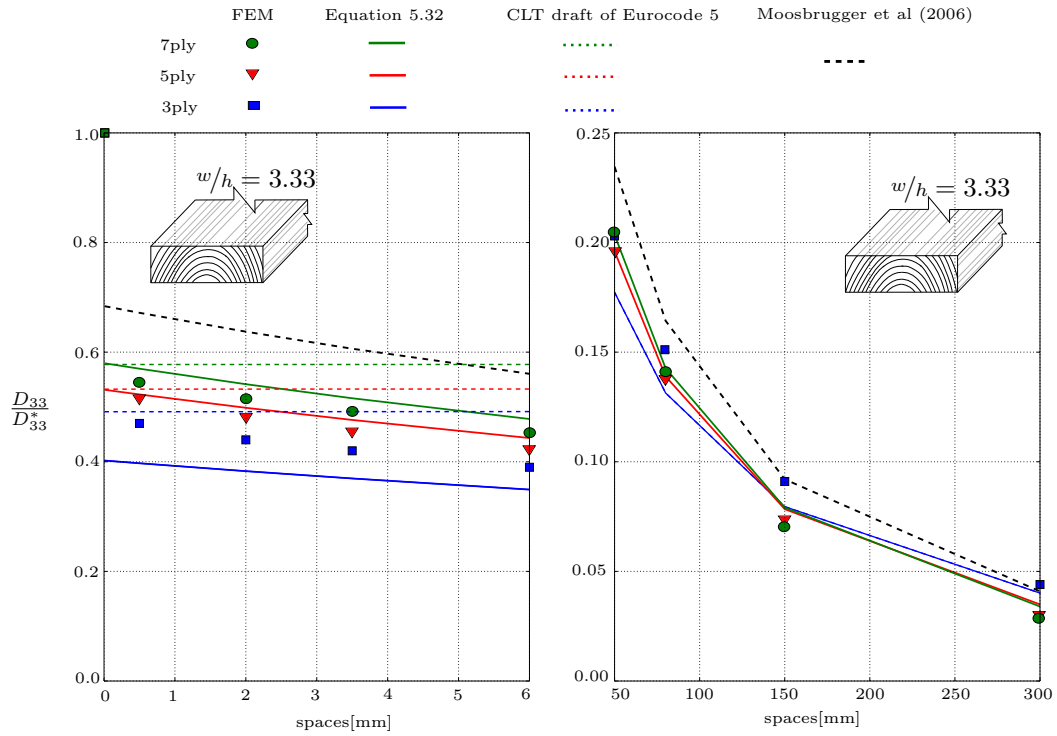


Figure 5.14: Comparison between closed-form solution, FE results and existing approaches for the torsional stiffness D_{33} . $w/h = 3.33$

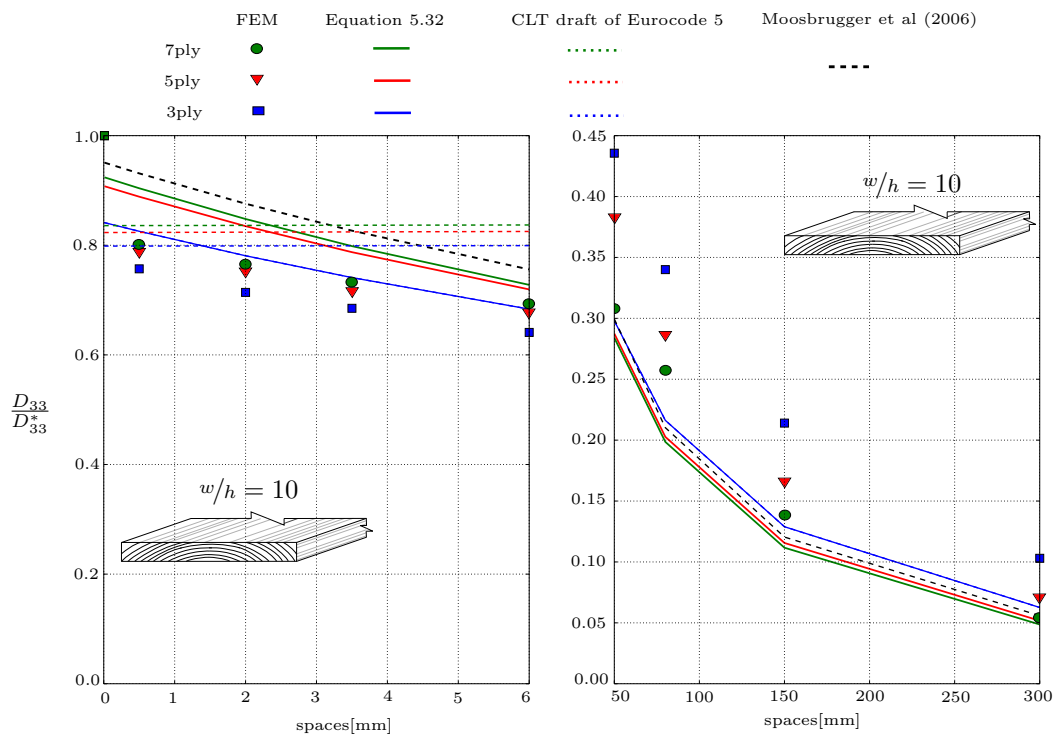


Figure 5.15: Comparison between closed-form solution, FE results and existing approaches for the torsional stiffness D_{33} . $w/h = 10$

5. CLOSED-FORM SOLUTIONS FOR SPACED CLT

underestimation could be that the torsional warping of thin lamellas is prevented when they are glued together, leading to a higher global torsional stiffness than expected. The closed-form approach considers a uniform torsional warping of lamellas and hence it underestimates the torsional stiffness of spaced CLT made of thin lamellas.

The current approach of the working draft on CLT design of the new version of Eurocode 5 1-1 (EN1995-1-1 2015) is based on FE fitting parameters as a function of number of layers for predicting the in-plane shear and torsional stiffness of shortly spaced crosslam (Bogensperger et al 2010; Silly 2010). This methods give a single value of reduced stiffnesses by the unglued lateral lamellas, neglecting the influence of spaces up to 6 mm. For simply laterally unglued panels ($s \approx 0$), the reduced in-plane shear and torsional stiffness are in agreement with the FE homogenization results. However, as Figure 5.12 to Figure 5.15 show, the small gaps up to 6mm have a non-negligible influence of the reduction of spaced CLT in-plane stiffnesses. The closed-form solutions for estimating spaced CLT in-plane shear and torsional stiffness suggested in this thesis do not require fitting parameters and can precisely take into account the influence of short spaces. This can lead to a future standardization of the obtained closed-form solution within this study.

5.6.3 Shear force compliance

From Figure 5.16 to Figure 5.18, the normalized shear force compliance f_{11}^{BG} predicted with the closed-form expression 5.75 and the numerical homogenization results are compared for different lay-ups. At small spaces, all closed-form solutions are almost superposed showing no dependency from the lamella's aspect ratio w/h , while the numerical homogenization shows dependency. This is because the transverse shear of lamellas having lateral free edges leads to additional stresses perpendicular to the grain which are dependent on the lamella's aspect ratio. This effects are well predicted by the FEM modeling but they cannot be taken into account by the closed-form approach. Nevertheless, a very good agreement for the 3-ply configuration is found, while increasing the number of layers yields progressive overestimation of the shear force compliance, especially at short spaces. This derives from the kinematic hypothesis of equal rotations of beams and blocks having the same orientation (L or T) made in Section 5.4.1. Indeed, if for the 3-ply lay-up such hypothesis is trivially satisfied, the more the number of layers increases, the more this hypothesis deviates from the actual kinematic. However, for 5-ply and 7-ply, the closed form expression still returns an acceptable approximation of the reference behavior. Globally, the derived closed-form solution for predicting the shear force compliance of spaced CLT gives good agreement with the reference numerical results at both short and large spaces. On the contrary, the simplified approach of volume fraction overestimates the reduction of the shear force compliance, especially at large spaces.

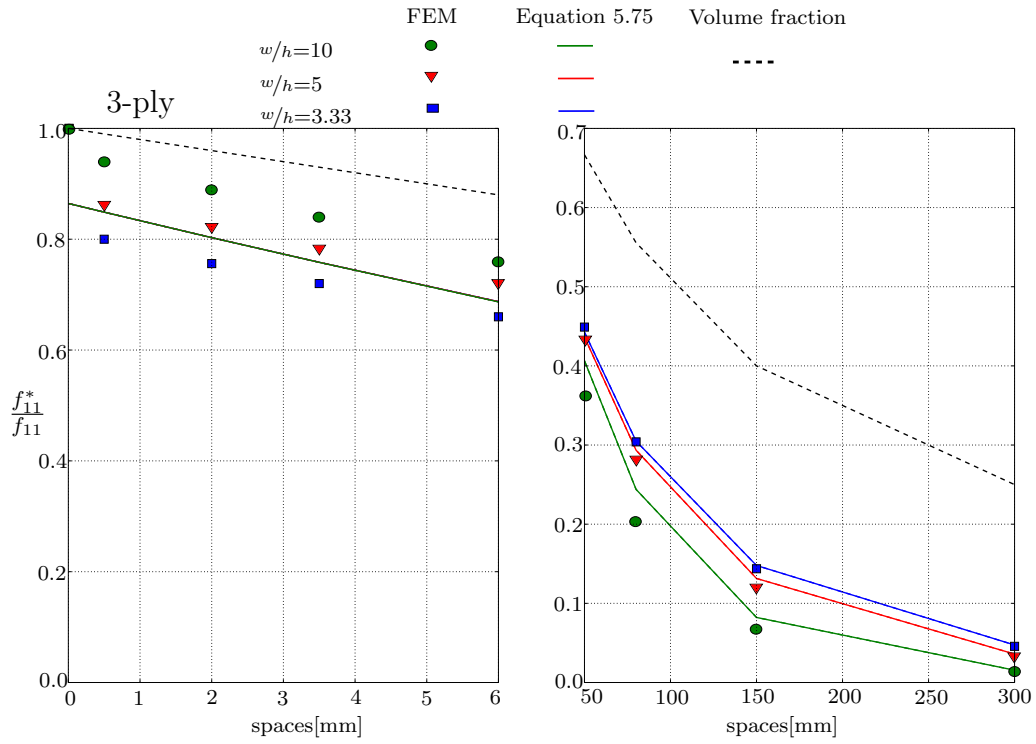


Figure 5.16: Comparison between closed-form solution, homogenization results and volume fraction approach for the shear force compliance f_{11} . 3-ply

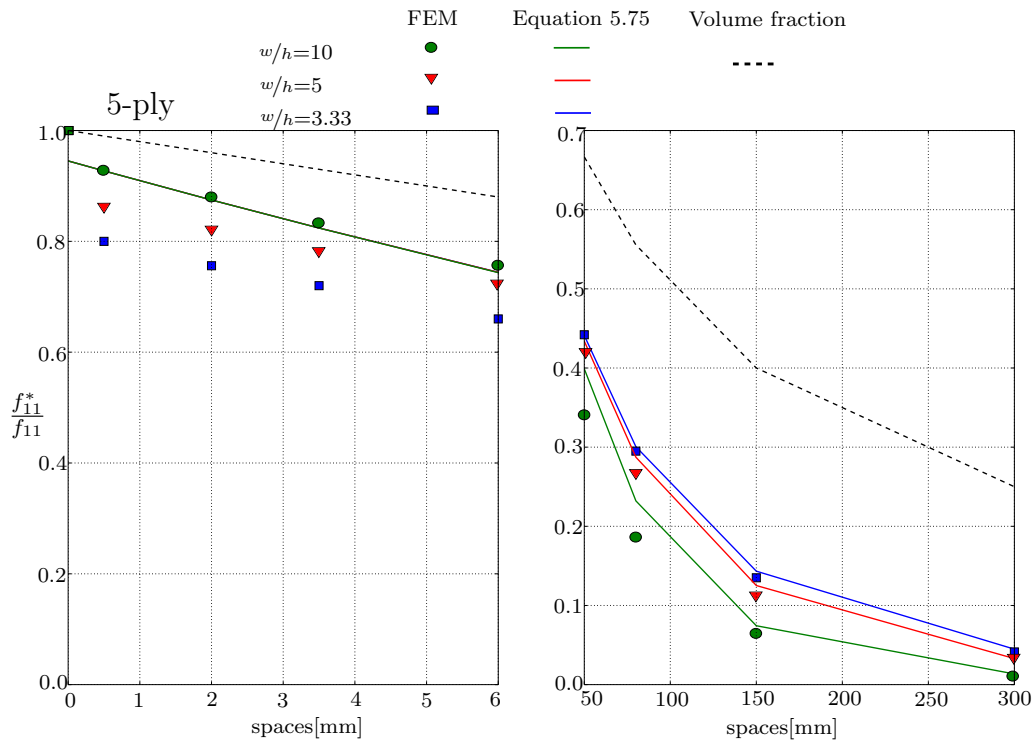


Figure 5.17: Comparison between closed-form solution, homogenization results and volume fraction approach for the shear force compliance f_{11} . 5-ply

5. CLOSED-FORM SOLUTIONS FOR SPACED CLT

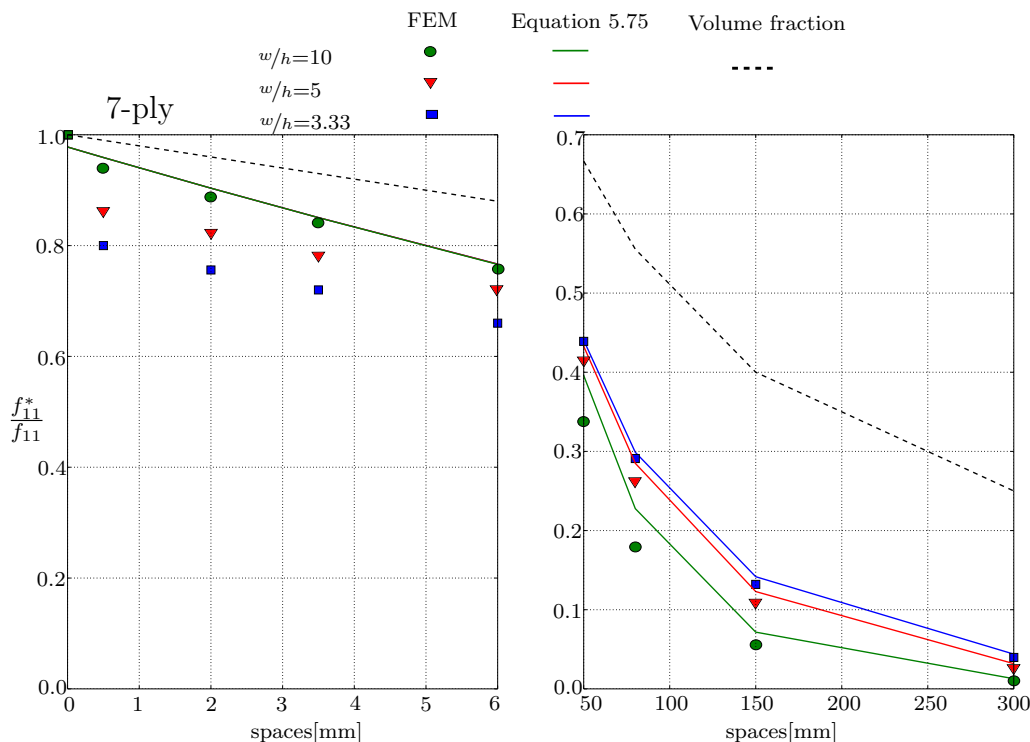


Figure 5.18: Comparison between closed-form solution, homogenization results and volume fraction approach for the shear force compliance f_{11} . 7-ply

5.6.4 Maximum longitudinal and rolling shear stresses

The suggested closed-form expressions 5.77 and 5.79 for predicting the maximum longitudinal and rolling shear stresses in spaced CLT under out-of-plane loads are in this section compared to the FE stresses found with the numerical homogenization (see Section 4.3.4). Dealing with the longitudinal stresses, there are no stress concentration (see Figure 4.7) and therefore the maximum value in the top or bottom beams can be simply identified. In contrast, the rolling shear stresses show stress concentration due to the presence of free edges (see Figure 4.19). Figure 5.19 shows the distribution of the rolling shear stress along the width of a transverse lamella. Only half width of the lamellas is showed, and the central point of lamella $x_1 = 0$ is chosen as the point where to evaluate the rolling shear stress. Hence the maximum value of rolling shear stress is numerically evaluated in the central point of the lamella closest to neutral axis of the panel.

Figure 5.20 to Figure 5.23 presents the relative distance between the numerical and closed-form maximum stresses as a function of spaces and for different lay-ups. The relative distance is defined as:

$$\sigma^{max, Norm} = \frac{\sigma^{max, Num} - \sigma^{max, Closed}}{\sigma^{max, Num}} \quad (5.82)$$

The closed-form prediction of maximum longitudinal stress returns a very good agreement with reference numerical results, showing relative distance between 0% and 4%.

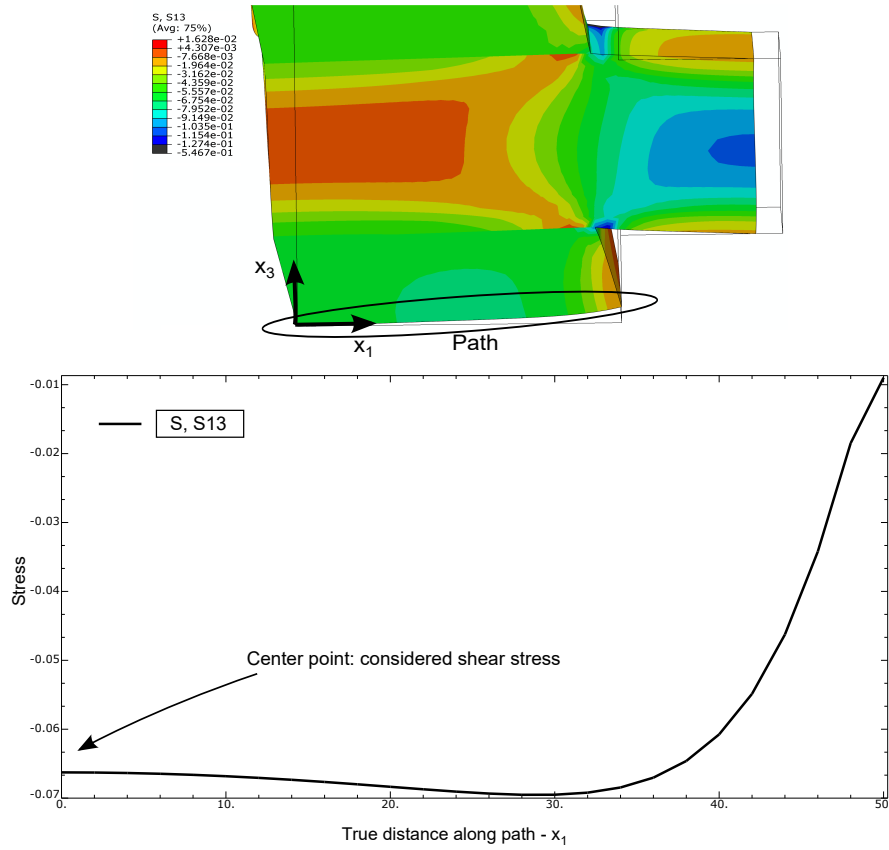


Figure 5.19: Distribution of rolling shear stress along the width of the half central lamella of a 7-ply ($w = 100\text{mm}$, $s = 50\text{mm}$, $h = 30\text{mm}$)

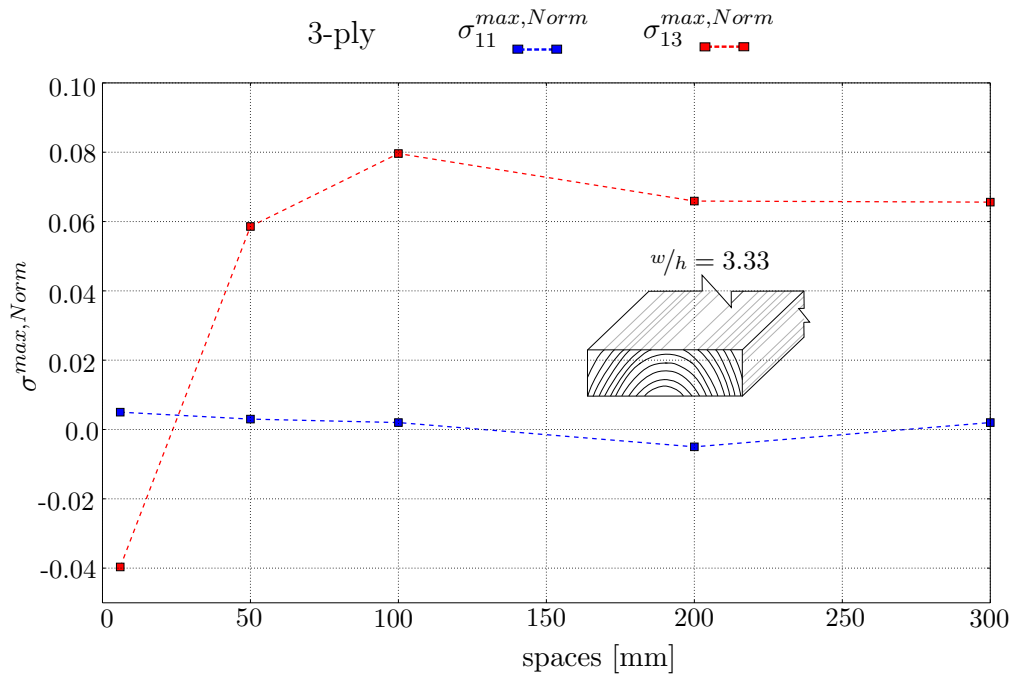


Figure 5.20: Relative distance between numerical and closed-form maximum longitudinal and rolling shear stresses in spaced CLT. 3-ply, $w/h = 3.33$

5. CLOSED-FORM SOLUTIONS FOR SPACED CLT

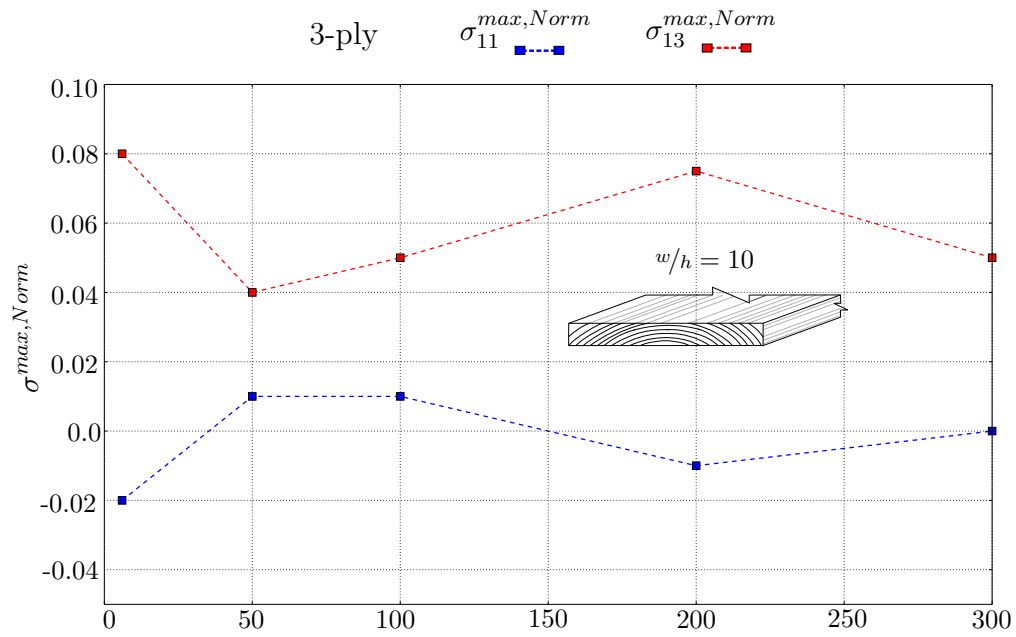


Figure 5.21: Relative distance between numerical and closed-form maximum longitudinal and rolling shear stresses in spaced CLT. 3ply, $w/h = 10$

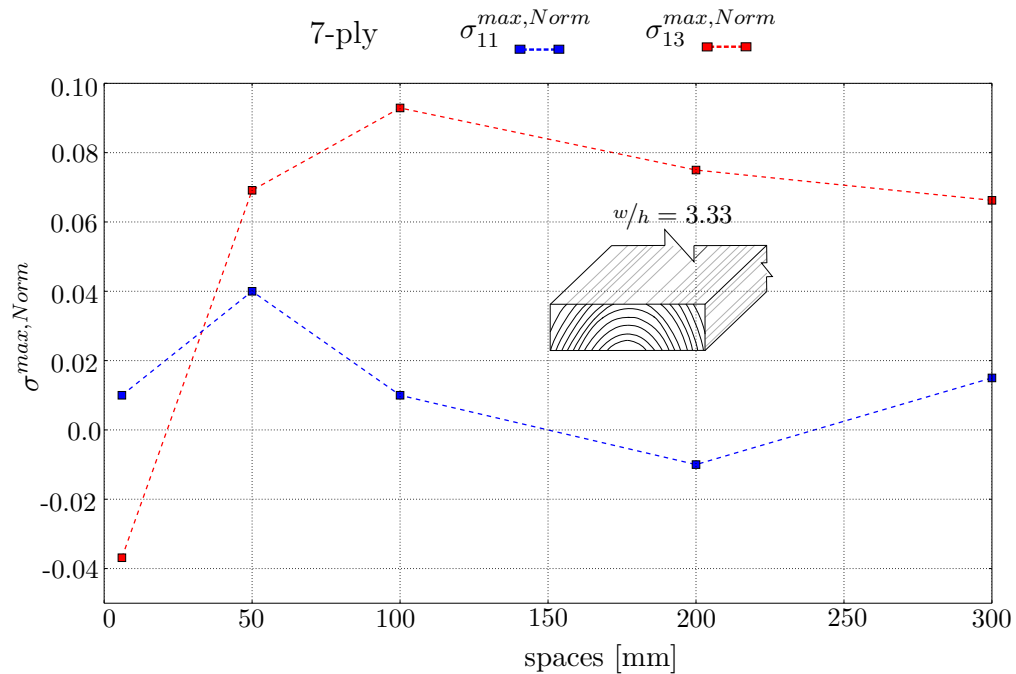


Figure 5.22: Relative distance between numerical and closed-form maximum longitudinal and rolling shear stresses in spaced CLT. 7ply, $w/h = 3.33$

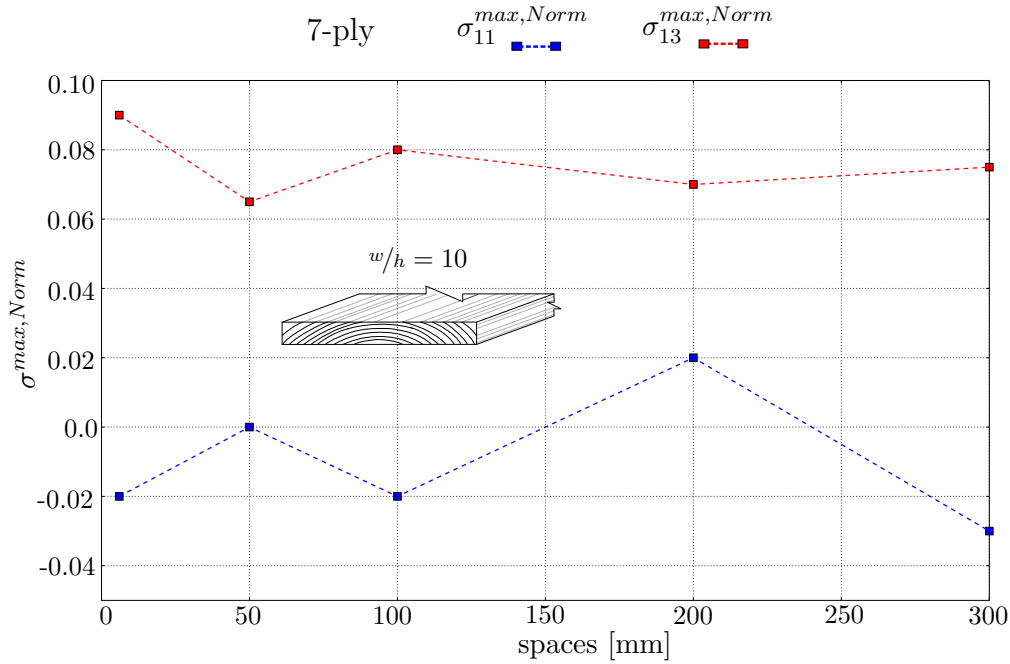


Figure 5.23: Relative distance between numerical and closed-form maximum longitudinal and rolling shear stresses in spaced CLT. 7ply, $w/h = 10$

In particular, for a 3-ply of Figure 5.20 and Figure 5.20, the relative distance is very close to 0%. For the 7-ply configuration, the closed-form prediction of maximum longitudinal stress can reach up to 4% of deviation from the FE reference. For both 3-ply and 7-ply lay-ups, the closed-form prediction of maximum rolling shear stress is generally overestimated between 4% and 10%. However, in the case of thick lamellas having short spaces the rolling shear stress stress is underestimated of about 4%. Globally, the obtained relative distance between -4% and +10% is a very good approximation by the derived closed-form solutions, considering the extremely lower computational costs and simplicity of application compared to the FE homogenization. The prediction of longitudinal stress is accurate, while the maximum rolling shear stresses in spaced CLT can be predicted with a slight overestimation but less than 10%, that is, from an engineering point of view, on the safe side but not too conservative.

5.7 Conclusion

In this Chapter, closed-form solutions have been derived for predicting the elastic mechanical behavior of regularly spaced CLT panels. The Bending-Gradient homogenization scheme presented in Chapter 5 has been applied to a simplified geometry of a periodic unit-cell made of beams connected by means of wooden blocks. Under membrane and bending strains, the wooden blocks have been modeled as springs having rotational stiffness, while for transverse shear strains a shear kinematics of the whole block has been imposed and the associated strain energy has been estimated. Classical beam equations have been applied in order to derive their contribution to the unit-cell

5. CLOSED-FORM SOLUTIONS FOR SPACED CLT

strain energy.

The final closed-form expressions for predicting bending, in-plane shear, torsional and shear force stiffness have been compared to the numerical homogenization. The bending stiffness expression is equivalent to the Classical Lamination Theory with volume fractions already successfully compared in Chapter 5. The suggested closed-form solution for in-plane shear returns a very good agreement with the numerical results. Moreover, this solution can improve the similar existing approach of Moosbrugger et al (2006). The obtained expression of torsional stiffness gives good approximation when the lamellas are thick, while for thin lamellas such solution deviates from the reference results. The derived expression of shear force compliance for spaced CLT is based on a simplified hypothesis on the shear kinematics of the unit-cell. For the 3-ply lay-up such hypothesis is satisfied and the closed-form solution for the 3-ply shear force stiffness is in very good agreement with numerical results. When increasing the number of layers, the simplified hypothesis slightly deviates from the actual more complex kinematic. However, the closed-form solutions for the shear force compliance of 5-ply and 7-ply still return an acceptable approximation of the reference behavior. Finally, closed-form expressions for estimating the maximum longitudinal and rolling shear stress acting on spaced CLT in bending have been derived. The relative distance between the maximum stresses predicted with the closed-form solution and numerical homogenization is between -4% and +10%, which is a good approximation.

Globally, the comparison between the closed-form solutions and the numerical homogenization returns good agreement. The cases where the closed-form solutions deviate from the reference results can be useful to understand the limits of application of such formulations. The simplified expressions derived in this work can be finally used for predicting the mechanical behavior of standard and innovative spaced CLT in practical applications.

Chapter 6

Fire behavior of standard CLT floors: a stiffness-based approach

Note: This Chapter has been submitted for publication with the title *A stiffness-based approach to predict the fire behavior of CLT floors*

Abstract. In this Chapter, the fire behavior of standard CLT floors is investigated predicting the experimental deflection during fire exposure with advanced and simplified methods. The simplified approach is the Reduced Cross Section Method (RCSM) of EN 1995 1-2 (EN1995-1-2 2004), while the more refined modeling is based on heat transfer prediction and reduced stiffness. The more accurate modeling returned a better agreement with the experimental reference than two existing RCSM approaches. Finally, based on the advanced modeling, a proposal for a possible improvement of the current version of the RCSM is suggested.

Résumé. Ce Chapitre présente une étude sur le comportement au feu des planchers CLT classiques qui pourrait permettre d'améliorer la méthode de dimensionnement actuelle. La flèche mesurée pendant l'exposition au feu des planchers est prédite avec une modélisation avancée et des méthodes simplifiées. L'approche simplifiée est la Méthode de la Section Réduite (RCSM) de la norme EN 1995 1-2 (EN1995-1-2 2004), alors que la modélisation plus raffinée est basée sur la prédiction du transfert thermique et sur les raideurs réduites. La modélisation plus raffinée permet d'obtenir une meilleure concordance avec la référence expérimentale par rapport à deux approches existantes basées sur la RCSM. Enfin, en s'appuyant sur la modélisation avancée, une proposition pour une possible amélioration de la version actuelle de la méthode RCSM de la norme EN 1995 1-2 est suggérée.

6.1 Introduction

The development of timber structures has to be followed by a progressive enhancement of knowledge about their fire safety, especially because of the increasing heights of

6. FIRE BEHAVIOR OF STANDARD CLT FLOORS: A STIFFNESS-BASED APPROACH

timber buildings that demand higher fire resistance. This is even more important when dealing with relatively recent products such as CLT panels. Indeed, the current version of EN 1995 1-2 (EN1995-1-2 2004) includes a fire design method for timber structures derived in the 80's (Schaffer 1984) and originally developed for simply supported Glued Laminated Timber beams. This method, called the Reduced Cross Section Method (RCSM), allows considering mechanical properties of wood at ambient temperature combined with a reduction of cross section. Due to its simplicity, this approach is very common among engineers and can be applied to timber products since wood has a low thermal conductivity and therefore the temperature gradient end not so far from the char front (from 35mm to 80mm in ISO fire, depending on the protection). However, this thermal gradient reduces wood's mechanical properties near the char front. This effect is taken into account by the RCSM removing an additional layer of 7mm considered to have no mechanical properties (also called zero-strength layer ZSTL, or d_0 as called in EN 1995 1-2) for design purposes. Actually, such depth depends on the kind of fire exposure (ISO or natural fire), the time of exposure and the kind of acting stresses (tension, compression or shear) (Schmid et al 2016). Moreover, recent studies (Schmid et al 2012; 2014; Lineham et al 2016) showed that the predicted behavior of timber members exposed to fire using the current RCSM approach is not always conservative. Furthermore, falling-off of layers can occur for the presence of glued interfaces between layers which show lower mechanical properties at high temperatures than wood. Indeed, when the char front is not yet at the glued interface between layers, the temperature gradient decrease the mechanical properties of glue and can lead to premature falling-off of layers and a consequent increase in charring rates. This phenomenon has been observed in CLT floors exposed to fire by Frangi et al (2009b), and the proposed approach of EN 1995 1-2 (EN1995-1-2 2004) for initially protected surfaces seemed to well reproduce this delamination phenomenon. However, other studies found very few falling-off of layers (Craft et al 2011; Osborne et al 2012) or a falling-off phenomenon that has negligible influence compared to the design in ambient conditions (Klippel et al 2014). This discrepancy is mainly due to the multitude of parameters that influence such phenomenon, like the type of glue, the thickness of glue lines, the kind of fire exposure, the presence of gaps between lateral boards of each layer and so on. Hence, it is worth to investigate about the influence of a possible falling-off of layers on the mechanical response of fire-exposed timber members.

Fire tests on loaded timber elements (Schmid et al 2010; Menis et al 2012; Fragiocomo et al 2013) are useful to understand the actual thermal-mechanical behavior of the specimen, but they are expensive, time-consuming and sometimes it is not straightforward to obtain reliable information on the actual load-carrying capacity of the panel of the specimen. This is also due to the fact that, in most of the cases, the test is stopped before the failure of the specimen for the safety of people and equipment. Therefore, the evolution of panels deformation during fire exposure is the only information about the variation of mechanical properties during the fire test.

The aim of this study is to use the measured deflections of three CLT floors exposed

to ISO fire for comparing different methods that can be applied for predicting the deflection. In this Chapter, two existing RCSM approaches, a more refined method and a new RCSM approach based on a zero stiffness layer (ZSSL) are compared. Even if the existing RCSM approaches were originally derived for predicting the residual load-carrying capacity of timber members, it may be extended to the prediction of deflection, since the stiffness properties are also affected by the thermal gradient after the char front. Moreover, once the panel is designed on the basis of the existing RCSM for the load-carrying capacity, it could be interesting to investigate about the corresponding deflection predicted using these methods.

First, the available experimental data of bending tests on fire exposed CLT floors is introduced. The subsequent section presents the advanced and simplified modeling in order to reproduce the experimental deflection. Then, the comparison between the predicted and experimental deflection of fire exposed CLT floors is presented. Finally, the results are discussed and the main conclusions are summarized.

6.2 Fire tests on CLT floors

6.2.1 Description of fire tests

Three CLT floors from three different producers have been tested in bending while exposed to ISO fire on their lower face in tension. The out-of-plane load remained constant during fire exposure and the panels were simply supported on two sides. Thermocouples were placed in several sections and over the thickness in order to measure the temperature profiles. The deflection was measured with LVDTs at panel mid-span and the displacement rate was constantly monitored. The end of tests was determined when reaching the safety criterion of (i) maximal displacement rate or (ii) when rupture occurred. Moreover, the fire test could also be stopped when reaching an established time of fire exposure without satisfying any safety criterion. Table 6.1 shows the main properties of the fire tests on CLT floors. All panels were made of Norway spruce (*Picea abies*) lamellas of strength class C24 and glued with one-component polyurethane glue. The panel-to-panel assembling was made with screwed LVL junction and protected with fire insulating joints that ensured the integrity during fire exposure. Suddenly after the end of fire test, the specimen was removed to fire exposure and the fire on its exposed side extinguished with water, which took approximately 6-8 min. Figure 6.1 shows that there were no alteration of panels supports geometry due to fire exposure, allowing therefore the hypothesis of respected simple supported boundary condition for the subsequent modeling step.

6.2.2 Temperature profiles

The temperature evolution within the panels during fire exposure has been measured by means of thermocouples along the cross section. Figure 6.2 presents the position

6. FIRE BEHAVIOR OF STANDARD CLT FLOORS: A STIFFNESS-BASED APPROACH

Test number	Test-1	Test-2	Test-3
Span [m]	4.2	4.6	4.6
Width [m]	2.97	2.6	2.97
Thickness [mm]	195	160	182
Load [kN]	40	40	60
Load distribution	4-points	4-points	Uniform
Distance of point load from supports [m]	1.2	1.2	-
Sections with thermocouples	9	1	4
Thermocouples per section	9	4	10
Exposure time [min]	150	86	90
Safety criterion reached	Displacement rate	Failure	None

Table 6.1: Properties of the tested specimens of CLT floors

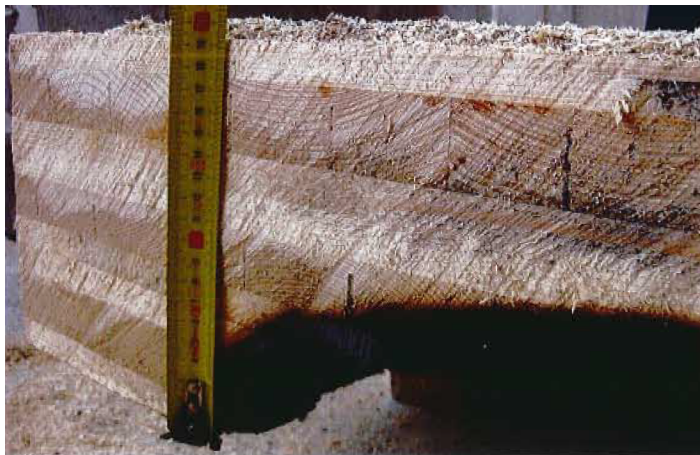


Figure 6.1: Reduced cross section of Test-1 after the fire exposure

6.2 Fire tests on CLT floors

of thermocouples over the thickness for the three tested floors and the directions of each layer. The shielded thermocouples were of type K with a diameter of 1.5mm and drilled inside the specimens by means of an appropriate driller that ensured the perfect straightness and placed in a bore hole having approximately 3mm diameter. Due to

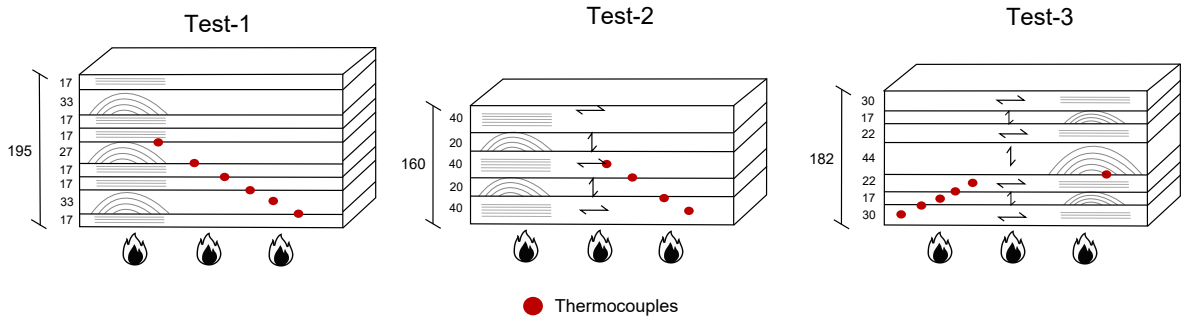


Figure 6.2: Lay-up of CLT floors and position of thermocouples for the three fire tests. Dimensions in [mm]

its high number of thermocouples (9 sections along the span and 9 thermocouples per section) and to the certainty of thermocouple position, Test-1 has the most certain documentation on temperature profiles over the CLT thickness. For this reason, in this Chapter are compared the measured and calculated temperatures only for the Test-1. Concerning the Test-2 and the Test-3 only the comparison of measured and predicted deflections are presented. In Figure 6.3 are plotted the registrations of Test-1 thermocouples placed at 84 mm from the bottom exposed side during the test. The

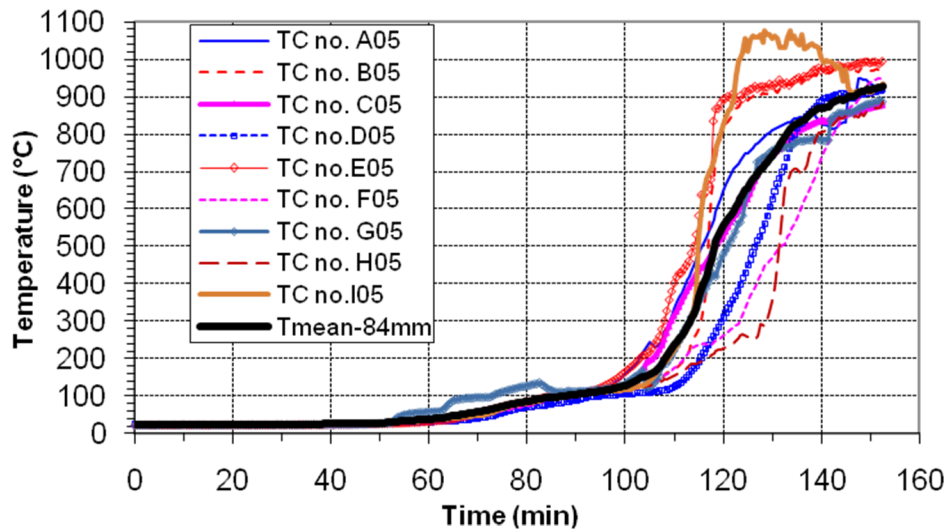


Figure 6.3: Evolution of the measured temperatures in Test-1 at 84mm from the bottom side

solid black line is the considered mean temperature at 84 mm (between layers 4 and 5, see Figure 6.2) thickness from the nine sections along the panels span. The significant difference between measured temperatures from different sections derives from the local delamination of timber pieces that yields a local important increase of temperatures.

6. FIRE BEHAVIOR OF STANDARD CLT FLOORS: A STIFFNESS-BASED APPROACH

6.2.3 Charring rates

Starting from the temperature profiles registered by the thermocouples during the test and assuming 300°C to be the wood charring temperature, one can simply derive the average charring rates $\beta_{\text{mean},i}$ over the CLT thickness. Table 6.2 presents the average computed charring rates for several layers of the three tests during the fire exposure, considering mean temperatures from the available sections. The numbering of layers follows the order of layers exposed to fire.

Test-1			Test-2			Test-3		
Layer	Depth [mm]	$\beta_{\text{mean},i}$ [$\frac{\text{mm}}{\text{min}}$]	Layer	Depth [mm]	$\beta_{\text{mean},i}$ [$\frac{\text{mm}}{\text{min}}$]	Layer	Depth [mm]	$\beta_{\text{mean},i}$ [$\frac{\text{mm}}{\text{min}}$]
1	17	0.67	1	40	0.70	1	30	0.63
1/2(2)	16.5	1.38	2	20	1.34	1/2(2)	8.5	1.70
2	33	0.81				2	17	1.15
3	17	0.77				1/2(3)	11	1.35
4	17	0.68				3	22	1.60

Table 6.2: Calculated charring rates of the three fire tests from mean measured temperatures. In green the nearly respected charring rate of solid wood according to EN 1995 1-2 (0.65mm/min) while the red gradient shows higher charring rates

For the three tests, the great increase in the charring rate when passing from the first to the second layer clearly shows that a delamination of layers occurred. Moreover, the charring rate within layer 2, directly exposed to fire after the delamination of layer 1, is about the double of the previous charring rate, exactly as established by the design approach of initially protected surfaces of EN 1995 1-2. Concerning Test-1, the charring rate across interfaces of layers 2/3 and layers 3/4 nearly respected the charring rate of solid wood (0.65 mm/min in EN 1995 1-2) and therefore no significant delamination phenomena should have occurred. Dealing with Test-2, it was not possible to estimate the charring rates for more than the second layer, due to the shortness of the fire test. Finally, the calculated charring rates for Test-3 highlighted possible delamination phenomena for more than the first layer, leading to a significant increase of mid-span deflection during this Test, as will be presented in the next paragraph. However, the lower certainty on temperature registration for Test-3 compared to Test-1 may somehow overestimate the estimated charring rates. The variation of the estimated charring rates showed in Table 6.2 can be also represented in the char depth/time graph showed in Figure 6.4.

6.2.4 Deflection of fire exposed CLT floors

During the fire tests on loaded CLT floors, the mid-span, deflection was constantly measured by means of Linear Variable Displacement Transducers (LVDT) placed on the upper side in compression. Figure 6.5 plots the evolution of mid-span deflection during fire exposure of the three tested CLT. Test-1 reached the safety criterion of maximum displacement rate at 150 minutes, highlighted by the acceleration of the increase of its mid-span displacement curve versus time. This means also that the specimen was close

6.2 Fire tests on CLT floors

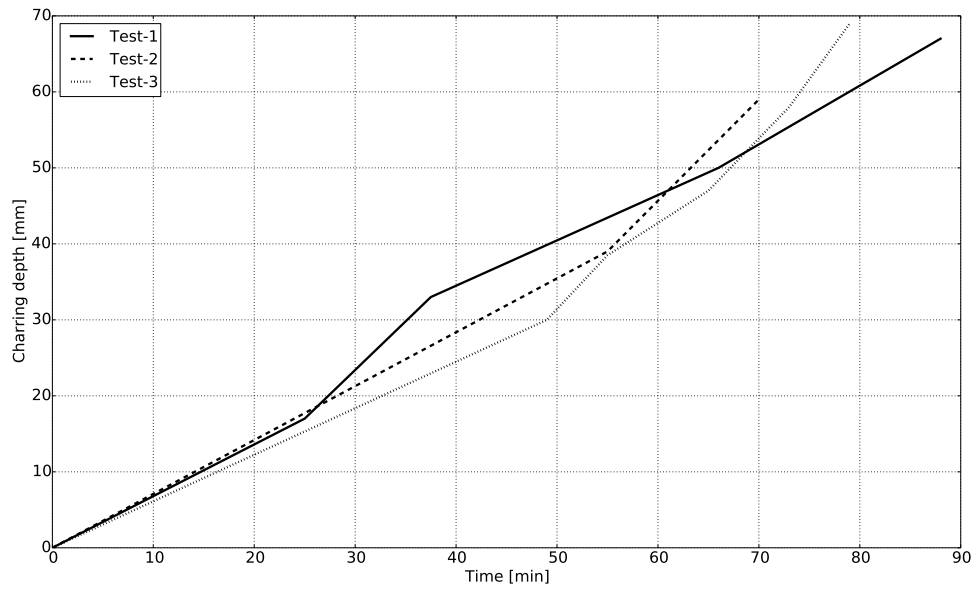


Figure 6.4: Char depth as a function of exposure time for the three tests

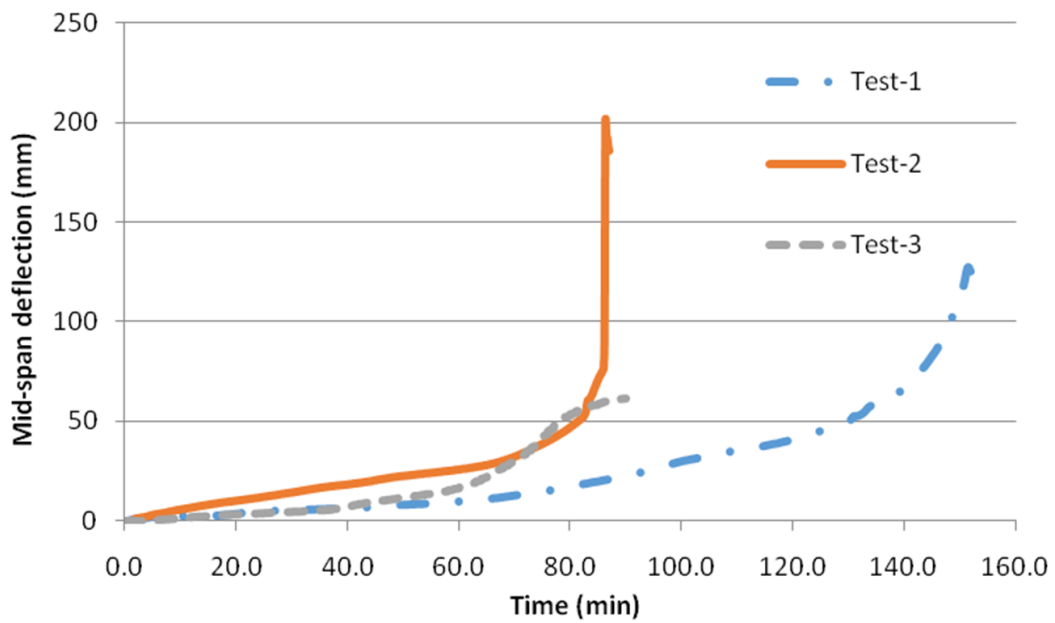


Figure 6.5: Evolution of the mid-span deflection during the three fire tests on CLT floors

6. FIRE BEHAVIOR OF STANDARD CLT FLOORS: A STIFFNESS-BASED APPROACH

to the failure point at that time of fire exposure. The specimen of Test-2 failed brittely on the tension side at 86 min of fire test, as the respective displacement curve shows. Finally, Test-3 was stopped after 90 minutes without reaching any safety criterion. The evolution of the mid-span deflection for Test-3 shows an acceleration at about one hour of fire exposure, with a subsequent smoother trend. The calculated charring rates, based on average measured temperatures, highlighted delamination phenomena at this exposure time which can explain the increase in displacement rate. The evolution of Test-1 deflection shows a slight trend variation due to the progressive charring of layers with or without load-carrying capacity. On the contrary, the floor of Test-2 presents a nearly linear trend of deflection variation until the failure, since almost only the first thick longitudinal layer has been affected by the combustion.

6.3 Modeling

In this section the modeling procedure to reproduce the deflection of tested CLT floors is presented, as well as the design approaches based on the RCSM which will be compared. Two types of advanced modeling are used: heat transfer modeling and thermo-mechanical modeling. The heat transfer modeling is based on temperature prediction with SAFIR (ArGEnCo 2011) software. Then, the mid-span deflection of the floor is predicted using the Bending-Gradient plate theory for thick plates (Lebée and Sab 2011a), combined with woods reduced properties.

6.3.1 Advanced modeling of heat transfer

The temperature evolution over the panels thickness during fire exposure was predicted with SAFIR software (ArGEnCo 2011). CLT panels were modeled as solid wood, with perfect connections between layers. The temperature evolution over the panels thickness during fire exposure was predicted with SAFIR software. CLT panels were modeled as solid wood, with perfect connections between layers. The density of specimens was measured and found to be in accordance with the mean value of 420 Kg/m^3 specified in EN 338 (EN 2009). Preliminary analyses investigated on the value to use for moisture content, fitting the predicted temperature to thermocouples registrations for Test-1, leading to the value of 12%. The emissivity (ε) of the modeled wood was set to 0.8, while the coefficients of convection of heated (h_h) and unheated (h_c) surfaces were assumed to be respectively $25 \text{ W/m}^2\text{K}$ and $4 \text{ W/m}^2\text{K}$. One dimensional uniform mesh of 1 mm was applied as a discretization over the panel thickness for the temperature prediction. Figure 6.6 plots the comparison between predicted and experimental temperature profiles during Test-1 across the specimen thickness. The falling-off of layer 1 of Test-1 pointed out in Table 2 and Figure 5 probably leads to the sharp increase of the measured temperatures at 20 minutes (blue curve) by the thermocouples at layers 1/2 interface. Globally, the predicted temperatures are in good agreement with the

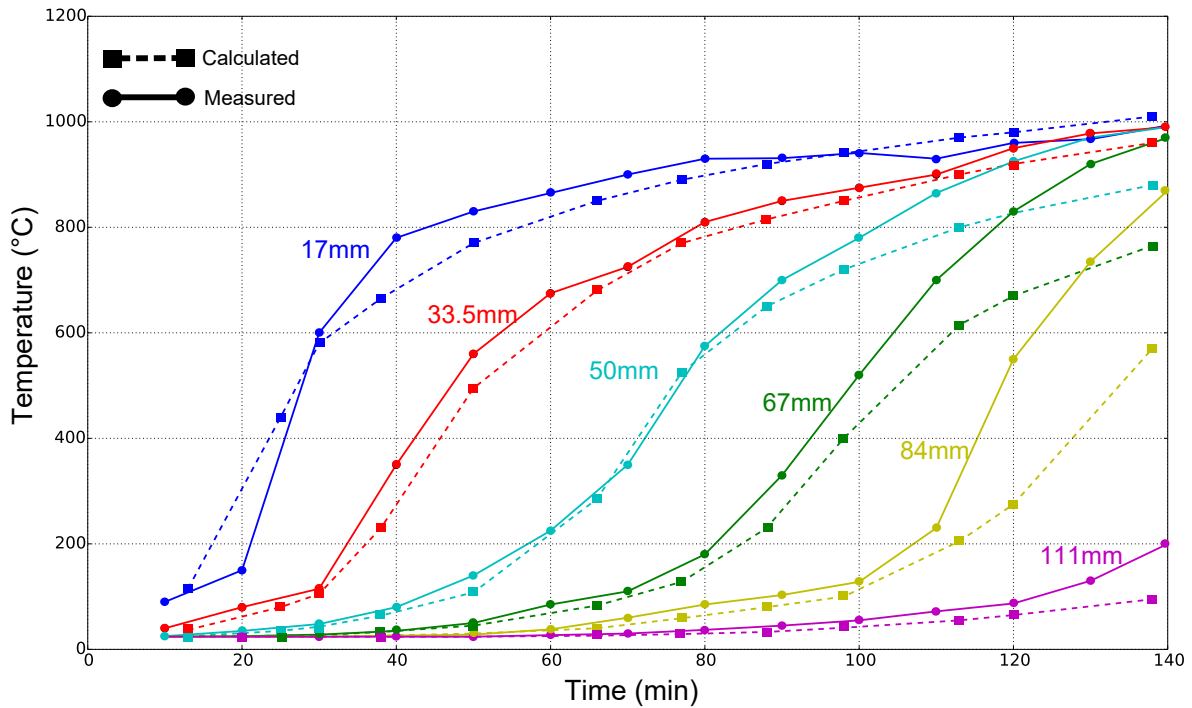


Figure 6.6: Evolution of the predicted and measured temperatures within the floor of Test-1

measured values during the fire test. However, slightly lower temperatures than the reference are predicted at high exposure times and for deep sections.

6.3.2 Thermo-mechanical modeling

The thermo-mechanical behavior of CLT floors has been modeled with a “multilayer” model, with each layer having the mesh thickness of 1 mm. Wood is an orthotropic material with three principal axes and therefore its elastic behavior is defined by three Youngs moduli, three shear moduli and three Poissons ratios. However, since within timber boards of CLT is not possible to know the local orientation of wood axes, wood can be modeled as a transversely isotropic material (Chapter 2) (EN 2009) having only a longitudinal (0) and transverse (90) direction. Further analyses highlighted the negligible influence of Poissons ratios on the deflection prediction and therefore are set to zero. Since no characterization of the raw material has been done, the elastic moduli of wood according to strength class C24 and a rolling shear modulus (G_{90}) of 50 MPa were considered (Table 6.3). Once the temperature profile is established for

Modulus of Elasticity	E_0	E_{90}	G_0	G_{90}
Stiffness [MPa]	11000	370	690	50

Table 6.3: Stiffness properties of C24 strength class timber according to EN 338

each considered exposure time, the elastic moduli changed as a function of temperature

6. FIRE BEHAVIOR OF STANDARD CLT FLOORS: A STIFFNESS-BASED APPROACH

using the reduction coefficient $k_{\theta,E}$ given by laws of EN 1995 1-2 (Figure 6.7). Different reductions of Young's modulus for the upper or lower part of the CLT floor (compression or tension side) have been taken into account. Since no reduction coefficient of the shear moduli has been given in EN 1995 1-2, the same law as compressive Young's modulus has been adopted for them. Finally, with the reduced properties for each 1mm

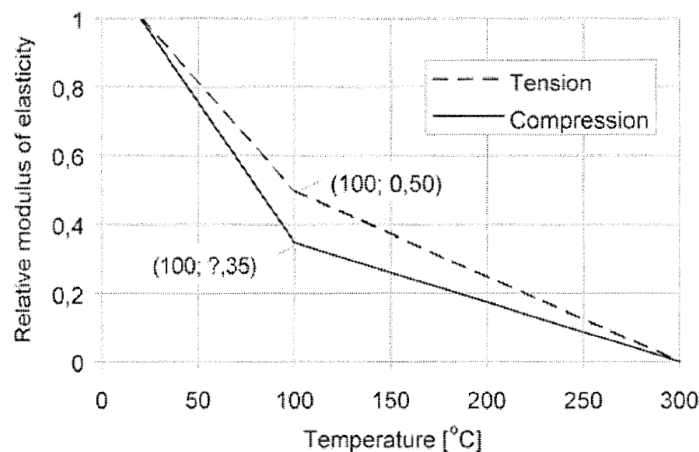


Figure 6.7: Effect of temperature on modulus of elasticity parallel to grain of softwood (EN1995-1-2 2004)

layer, the mid-span deflection is computed with the Bending-Gradient plate theory for thick layered plates (Lebé and Sab 2011a) already described in Section 4.2.1 of Chapter Chapter 4. According to this method, the elastic properties of the mesh are homogenized with a semi-analytical procedure in order to obtain the equivalent out-of-plane bending and transverse shear stiffnesses of the panel. This calculation is performed at each increment of exposure time in order to predict the evolution of mid-span deflection.

6.3.3 Reduced Cross Section modeling

Since recent studies pointed out that the current version of the RCSM is not always conservative, several attempts to improve the RCSM without changing its simple principle have been done. In the next paragraphs, three methods to determine the geometry of the effective cross section are presented. Once the effective geometry is established, properties at ambient conditions of C24 timber from EN 338 are combined with the plate theory in order to predict the mid-span deflection according to the RCSM.

6.3.3.1 Existing RCSM approaches

- **RCSM-1.** The first existing RCSM approach has been derived by Schmid et al (2012) fitting results of advanced numerical simulations on timber members in bending. According to this method, the charring rate is uniform as prescribed in the EN 1995 1-2 (0.65 mm/min), while the zero-strength layer (ZSTL) layer is derived as a function

of panels total thickness and of the exposed side. Applying this approach to the three tested panels leads to the following values of ZSTL: Test-1 = 11 mm; Test-2 = 10.7 mm; Test-3 = 10.8 mm.

- **RCSM-2**. The second simplified design model (Frangi et al 2009b) is based on the initially protected surfaces approach of EN 1995 1-2, in order to take into account the delamination phenomenon discussed in the previous section. Hence, a double charring rate (1.3 mm/min) is considered after the complete charring of each layer (delamination moment), until the char depth exceeds 25 mm. Beyond these 25 mm of char depth, the charring rate returns at 0.65 mm/min. Within this method, the value of ZSTL was not established, hence the value set by the EN 1995 1-2 (7mm) is combined with RCSM-2.

6.3.3.2 Proposal for improving the RCSM

More than the two presented existing models, a new simplified approach based on the RCSM is suggested in this study (**RCSM-3**). The principle is to define the reduced section of the floors taking into account the reduction factor for modulus of elasticity $k_{\theta,E}$. In other words, the basic idea is to calculate the reduced thickness of each discretized mesh by the advanced modeling as a function of the temperature calculated with Safir software. Then, for each fire exposure time, the zero stiffness layer (ZSSL) of the floor is the sum of all reduced thicknesses of meshes. The suggested deriva-

1mm	20°C	1.00	$(1-1)*1 = 0 \text{ mm}$
1mm	30°C	0.90	$(1-0.9)*1 = 0.1 \text{ mm}$

1mm	180°C	0.30	$(1-0.3)*1 = 0.7 \text{ mm}$
1mm	240°C	0.15	$(1-0.15)*1 = 0.85 \text{ mm}$
h = 0.65*time T > 300°C charred wood			



Figure 6.8: Principle of determination of the ZSSL as a function of exposure time

tion of the ZSSL is therefore based on the hypothesis that at established reduction of stiffnesses corresponds the same reduction of geometry (or loss of material). Results from Chapter 4 showed that this hypothesis is valid when dealing with the bending deflection, without contribution of transverse shear. On the contrary, such hypothesis is not anymore valid concerning the transverse shear deflection. However, since the geometry and the lay-up of the considered panels yield a low contribution of transverse shear to global deflection (in the range of 10%-12%), this principle can be applied to the tested panels with a low margin of error. When plotting the estimated ZSSL versus the time of fire exposure, a plot like the one showed in Figure 6.9 can be found. From Figure 6.9 it is clear that the ZSSL increases during exposure time, reaching values

6. FIRE BEHAVIOR OF STANDARD CLT FLOORS: A STIFFNESS-BASED APPROACH

much higher than the constant 7mm prescribed in the EN 1995 1-2. On the basis of

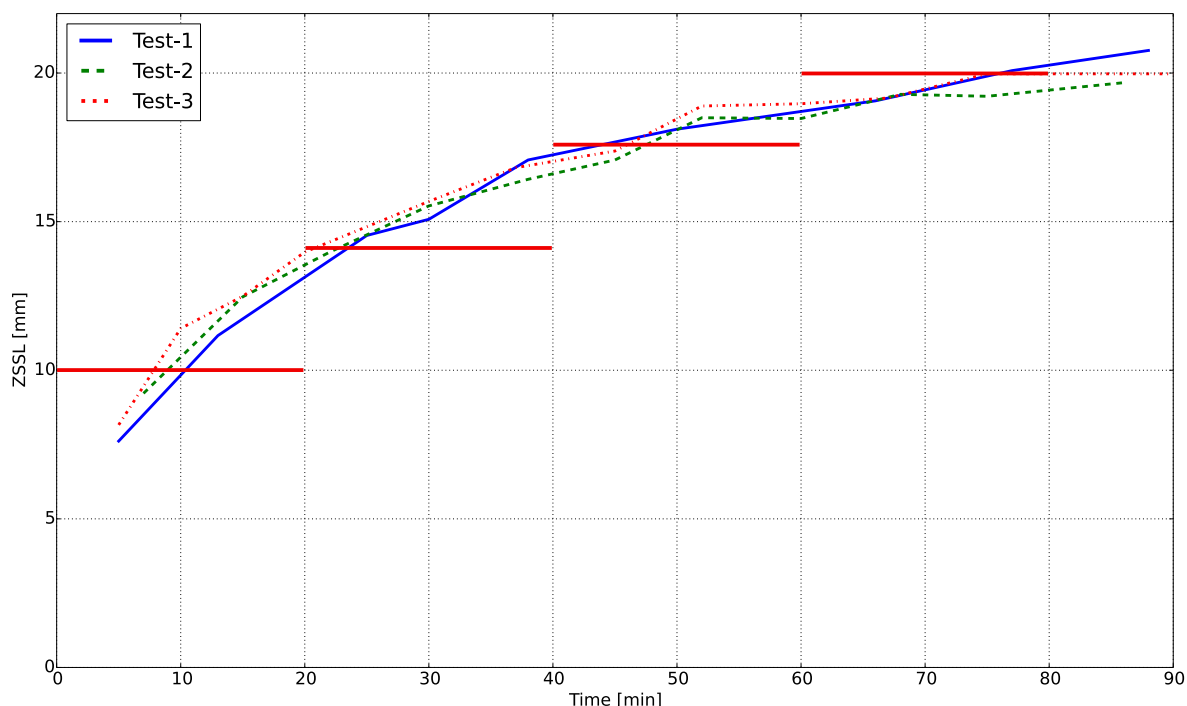


Figure 6.9: Evolution of the estimated zero stiffness layer (ZSSL) for the three tests as a function of exposure time. The red lines shows the considered values for four ranges of time

Figure 6.9, values of ZSSL as a function of time are therefore suggested, in order to take into account the increasing heat flux received by the CLT panel during fire exposure. Finally, a simplified design approach can be obtained setting four values of zero stiffness layer for four ranges of time as in Table 6.4. The slight differences between the estimated values of ZSSL for the three tests in Figure 6.9 shows that the suggested ranges in Table 4 can be used for the new suggested RCSM.

Time t [min]	$t < 20$	$20 < t < 40$	$40 < t < 60$	$t > 60$
ZSSL [mm]	10	14	17	20

Table 6.4: Suggested values of ZSSL as a function of exposure time

6.4 Comparison

The comparison between the predicted and experimental mid-span deflection for the three fire tests on CLT are showed from Figure 10 to Figure 12. As already introduced in 3.2, the RCSM-1 method is according to Schmid et al (2012), the RCSM-2 is according to Frangi et al (2009b) and RCSM-3 considers the ZSSL as a function of time. For the three approaches based on reduced cross section, the k_0 used for the calculation of

ZSTL and ZSSL are computed as in EN 1995 1-2. The advanced modeling based on

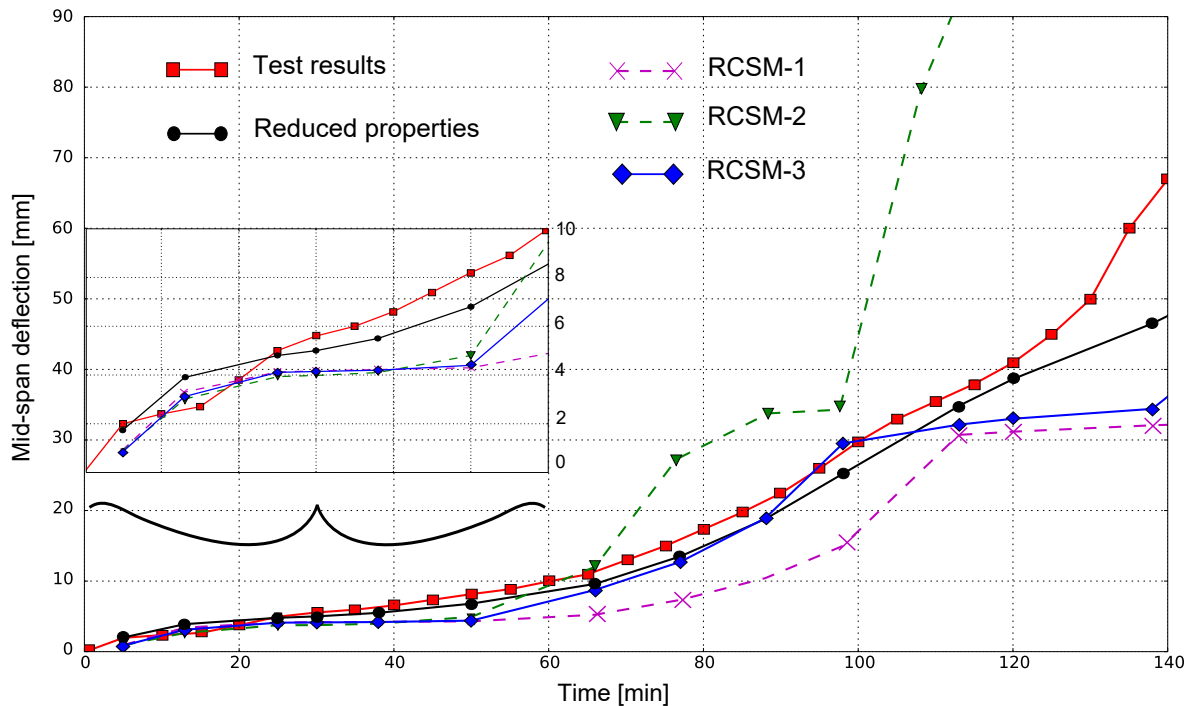


Figure 6.10: Comparison between the experimental and predicted mid-span deflection of Test-1

reduced properties returns the mid-span deflection that less deviates from experimental results for the three tests. The evolution of the deflection predicted by all RCSM methods shows plateau corresponding to the non-contribution of cross layers to global stiffness but not highlighted by test results. By contrast, the advanced modeling based on reduced stiffness is able to follow the experimental evolution of deflection, showing that the actual phenomenon is a progressive reduction of properties and not a reduction of geometry. The RCSM-3 based on the time-dependency of the ZSSL gives a better description of the measured deflection compared to other RCSM approaches. The RCSM-1 approach underestimates the deflection of the three fire tests. Despite of the delamination of the first layer in Test-1 previously highlighted, the RCSM-2 (derived to take into account such phenomenon) overestimates the Test-1 deflection. The deflection of Test-2 is underestimated by both existing RCSM approaches. Dealing with Test-3, all the RCSM methods show similar slope of the deflection evolution trend, but with an offset due to the different ways of estimating the residual cross section. Indeed, the double charring rate considered by RCSM-2 compensates somehow the higher values of the additional layer to remove of RCSM-3, while RCSM-1 predicts lower deflection since it considers lower values of the ZSTL. In the final parts of Figure 6.10 and Figure 6.11, all methods underestimate the deflection. This is because both of specimens were close to failure at those exposure times and hence the increasing non-linear contributions to deflection cannot be taken into account by the plate theory.

6. FIRE BEHAVIOR OF STANDARD CLT FLOORS: A STIFFNESS-BASED APPROACH

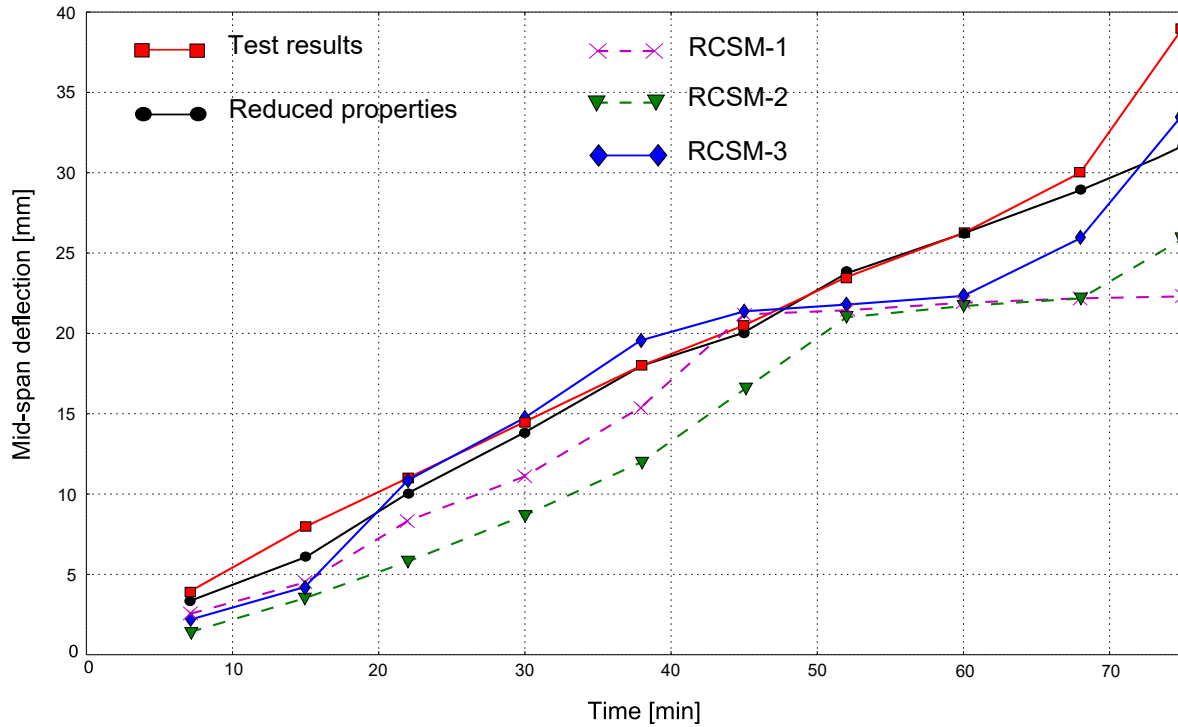


Figure 6.11: Comparison between the experimental and predicted mid-span deflection of Test-2

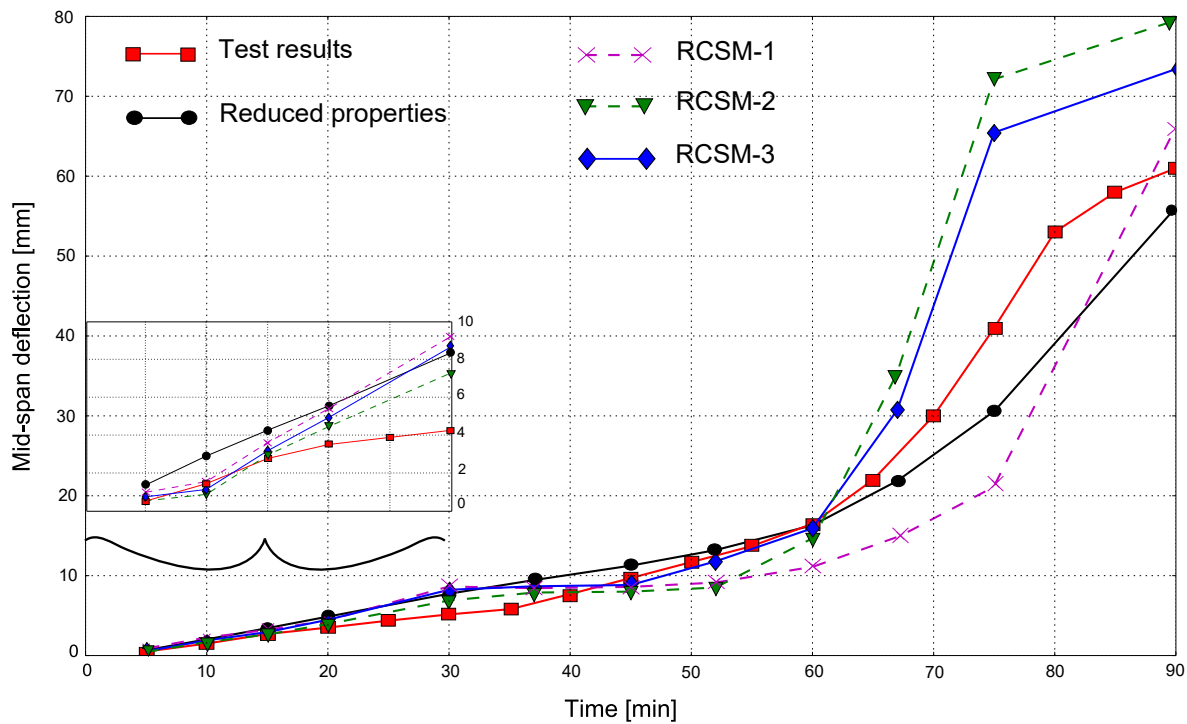


Figure 6.12: Comparison between the experimental and predicted mid-span deflection of Test-3

6.5 Discussion

The stiffness-based approach (RCSM-3) presented in this Chapter shows that, in most of the cases, the calculated deflections are in agreement with the measured deflections while the existing RCSM approaches globally deviate from test results. However, as is known, the existing RCSM approaches were originally derived for predicting the load-carrying capacity of timber elements, hence, the differences observed between measured and calculated deflections are understandable. Consequently, in order to correctly model the fire behavior of CLT floors, it could be interesting to enhance the research in order to define the best method for the designs of these structural elements. Perhaps the method based on ZSSL suggested in this study could be interesting for CLT floors, but has to be further investigated for different configurations and different load levels.

Dealing with the sensitivity of predicted results, like in every modeling procedure, the predicted results can be affected by the variation of input material parameters. Unfortunately, the raw material of CLT has not been tested in ambient conditions and the input mechanical properties for the modeling are based on mean stiffnesses given by C24 strength class in EN 338. However, the model to predict the panels mechanical behavior in ambient conditions implemented in this work (the plate theory) is based on linear elasticity, like common engineering methods. Hence, a given variation of wood stiffnesses yields the same variation of mechanical response. On the contrary, physical properties of the modeled material such as conductivity, relative humidity or volume specific heat can lead to significant variation of predicted temperatures and therefore even greater variation of the predicted mechanical behavior with the advanced modeling. More accuracy in determining the physical and mechanical properties of the raw material is therefore encouraged for future researches.

The delamination phenomenon is a complex mechanism influenced by a multitude of parameters and therefore very difficult to predict. It can occur locally, with delamination of small pieces of wood, or with a complete falling-off of layer. The charring rate estimation with thermocouples registration pointed partial delamination phenomena for the three considered tests. In particular, the calculated charring rates of Test-3 pointed out delamination of more than the first layer. The same Test-3 showed an acceleration of mid-span deflection that may be due to such delamination phenomenon. On the contrary, the less pronounced delamination of Test-1 and Test-2 had no visible influence on the global evolution of deflection. This discrepancy confirms the complexity of this phenomenon and suggests enhancing the studies about the effective influence of delamination on structural fire safety of laminated timber structures. It seems that the existing RCSM-2 model can lead to quite conservative results in the cases without delamination and to better results in cases of delamination.

6. FIRE BEHAVIOR OF STANDARD CLT FLOORS: A STIFFNESS-BASED APPROACH

6.6 Conclusion

In the present Chapter, the experimental deflection of fire exposed CLT floors has been predicted with advanced modeling based on reduced properties and the simplified approach of the RCSM. The best way to correctly simulate the fire behavior of CLT floors is by means of an advanced modeling. However, the methods based on the RCSM approach are more convenient for practical applications by engineers. This is the reason why it would be interesting to find the best RCSM method for the calculation of deflection and perhaps the design of CLT in fire conditions.

The results presented within this study show that RCSM-3 based on the time-dependency of the additional layer to remove could be a relevant method for simulating the fire behavior of CLT floors. This approach is a research path which seems interesting to investigate, in order to define the relevant method for the fire design of CLT floors to be taken into account by the on-going revision process of EN 1995 1-2 (EN1995-1-2 2004). However, this method has to be further investigated for different configuration of floors and under different load conditions.

Chapter 7

Conclusions and outlooks

In the present thesis, the mechanical behavior of regularly spaced CLT panels has been investigated by means of modeling and experimental validation. The influence of both short spaces of standard CLT and large spaces of innovative panels on the mechanical response has been analyzed.

First, continuous or discontinuous layers of standard CLT panels have been modeled with an equivalent layer model based on simplified hypotheses on mechanical properties. The combination with the exact 3D analytical solution (Pagano 1969) and a failure criterion for wood (van der Put 1982) returned a rather good comparison with a reference bending test of the literature (Hochreiner et al 2013). The 3D solution enabled a good description of local punching effects and interactions between shear stress and stress perpendicular to the grain. From the modeling-experimental comparison, it appeared that gluing lateral boards have a negligible influence on bending stiffness and a moderate influence on failure load and failure modes. The discontinuous equivalent layer returned the best fit with the experimental evidence. Then, parameter studies about the influence of several CLT properties on elastic and failure behavior pointed out interesting features for CLT applications. In particular, innovative orientations of transverse layers can, in some cases, lead to an improved mechanical behavior, confirming recent experimental studies of the literature (Chen and Lam 2013; Buck et al 2016). However, there are also several cases where an innovative lamination of CLT layer can yield significant losses in the load-carrying capacity of the panel.

The equivalent-layer approach is not able to exactly quantify the influence of small gaps on the mechanical behavior, as well as to predict the effect of increasing the spaces between lamellas up to hundreds of millimeters. Hence, a reference experimental behavior of spaced CLT was set. Dealing with the out-of-plane behavior, 4-points bending tests have been performed on standard and innovative panels. Test results highlighted that enlarging the spaces yields a progressive increase of the shear part of the deflection and a failure mode transition from bending to transverse shear. The reference in-plane shear behavior of spaced CLT diaphragms was chosen on the basis of an experimental investigation of the literature (Brandner et al 2015) on standard panels.

7. CONCLUSIONS AND OUTLOOKS

The identified existing approach for predicting spaced CLT out-of-plane behavior is combining a method for massive panels (Kreuzinger 1999) to wood properties reduced by the volume fraction within the panel. Dealing with the in-plane shear stiffness, the closed-form solution by Moosbrugger et al (2006) is applied to both short and large spaces between lamellas. Since such existing methods are simplified approaches, a more refined modeling is needed for predicting spaced CLT mechanical behavior and for enabling a better understanding of spaced CLT mechanics. The great influence of shear effects when increasing the spaces motivated the choice of a thick plate theory (Lebéé and Sab 2011a) for predicting the elastic behavior of spaced CLT. A homogenization scheme based on FE energy equivalence with a periodic unit-cell (Lebéé and Sab 2012) was implemented in order to apply the plate theory to the panel's geometry. It turns out that the reduction of bending stiffness as a function of increasing spaces follows the volume fraction within the panel. Hence, the volume fraction approach returns the same results as homogenization and is in good agreement with test results. Dealing with in-plane shear stiffness, in most of the cases the existing closed-form solution by Moosbrugger et al (2006) deviates from homogenization results, which returns good agreement with the experiment of the literature. Finally, the reduction of the shear force stiffness due to the presence of spaces does not follow the volume fraction within the panel, leading to an overestimation of the stiffness by the volume fraction approach. In contrast, the homogenization model returned very good agreement with the experimental values of shear force stiffness. Finally, the maximum longitudinal and shear stresses of the tested panels at failure point predicted with the homogenization scheme were in good agreement with mean tensile and rolling shear strength of the literature. This confirms the experimental transition from bending to shear failure modes observed during the 4-points bending tests.

The computational costs of the FE homogenization modeling motivated the derivation of approximated closed-form solutions for predicting spaced CLT elastic behavior. The unit-cell was modeled as 3D space frame of Timoshenko beams connected each other with deformable wooden blocks. The deformable blocks have been simply modeled as rotational springs when submitted to in-plane shear, following several approaches of the literature. By contrast, when submitted to transverse shear, a transverse shear kinematics has been imposed to the whole block. Basically, the same energy equivalence principle of the FE homogenization has been applied to a simplified geometry of the unit-cell in order to estimate the strain energy with closed-form expression. The derived closed-form expression of bending and membrane stiffnesses are based on the volume fraction approach and therefore return very good match with the reference behavior. Dealing with in-plane shear and torsional stiffnesses, simplified closed-form solutions have been suggested, which predict stiffnesses in agreement with the reference numerical results. Several simplified hypotheses have been done as well on the transverse shear kinematics of the unit-cell, leading to closed-form expressions for spaced CLT transverse shear stiffness giving a good agreement with the numerical homogenization. The derived closed-form solutions give a better prediction of in-plane shear,

torsional and transverse shear stiffnesses of standard CLT than the approach currently adopted by the working draft for CLT design of the revised version of Eurocode 5 1-1 (EN1995-1-1 2015). This suggests a possible future standardization of the obtained closed-form solutions for predicting the stiffnesses of crosslam having lateral spaces up to 6 mm (EN-16351 2016). Finally, closed-form solutions for predicting the maximum longitudinal and rolling shear stress of spaced CLT have been derived. The comparison with FE maximum stresses pointed out that the closed-form expressions return a good prediction of the maximum stress. The longitudinal stresses are very well predicted, while the rolling shear stresses are generally slightly overestimated up to 10% that is, from an engineering point of view, on the safe side but not too conservative.

The study on the fire behavior of standard CLT floors aimed to suggest a possible improvement of the existing structural fire design for timber members of the Eurocode 5 1-2 (EN1995-1-2 2004) reproducing the experimental data with advanced and simplified modeling. The deflection of CLT floors exposed to fire has been used to obtain information on the elastic properties of the panel during fire exposure. The available experimental data included three fire tests on out-of-plane loaded CLT panels. The advanced modeling was based on FE heat transfer prediction and reduced stiffnesses with the Eurocode's law. The simplified modeling was based on the Reduced Cross Section Method (RCSM) of the Eurocode 5 1-2 which considers reduced geometry instead of reduced properties of wood during fire exposure. More than two existing RCSM approaches, a proposal for improving the current version of the RCSM has been suggested. The principle is to use the heat transfer predicted with the advanced modeling in order to make the the additional layer to remove dependent on the exposure time. For the three fire tests, the experimental deflection has been well predicted with the advanced modeling, while the existing RCSM deviated from the reference deflection. In contrast, the suggested approach based on time-dependent additional layer to remove returned a good comparison with the advanced modeling and test results. This approach of considering a time-dependent value of the additional layer to remove within the RCSM may be a research path to follow in order to find the relevant method for the fire design of CLT panels.

7.1 Limitations

This thesis deals with the elastic and deterministic mechanical behavior of spaced CLT. Dealing with timber failure behavior, there is a great influence of natural variability such as wood's defects or knots. However, this variability has not been taken into account, as well as damage or ductile effects of wood constitutive behavior. Therefore, timber failure in the present work, especially longitudinal tensile failure, has been defined as the reach of strength values by means of elastic stresses.

Dealing with the homogenization modeling, for both FE and closed-form approaches the mirror symmetry with respect to panel's mid plane has to be satisfied. Moreover,

7. CONCLUSIONS AND OUTLOOKS

the derived closed-form expressions for stiffnesses and maximum stresses consider all layers having the same thickness. This in order to obtain closed-form solutions as simple as possible. However, the suggested closed-form expressions could be extended to panels having layers with varying thickness, at the price of more complex equations. Due to time constraints, the terms f_{33}^{BG} and f_{66}^{BG} related to the additional Bending-Gradient shear variables R_3 and R_6 have not been compared to the reference FE homogenization. Hence, the suitability of the suggested closed-form approach have to be further checked to return a good estimation of also these additional terms of the shear force compliance.

The suggestion for a possible improvement of the current fire design model in Chapter 6 has been based upon a “stiffness approach”, because of the deflection of fire exposed CLT floors used as the mechanical information to predict. Therefore, the additional layer to remove for the RCSM modeling derived as a function of exposure time compensate the losses in stiffness (zero stiffness layer). However, the fire design of timber members is mostly governed by the Ultimate Limit States, and therefore the additional layer to remove should compensate the losses in strength (zero strength layer). From an engineering point of view this approximation can be considered reasonable, but it has to be kept in mind when comparing existing RCSM approaches in Chapter 6 which have been derived for predicting the load-carrying capacity of fire-exposed timber members.

7.2 Outlooks

The present thesis is a first attempt to explore the possibilities of application of lightweight CLT panels in the modern timber construction. Furthermore, the mechanical behavior of standard CLT panels has been investigated in ambient and fire conditions as well. Based on the comparison between predicted and experimental results, simplified modeling tools useful for practical applications have been derived.

The approach based on elastic and deterministic modeling can be improved considering the uncertainties deriving from timber natural variability. This involves a probabilistic modeling that can be integrated in future in the presented modeling. This can be particularly interesting since the CLT “system effect” that increases the raw material stiffness and strength (see Chapter 2) is progressively lost when the spaces increase, leading isolated knots exposed in free edges (see Chapter 4). This effect may be correctly modeled with a probabilistic approach.

As already introduced in the previous paragraph, the developed modeling tools are valid for simplified geometry of spaced CLT. Hence, an outlook of the present work could be studying more complex geometries of spaced CLT panels, with layers having different thicknesses or different orientation of transverse layers that could limit the shear compliance of the panel (see Chapter 2). Moreover, CLT offers the potential application to free-form structures, in which the panels can be entirely rotated, with

all layers in a cross-grain condition (Cheng et al 2016). In this case, the additional shear variables handled by the Bending-Gradient plate theory are needed in order to correctly predict transverse shear effects. The periodic alternation along the panel could be different than wood/insulating material. For instance, massive panels having a regular alternation of lamellas of different strength class or different species can be modeled exactly as presented in this thesis. This can respond to the current demand within the timber construction field of using local wood species.

Finally, the stiffness-based approach suggested in Chapter 6 for improving the current fire design model of EN1995-1-2 (2004) suggests a research path that may be followed in future in order to investigate about the time-dependency of the zero strength layer. In addition, the influence of short spaces between lateral lamellas in CLT exposed to fire on the thermo-mechanical response may be further investigated coupling the modeling tools in ambient and fire conditions developed in this thesis.

Acknowledgments

The authors gratefully acknowledge the research team composed of G. Hochreiner, J. Fussl and J. Eberhardsteiner (Vienna University of Technology, Institute for the mechanics of materials and structures) for sharing their experimental data. The producers Binderholz gmbh and Techniwood SAS are also acknowledged for supplying the specimens for the experimental investigation.

7. CONCLUSIONS AND OUTLOOKS

Bibliography

- Aicher S, Dill-Langer S (2000) Basic considerations to rolling shear modulus in wooden boards. Tech. rep., Otto Graf Journal 4
- Andreolli M, Tomasi R, Polastri A (2012) Experimental investigation on in-plane behaviour of crosslaminated-timber elements. In: International Council for Research and Innovation in Building and Construction, Working Commission W18 5, 6
- ANSI/APA (2012) ANSI/APA PRG 320-2012 Standards for performance-rated cross-laminated timber. ANSI/APA, Tacoma, US 6
- Araki Y, Nakajima S, Yamaguchi Y, Nakagawa T, Miyatake A, Yasumura M (2014) In-plane shear test of full scale cross laminated timber panels. In: Proceedings of the 13th World Conference on Timber Engineering 5
- ArGEnCo (2011) SAFIR (software), version 2011.b.3. University of Liege 112
- Bernasconi A (2016) Four Residential towers as CLT timber construction in the city of Milan. In: Proceedings of the 14th World Conference on Timber Engineering, Vienna (AUT) 2
- Blass H, Fellmoser P (2004a) Design of solid wood panels with cross layers. In: Proceedings of the 8th World Conference on Timber Engineering 5, 21, 27, 68
- Blass H, Fellmoser P (2004b) Influence of rolling shear modulus on strength and stiffness of structural bonded timber elements. In: International Council for Research and Innovation in Building and Construction, Working Commission W18 4, 27
- Blass H, Goerlacher R (2002) Zum Trag- und Verformungsverhalten von BrettsperrholzElementen bei Beanspruchung in Plattenebene. Bauen mit Holz 11:30–34 83
- Blass H, Gorklacher R (2000) Rolling shear in structural bonded timber elements. In: International conference on wood and wood fiber composites 4, 8, 27, 46
- Blass H, Schadle P (2011) Ductility aspects of reinforced and non-reinforced timber joints. Engineering Structures 33(11):3018–3026 2

BIBLIOGRAPHY

- Bogensperger T, Jobstl R (2015) Concentrated load introduction in CLT elements perpendicular to plane. In: Proceedings of the 2nd International Network on Timber Engineering Research meeting 2
- Bogensperger T, Moosbrugger T, Silly G (2010) Verification of CLT-plates under loads in plane. In: Proceedings of the 11th World Conference on Timber Engineering 6, 7, 57, 98
- Bogensperger T, Augustin M, Schickhofer G (2011) Properties of CLT panels exposed to compression perpendicular to their plane. In: Proceedings of the 44th CIB W18 meeting 5
- Branco JM, Kekeliak M, Lourenco PB (2014) In-plane stiffness of timber floors strengthened with CLT. *European Journal of Wood and Wood Products* 73(3):313–323 3
- Brandner R, Schickhofer G (2014) Properties of cross laminated timber (CLT) in compression perpendicular to grain. In: Proceedings of the 1st International Network on Timber Engineering Research meeting 5
- Brandner R, Bogensperger T, Schickhofer G (2013) In plane Shear Strength of Cross Laminated Timber (CLT): Test Configuration, Quantification and influencing Parameters . In: International Council for Research and Innovation in Building and Construction, Working Commission W18 5, 57
- Brandner R, Dietsch P, Droscher J, Shulte-Wrede M, Kreuzinger H, Sieder M, Schickhofer G, Winter S (2015) Shear properties of Cross Laminated Timber (CLT) under in-plane load: test configuration and experimental study. In: Proceedings of the 2nd International Network on Timber Engineering Research meeting 5, 32, 34, 43, 44, 60, 71, 121
- Brandner R, Flatscher G, Ringhofer A, Schickhofer G, Thiel A (2016) Cross Laminated Timber (CLT): overview and development. *European Journal of Wood and Wood Products* 74(3):331–351 2
- Buck D, Xiaodong W, hangman O, Gustafsson A (2016) Bending properties of Cross Laminated Timber (CLT) with a 45° alternating layer configuration. *BioResources* 11:2 4, 5, 29, 31, 32, 121
- Cabrero JM, Blanco C, Gebremedhin KG, Martin-Meizoso A (1984) Assessment of phenomenological failure criteria for wood. *Mathematical Methods in the Applied Sciences* 6(2):159–191 18
- Caillerie D (1984) Thin elastic and periodic plates. *Mathematical Methods in the Applied Science* 6(2):159–191 48, 49

BIBLIOGRAPHY

- Chen Y, Lam F (2013) Bending performance of box-based Cross-Laminated Timber systems. *Journal of Structural Engineering* 139(12) 4, 5, 29, 121
- Cheng A, Schneider J, Tannert T (2016) Effective out-of-plane stiffness and strength of rotated Cross Laminated Timber panels. In: *Proceedings of the 14th World Conference on Timber Engineering* 125
- Craft S, Desjardins R, Mehaffey J (2011) Investigation of the behaviour of CLT panels exposed to fire. In: *Proceedings of the 12th International Conference Fire and Materials* 3, 9, 106
- Czaderski C, Steiger R, Howald M, Olia S, Gulzow A, Niemz P (2007) Tests and calculations on 3-layered cross-laminated solid wood panels supported at all edges. *European Journal of Wood and Wood Products* 65:383–402 4, 27, 92
- Dahl K (2009) Mechanical properties of clear wood from Norway spruce. PhD thesis, Norwegian University of science and technology 16, 17
- DIN (2004) DIN 1052:2004 Design rules for timber buildings (in German). German Institute of Standardization, Berlin, Germany 5
- DIN (2012) DIN 4074-1:2012-06: Strength classes for Norway spruce timber (in German). German Institute of Standardization, Berlin, Germany 38
- Eberhardsteiner J (2002) Mechanical behavior of Spruce (in German). Springer, Vienna, Austria 17
- Ehrhart T, Brandner R, Schickofer G, Frangi A (2015) Rolling Shear Properties of some European Timber Species with Focus on Cross Laminated Timber (CLT): Test Configuration and Parameter Study. In: *Proceedings of the 2nd International Network on Timber Engineering Research meeting* 4, 42, 64, 68
- EN (2009) EN 338: Structural timber - strength classes. European Committee for Standardization, CEN, Bruxelles, Belgium 4, 15, 27, 39, 112, 113
- EN-16351 (2016) Timber Structures: Cross Laminated Timber, requirements. European Committee for Standardization, CEN, Bruxelles, Belgium 6, 7, 51, 123
- EN1995-1-1 (2004) EN 1995 1-1: Design of timber structures. Part 1-1: General Common rules and rules for buildings. European Committee for Standardization, CEN, Bruxelles, Belgium 5, 8, 21, 80
- EN1995-1-1 (2015) Working draft of CLT design in a revised Eurocode 5-1-1. Version 2015-10-30 (confidential). European Committee for Standardization, CEN, Bruxelles, Belgium 6, 7, 95, 98, 123

BIBLIOGRAPHY

- EN1995-1-2 (2004) EN 1995 1-2: Design of timber structures. Part 1-2: Structural fire design. European Committee for Standardization, CEN, Bruxelles, Belgium 3, 9, 10, 105, 106, 114, 120, 123, 125
- ETA (2013) ETA - 06/0009: Binderholz Cross Laminated Timber BBS. Binderholz Bausysteme GmbH, Zillertalstrasse 39 6263 Fügen, Austria 27
- Fast P, Gafner B, Jackson R, Li J (2014) Case study: an 18-storey tall mass timber hybrid student residence at the University of British Columbia, Vancouver. In: Proceedings of the 13th World Conference on Timber Engineering 2
- Flaig M, Blass H (2014) Bending strength of Cross Laminated Timber beams loaded in plane. . In: Proceedings of the 13th World Conference on Timber Engineering 70
- Flatscher G, Bratulic K, Schickhofer G (2014) Screwed joints in Cross Laminated Timber structures. In: Proceedings of the 13th World Conference on Timber Engineering 2
- Flores E, Saavedra K, Hinojosa J, Chandra Y, Das R (2016) Multi-scale modelling of rolling shear failure in cross-laminated timber structures by homogenisation and cohesive zone models. *International Journal of Solids and Structures* 81:219–232 6, 7
- Fragiacomo M, Dujic B, Sustersic I (2011) Elastic and ductile design of multi-storey crosslam massive wooden buildings under seismic actions. *Engineering Structures* 33(11):3043–3053 2
- Fragiacomo M, Menis A, Clemente I, Bochicchio G (2013) Fire resistance of cross-laminated timber panels loaded out-of-plane. *Journal of Structural Engineering* 139(12) 106
- Frangi A, Fontana M, Hugi E, Jobstl R (2009b) Fire Behaviour of Cross-Laminated Solid Timber Panels. *Fire Safety Science* 44(8):1078–1087 3, 9, 106, 115, 116
- Gagnon S, Pirvu C (2013) CLT handbook: Cross Laminated Timber. FPInnovations, Qubec, Canada 6
- Gagnon S, Mohammad M, Toro W, Popovski M (2014) Evaluation of the in-plane shear strength of CLT . In: Proceedings of the 13th World Conference on Timber Engineering 5
- Gavric I, Fragiaco M, Ceccotti A (2015) Cyclic behaviour of typical metal connectors for cross-laminated (CLT) structures. *Materials and Structures* 48(6):1841–1857 2
- Grandvuinet T, Muszynski L (2016) Effects of knots and slope of grains on the rolling shear in dimensional timber used in CLT core layers. In: Proceedings of the 14th World Conference on Timber Engineering 4, 27, 68

BIBLIOGRAPHY

- Hochreiner G, Fussl J, Eberhardsteiner J (2013) Cross Laminated Timber plates subjected to concentrated loading. Experimental identification of failure mechanisms. *Strain* 50(1):68–71 2, 4, 6, 7, 13, 14, 15, 16, 64, 121
- Hochreiner G, Fussl J, Serrano E, Eberhardsteiner J (2014) Influence of wooden board strength class on the performance of Cross Laminated Timber plates investigated by means of full-field deformations measurements. *Strain* 50(2):161–173 4, 27, 92
- Jeitler G (2004) Versuchstechnische ermittlung der verdrehungskenngrößen von orthogonal verklebten brett lamellen (German). TU Graz - Graz University of Technology, Graz, Austria 83
- Joebstl R, Bogensperger T, Schickhofer G, Jeitler G (2004) Mechanical Behaviour of Two Orthogonally Glued Boards. In: *Proceedings of the 8th World Conference on Timber Engineering* 75, 83
- Joebstl R, Moosbrugger T, Bogensperger T, Schickhofer G (2006) A contribution to the design and system effect of cross laminated timber (CLT). In: *International Council for Research and Innovation in Building and Construction, Working Commission W18* 2, 27
- Keunecke D, Hering S, Niemz P (2008) Three-dimensional elastic behaviour of common yew and Norway spruce. *Wood Science and Technology* 42(8):633–647 16, 17, 42
- Kirchhoff G (1850) On the equilibrium and kinematics of an elastic plate (in German). *Journal of Pure and Applied Mathematics* 40:51–88 28
- Klippel M, Leyder C, Frangi A, Fontana M, Lam F, Ceccotti A (2014) Fire tests on loaded Cross Laminated Timber wall and floor elements. In: *11th international symposium on Fire Safety Science* 9, 106
- Kohn R, Vogelius M (1984) A new model for thin plates with rapidly varying thickness. *International Journal of Solids and Structures* 20(4):333–350 48
- Kreuzinger H (1999) Plate and shell structures. A model for common calculation tools (in German). *Bauen mit Holz* 1:34–39 5, 21, 46, 56, 66, 80, 87, 122
- Lebée A, Sab K (2011a) A Bending-Gradient model for thick plates, Part I: Theory. *International Journal of Solids and Structures* 48:2878–2888 21, 45, 46, 47, 48, 112, 114, 122
- Lebée A, Sab K (2011b) A Bending-Gradient model for thick plates, Part II: Closed-form solutions for cylindrical bending of laminates. *International Journal of Solids and Structures* 48:2889–2901 46, 47, 52

BIBLIOGRAPHY

- Lebée A, Sab K (2012) Homogenization of thick periodic plates: Application of the Bending-Gradient plate theory to a folded core sandwich panel. *International Journal of Solids and Structures* 49:2778–2792 32, 45, 46, 50, 122
- Lebée A, Sab K (2013) Homogenization of a space frame as a thick plate: Application of the Bending-Gradient theory to a beam lattice. *Computer and Structures* 70:88–101 32, 61, 74, 76, 80, 84
- Lebée A, Sab K (2015a) On the generalization of Reissner plate theory to laminated-plates, Part I: Theory. *Journal of Elasticity* 48
- Lebée A, Sab K (2015b) On the generalization of Reissner plate theory to laminated-plates, Part II: Comparison with the Bending-Gradient theory. *Journal of Elasticity* 48, 64
- Li M, Lam F, Li Y (2014) Evaluating rolling shear strength properties of cross laminated timber by torsional shear tests. In: *Proceedings of the 13th World Conference on Timber Engineering* 4
- Lineham S, Thomson D, Bartlett A, Bisby L, Hadden R (2016) Structural response of fire exposed cross-laminated timber beams under sustained loads. *Fire Safety Journal* pp 23–34 9, 106
- March HW (1936) Bending of a Centrally Loaded Rectangular Strip of Plywood. *Physics (College Park Md)* 7(1), DOI 10.1063/1.1745342 28
- Menis A, Fragiaco M, Clemente I (2012) Numerical investigation of the fire resistance of protected cross-laminated timber floor panels. *Structural Engineering International* 4(22):523–532 106
- Mestek P (2011) Cross laminated timber panels under concentrated loads: design with local shear reinforcement (in german). PhD thesis, Munich University of Technology 4, 27, 92
- Mestek P, Kreuzinger H, Winter S (2008) Design of Cross Laminated Timber (CLT). In: *Proceedings of the 10th World Conference on Timber Engineering* 21
- Moosbrugger T, Guggenberger W, Bogensperger T (2006) Cross Laminated Timber wall segments under homogeneous shear with and without openings. In: *Proceedings of the 9th World Conference on Timber Engineering* 7, 8, 21, 32, 46, 51, 60, 71, 75, 83, 84, 95, 104, 122
- Moroder D, FSarti, Smith T, Pampanin S, Buchanan A (2016) The influence of diaphragm stiffness on the dynamic behaviour of multi-storey timber buildings. In: *Proceedings of 14th World Conference on Timber Engineering, Vienna (AUT)* 5

BIBLIOGRAPHY

- Okabe M, Yasumura M, Kobayashi K, Fujita K (2014) Prediction of bending stiffness and moment carrying capacity of sugi cross-laminated timber. *Journal of Wood Science* 60(1):49–58 4, 92
- Osborne L, Dagenais C, Bénichou N (2012) Preliminary CLT Fire Resistance Testing Report. Advanced Building Systems Serviceability and Fire Group, Point-Claire, Canada 9, 106
- Pagano N (1969) Exact solutions for rectangular bidirectional composites and sandwich plates. *Journal of composite materials* 4:20–34 13, 14, 16, 21, 46, 121
- Pagano N (1970) Influence of shear coupling in cylindrical bending of anisotropic laminates. *Journal of composite materials* 4:330–343 14, 16, 21
- Perret O, Lebé A, Douthe C, Sab K (2016) The Bending-Gradient theory for the linear buckling of thick plates: Application to Cross Laminated Timber panels. *International Journal of Solids and Structures* 87:139–152 5
- Polastri A (2014) An innovative connector system for fast and safe erection with CLT. In: IHF 2014, International Holzbau Forum 2
- van der Put T (1982) A general failure criterion for wood. In: Proceedings of 15th *Conseil Industriel des Bois-International*. Union of Forestry Research Organizations Meeting, Boras, Sweden 16, 18, 121
- Ranta-Maunus A, Drenzler J, Stapel P (2011) Strength of European Timber. Part 2: properties of spruce and pine tested in Gradewood project. VTT working papers 179, Technical Research Center of Finland, Qubec, Canada 68
- Sab K, Lebé A (2016) Homogenization of thin and thick heterogeneous plates. Wiley scientific publishing 47
- Schaffer E (1984) Structural fire design: Wood. Forest Products Laboratory, Madison, USA 106
- Schickhofer G, Bogensperger T, Moosbrugger T (2009) CLT Handbook: buildings with Cross Laminated Timber (in German). Technische Universitat Graz, Graz, Austria 1, 6
- Schickhofer G, Brandner R, Bauer H (2016) Introduction to CLT, Product Properties, Strength Classes. In: Proceedings of the joint COST FP1402 - FP1404 Conference on CLT 2, 5
- Schmid J, König J, Köhler J (2010) Fire exposed Cross Laminated Timber - Modeling and tests. In: Proceedings of the 11th World Conference on Timber Engineering, Trento (ITA) 106

BIBLIOGRAPHY

- Schmid J, König J, Just A (2012) The Reduced Cross Section Method for the design of timber structures exposed to fire Background, Limitations and new Developments. *Structural Engineering International* 22(4):514–522 3, 9, 106, 114, 116
- Schmid J, Klippel M, Just A, Frangi A (2014) Review and analysis of fire resistance tests of timber members in bending, tension and compression with respect to the Reduced Cross Section Method. *Fire Safety Journal* 68:81–99 9, 106
- Schmid J, Just A, Klippel M, Fragiaco M (2016) The Reduced Cross Section Method for evaluation of the fire resistance of timber members: discussion and determination of the Zero-strength layer. *Fire technology* 51(6):1285–1309 106
- Scotta R, Marchi L, Trutalli D, Pozza L (2016) A dissipative connector for CLT buildings: Concept, design and testing. *Materials* 9(3) 2
- Sebera V, Muszyński L, Tippner J, Noyel M, Pisaneschi T, Sundberg B (2013) FE analysis of CLT panel subjected to torsion and verified by DIC. *Materials and Structures* 1(9) 4
- Serrano E, Enquist B (2010) Compression strength perpendicular to grain in cross laminated timber. In: *Proceedings of the 11th World Conference on Timber Engineering* 5
- Sikora K, McPolin D, Harte A (2016) Effects of the thickness of cross-laminated timber (CLT) panels made from Irish Sitka spruce on mechanical performance in bending and shear. *Construction and building materials* 116:141–150 4
- Silly G (2010) Numerical study on in-plane shear and torsional stiffness of cross laminated timber (in German). PhD thesis, Graz University of Technology 7, 32, 51, 60, 98
- Soriano F, Pericot N, Sierra E (2016) Comparative analysis of the reinforcement of a traditional wood floor in collective housing. In *depth development with cross laminated timber and concrete. Case Studies in Construction Materials* 4:125–145 3
- Stapel P, van de Kuilen J (2014) Influence of cross-section and knot assessment on the strength of visually graded Norway spruce. *European Journal of Wood and Wooden Products* 72:213–227 27, 68
- Sturzenbecher R, Hofstetter K, Eberhardsteiner J (2010) Structural design of Cross Laminated Timber (CLT) by advanced plate theories. *Composite science and technology* 70:1368–1379 4
- Takabatake H, Yanagisawa N, Kawano T (1996) A simplified analysis of rectangular cellular plates. *International Journal of Solids and Structures* 33(14):2055–2074 46

BIBLIOGRAPHY

- Thai ND, DOttavio M, Caron JF (2013) Bending analysis of laminated and sandwich plates using a layer-wise stress model. *Composite Structures* 96:135–142 21
- Thiel A, Krenn H (2016) Buckling loads for cross-laminated timber elements under uniaxial in-plane compression. In: *Proceedings of the 14th World Conference on Timber Engineering, Vienna (AUT)* 5
- Tsai S, Wu E (1971) A general theory of strength for anisotropic materials. *Journal of composite materials* 5(1):58–80 17
- Viskovic A, Radogna D, Forlani M, Romano M (2016) Use of timber elements for reinforced concrete buildings seismic retrofitting and comfort rehabilitation. In: *Proceedings of 14th World Conference on Timber Engineering, Vienna (AUT)* 3
- WoodHandbook (2010) *Wood Handbook, Wood as Engineering Material*. The Forest Products Laboratory - US Department of Agriculture Forest Service, Madison, Wisconsin 42
- XlamDolomiti (2016) *Xlam Dolomiti on-line catalog*. Xlam Dolomiti S.R.L., Castel Ivano, Trento (ITA) 3
- Zhou Q, Gong M, Chui Y, Mohammad M (2014) Measurement of rolling shear modulus and strength of Cross Laminated Timber using bending and two plates shear tests. *Wood and fiber science* 46(2):1–11 4